Electronic and magnetic properties of two dimensional on-surface organic systems

Inauguraldissertation

zur

Erlangung der Würde eines Doktors der Philosophie

vorgelegt der

Philosophisch-Naturwissenschaftlichen Fakultät

der Universität Basel

von

Olha Popova

aus Tschernihiw, Ukraine

Basel, 2019

Genehmigt von der Philosophisch-Naturwissenschaftlichen Fakultät
auf Antrag von:

Prof. Dr. Thomas A. Jung
Prof. Dr. Ernst Meyer

Basel, 21 Mai 2019

Prof. Dr. Martin Spiess, Dekan

"*If you've never done anything wrong it's probably because you have never tried anything new*"
Albert Einstein

Abstract

The field of molecule-based technology has developed in parallel with nanotechnology over the past decades. However, these systems can offer their own unique functional properties for prospective applications, compared to more traditional, hard condensed matter-based nanotechnologies. This is due to the small size, low cost, and structural perfection that molecules have to offer. The essence of their properties goes beyond classical physics, due to their quantum nature. This fact makes molecule systems as equally fascinating from a physics prospective as they are for their potential use in new device industries. Surface and interface science is an active, interdisciplinary field with applications in chemistry and physics such as heterogeneous catalysis, energy conversion semiconductor and molecular electronics, organic spintronics and quantum magnetism, in particular at the organic-inorganic interface. In these nanoscale systems chemical bonding, electronic charge transfer and magnetic interactions at the interfaces play a fundamental role, and many of these effects are intimately coupled to the atomic structure. Thus knowledge of their structures on atomic scale is essential for the understanding of the underlying physics and for the development and performance of theoretical calculations. Complex self-assembled molecular layers on substrates with engineered architectures and tailored properties, are expected to play important role in the miniaturization and development of future devices at the nanoscale. The work presented in this thesis addresses the electronic properties of self-assembled metal-organic on-surface networks confining the surface electrons, and deeper understanding of the tuning of the electronic and magnetic properties of molecular adsorbates across those networks. The research is aimed at studying the interaction between the molecular adsorbates and the quantum confinement. This knowledge is essential e.g. for the development of organic molecule-based devices.

In summary, the strength of this thesis lies in the provision of systematic and comprehensive investigation of the interaction and surface-driven modifications of supported metal-organic complexes on noble metal surfaces, new insight into site specific electronic and magnetic properties of confined and delocalized surface states with specifically chosen molecular adsorbates. By varying the metal center of organic adsorbates,

one can change the density and distribution of the valence electrons in the metal center of the molecule. In other words, the original properties of the complex and the electronic and magnetic properties of the adsorbates are modified due to the presence or absence of the quantum confinement. The realization that the electronic and magnetic properties of the transition metal organic compound can be tailored selectively has created a large diversity of possible applications for these complexes. This includes the creation of exploratory single molecular data storage devices, the replacement of traditional semiconductor electronics by molecular electronics in supramolecular architectures, in magnetochemical sensors or as a means to control and fine tune the magnetic properties of complex architectures in spintronic devices, as well as other applications.

The ultimate achievement of this thesis is its contribution to the understanding of the precise mechanisms of confinement-adsorbate interaction. The work presented here provides a solid foundation towards improvement in the development of smart design of structures consisting of just few individual molecules and directly visualizing electron scattering and confinement.

Contents

Introduction

When length scales known from daily life are left behind, the applicability of knowledge from the macroscopic world must also be questioned. In modern micro- and nanotechnology, the knowledge from the macroscopic world cannot be transferred to the micro- and nanoscale. New material properties can improve current devices and pioneer the technological platform for new applications as the feature size becomes a relevant factor in nanosystems. In classical solid state physics, describing the bulk only is a good approximation of the macroscopic material properties: surface effects can be neglected, greatly simplifying the analytic description.
As Richard Feynman pointed out in his visionary talk "There's plenty of room at the bottom: an invitation to enter a new field of physics" the key to the nanoscale world can be found in microscopy techniques.

In nanostructures, confinement is usually related to the reflection of the electronic wave function at their surfaces or interfaces by combining different materials, giving rise to diverse optical and transport properties of semiconductor quantum dots, wires and wells [1]. As it was shown by numerous publications [2, 3, 4, 5, 6, 7], noble metal (111) surfaces host two dimensional electron gases (2DEG), which are ideal systems to study low-dimensional electronic properties dealing with electron scattering at the existing nanostructures. It is known, that if electrons are confined into the structures with a size comparable to the nanometer length, quantum size effects emerge. STM studies have demonstrated that Shockley states can be confined in parallel with a respect to the surface by artificially made nanoscale assemblies [8], for example, two-dimensional structures built atom-by-atom, so called *quantum corrals* [9], vacancy and adatom islands [10, 11], vicinal surfaces [12] and molecular nanoporous networks [13, 14]. Accordingly, the construction and exploration of coupled quantum dot systems is of great interest, both from fundamental scientific perspective and in view of potential application in fields of materials engineering, molecular electronics and quantum computing. In the following paragraph a brief discussion of the selected systems is provided, as they represent the fundamental base for this thesis.

Taking advantage of the cryogenic temperatures in combination with the ability

to position single atoms with the STM tip starting from the 90's, *quantum corrals* were assembled by repositioning Fe atoms on a Cu(111) surface [15]. The quantum mechanical interference patterns of surface states as standing waves were imaged [16]. In this case, standing wave patterns in electron density act like *"black dots"*, soaking up all of the wave amplitude imprinting of them. This phenomena Crommie *et al.* explained by a simple model considering the textbook *"particle in a box"* system and modeling the Fe atoms as an considerable boundary [9]. In a similar manner, quantum resonators were built atom-by-atom on a metal surface, and those can also trap surface state electrons [17]. However, since atom manipulation technique for the construction of corral structure is a relatively time consuming process, the fabrication of periodic two-dimensional structures at the larger scale is practically impossible.

Further on, control of production of highly regular low-dimensional nanostructures at the surfaces was achieved with hexagonal islands [18, 19] or triangular vacancy islands formed on Ag (111). This demanded less efforts then atom manipulation, since the structure was achieved by very soft sputtering of the surface [10]. These nanostructures were phenomenally similar to *quantum corrals* described earlier, but in case of hexagonal islands, discrete energy levels can be easily tuned with the lateral size. It was found that the standing wave patterns don't reflect individual eigenstates, but reflect their superpositions.

Not only steps or adatoms are able to scatter the surface electrons, but also organic molecules. They create standing wave patterns of surface state electrons by scattering them with the aromatic π system of the molecular aromatic core [20]. The concept which was transferred from supramolecular chemistry into the surface science [21], allowed to produce numerous amount of self-assembled on-surface molecular architectures with different symmetries and periodicity capable to interact with 2DEGs. For instance, the first molecular resonators were represented by 1D arrays of molecules at the metal surfaces [7]. In this case surface state resonances could be tuned by separation between the scattering molecular barriers while 2DEGs would remain practically unaffected in the direction parallel to the barriers. The strength of such quantum dot (QD) confinement depends on the geometry and periodicity of the network as well as on the deliberate choice of the molecules acting as potential barrier.

Adding more complex parameters into controlling the molecular architectures formation by the selection of functional groups of the molecular core, metal coordinating centers and the underlying template, various extended nanoporous networks were built [22, 23, 24, 25, 26]. These on-surface architectures were mainly stabilized by hydrogen bonds or metal-organic coordination [27, 28, 29, 30], showing extended order and quite low amount of defects. It is worth to notice here, that with the use of local techniques such as STM/STS, evidence of the electron confinement was shown inside the 2D architectures defined by molecular barriers [14, 22, 28]. Nevertheless, large broadening of the confined state already suggested certain interdot interaction [31]. ARPES measurements detected the presence of a shallow dispersive, cosine-shape electronic band matching the STS energy.

However, confined surface electrons within the pores of such molecular nanoporous networks turned out to be quite 'leaky'. The therm *lossy* scattering was proposed as the most correct explanation, as it reflects the fact that electrons might be scattered

from the surface states into the bulk states, and to contribute to the energy width of the confined states itself. Referring to the finite scattering barrier represented by the molecular building blocks, some degree of interdot coupling was allowed between neighboring pores. According to the concepts of band theory [32], this case shows that the formation of distinct electronic bands, as confirmed by Lobo-Checa *et al.* [14], for the 3deh-DPDI metal-organic nanoporous network supported by Cu(111) is possible. Owing to the high spatial resolution of STS technique, it was confirmed that the pores confine surface state into different localized states, in a similar fashion to previous examples [28]. In addition, dI/dV maps at the resonance peak energy and cross sections confirmed the localization of the quantum state inside each pore, resembling a quantum dot.

All previously mentioned examples of confinement presence across the porous networks summarized in this introduction build the base of this thesis. In the first chapter of the thesis (Chapter 1), the basic concepts of used methods and surface sensitive techniques are explained. Further investigation is still necessary to unravel the interplay between the electronic and geometric structure of the complex metal-organic structures on solid substrates, in particular the influence of the molecular structure of the adsorbate onto confinement properties and the intercoupling between QDs. The weak lateral forces applied by surface upon physiosorbed molecules, and the image charges which occur in metal substrates, allow the weak intermolecular forces to play a significant role in the formation of long-range order in the adsorbed phase. In Chapter 2 is shown that porphyrin based porous network can be self-assembled due to the combination of the charge transfer, electrostatic repelling forces and van der Waals strain. In the Chapter 3 is shown the electronic properties on the 3deh-DPDI network supported by Cu(111) substrate, studied by combination of different surface sensitive techniques combined with EBEM/EPWE theoretical simulations. Since nanoporous networks are serving as an ideal templates for hosting adsorbates, it is possible to tune electronic states of the quantum confinements by controlled selectivity of the adsorbates [33, 34]. While hosting molecular adsorbates across the network, the QD electronic structure can change dramatically. However, only few studies exist in the scientific literature about the interaction of selected molecular adsorbates with present quantum confinement[35, 36, 33]. Based on the sensitivity of surface states to the presence of the adsorbates and knowing that regular nanoporous structures stand out as ideal host templates [23, 33], in Chapter 4 and Chapter 5 this network is used to host octaethylporphyrins with selected metal centers inside the nanocavities. STS measurements show that confined state shifts in energy towards the Fermi level upon filling. This tendency, is qualitatively corroborated by ARPES measurements. These adsorbate-filling configurations are accurately simulated with EBEM/EPWE, examine into complexity of confinement and interdot coupling effects.

Notably, organic-electronics which relies on carbon-based materials and *spintronics*, which uses the electron-spin as a tool to store, recieve, transmit and manipulate information. Some terms like *molecular spintronics* refers to a combination of novel technologies. Storage, receiving, transmitting and manipulation of information is not only important for computers, but is also central part in the biological systems. Huge amount of information are encoded in the sequence of linear macromolecules -

DNA. This information encodes the sequence of polypeptides which from real molecular nanomachines via intra-molecular and inter-molecular self-assemblies. Biological systems give examples for the great potential of molecular nanotechnology. In Chapter 5 was investigated the effect of tuning magnetic properties of the metal ions of molecular adsorbates caused by interaction with the present quantum confinement, a topic, which was never reported in the scientific literature before.

In the last part of this thesis (Chapter 6) were investigated Mn complexes with triagonal prismatic geometry exhibiting unusual magnetic properties in the bulk crystalline samples at the Au(111) substrate. The complexes comprise an ionic compound with both an organic anion and an organic cation i.e. a completely different chemical architecture which can be deposited by sublimation.

1 Methods and Experimental setup

This chapter gives an overview of the main experimental techniques used in the research included in the thesis. Scanning Tunneling Microscopy (STM) was used to obtain structural information about the studied on-surface interfaces. Chemical composition of the samples as well as evolution of chemical reactions was investigated by X-Ray Photoelectron Spectroscopy (XPS). Electronic properties of the on-surface architectures were investigated by Scanning Tunneling Spectroscopy (STS), Angle Resolved Photoelectron Spectroscopy (ARPES) and Photoelectron Diffraction (PES). Finally, magnetic properties of molecular adsorbates were probed with X-Ray Magnetic Circular Dichroism (XMCD) on one hand, and with STS on another.

1.1 Ultra-High Vacuum

Owing to the stringent requirements of Ultra High Vacuum (UHV) in surface science experiments many of the samples have to be prepared *in situ* without breaking the UHV conditions between preparations and measurements. According to the kinetic theory of gasses, the flux I of gas molecules towards the surface is given by equation:

$$I = \frac{p}{\sqrt{2\pi m k_b T}} \tag{1.1}$$

where p [Pa] is the pressure in the experimental chamber, m [kg] is the mass of molecules or particles, k_b=1.38×10^{-23} kg · m^2 · s^{-2} · K^{-1} is the Boltzmann's constant and T [K] is temperature of the sample.

In the optimal conditions (p=10^5 Pa, T=300 K, m_{air}=4.83×10^{-26} kg), that would mean, sample for investigation with size around 1 cm^2 and with approximately 10^{15} adsorption sites, will be covered with air (assuming that every molecule which hits the sample stays adsorbed) within a picosecond. If pressure is in 10^{-6} mbar, sample will be covered within seconds, and in the case when the pressure is in UHV conditions, means 10^{-10} mbar, it takes several hours for sample to be covered in the pessimistic scenario – when all molecules/particles would stick to the surface. Thus, in order to reduce possible contamination of the sample of the interest, UHV conditions are

required for number of the surface sensitive techniques e.g. UPS, XPS, ARPES, XAS etc, where we want to minimize scattering of the electrons, or X-Ray absorption of the surrounding gas molecules. All experiments, which are presented in this thesis were performed under UHV conditions, which were reached by combination of different pumps involving rough pump, turbomolecular pumps, ion-getter pumps and titanium sublimation pumps according to the information from the following sources [37]. Part of the experiments were conducted at Nanolab, University of Basel, part at Surface Science Lab, Paul Scherrer Institute (PSI) East (Villigen, Switzerland), other part was performed at the different beamlines of the Swiss Light Source (SLS), synchrotron located at the PSI West. The samples were transferred between the labs and beamlines without breaking the vacuum using a vacuum suitcase.

1.2 Sample preparation

The surface was prepared by multiple cycles of Ar^+ ion sputtering at 2 keV at room temperature, followed by annealing to 800 K. The cleanliness and the quality of the surface structure and desired composition were controlled by STM and XPS. Studied molecules were thermally sublimed onto the surface with the use of the nine-cell commercial evaporator (Kentax, GmBH, Germany), at a rate about 0.5 ML/min , checked by a quartz microbalance, resulting in an average coverage in the submonolayer range up to a full molecular layer.

1.3 Surface Analysis I. Microscopy

Microscopy is the technical field of using instruments designed to view objects and areas of objects that cannot be seen within the resolution range of the normal eye. In general, microscopy information concerns surface crystallography, surface morphology and surface composition. Until the 1930th, microscopy relied on optical methods with a spatial resolution that was limited by Abbe's diffraction limit, i.e. $\sim$1 μm. To overcome this hurdle, Ernst Ruska developed new type of microscopy that uses high-energy electrons. Despite the strongly enhanced spatial resolution of Ruska's electron microscope, Erwin Mueller obtained the first atomically resolved images using field ion microscopy.

1.3.1 Physical bases of Scanning Tunneling Microscopy

Another major breakthrough in the field of microscopy was the invention of the STM in 1981 by Gerd Binning and Heinrich Rohrer [38], who were awarded with a Nobel Prize in 1986, and it significantly influenced surface science research. Since it allowed systematic study of the surfaces at the (sub-) nanometer scale in real space. In quantum world relatively small particles can pass through an energy barrier although their energy might be way smaller than the barrier itself. This so-called tunneling effect [39] carries the name of quantum tunneling and in consequence of uncertainly principle giving non-zero probability of finding particle on the other side of the barrier. In the

very simple model of rectangular barrier one can analytically solve the Schrödinger equation and demonstrate that tunneling is dependent on height and width of the barrier.

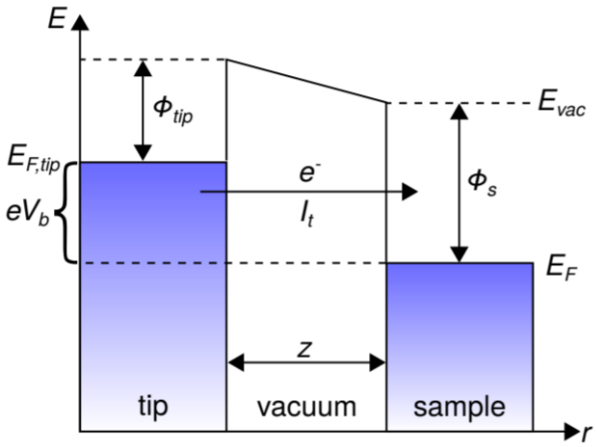

Figure 1.1: *Tunneling barrier scheme. Due to the quantum tunneling effect electron has a low probability to tunnel through rectangular barrier (vacuum) if the tip-sample distance z is small enough and a bias voltage V_{bias} is applied.*

One electrode is the STM tip with a work function Φ_T, the other is the sample surface with a work function Φ_s by a vacuum gap of the width z. The probability to tunnel through the barrier exponentially decreases with increasing the width of the barrier. This was the principle Binning and Rohrer used for creating the very first STM in the image where the distance between the apex of the sharp metallic tip and the sample d [m] represents the tunneling barrier for the electrons 1.1. When a small voltage U [V] between them is applied, electrons at the Fermi level E_{Fermi} (within the $e \cdot U$ energy range, e=1.602×10^{-19} C are excited and can tunnel through the barrier. In STM metallic tips are approached normally very close (~ 4 $\mathring{A}$) to (semi-) conducting surface. While applying bias voltage between the tip and sample ($< 3V$) would not permit the overcoming of the barrier between them in classical physics, in the case of quantum mechanics probability of the tunneling event increases. This probability and hence the resulting tunneling current decreases exponentially with tip-sample distance. The tunneling current I_t [A], regardless of its direction is given by the formula:

$$I_t \infty \sum_{E_f - eU}^{E_{Fermi}} |\psi_n(0)|^2 e^{-2kd} \tag{1.2}$$

Where $\psi_n(0)$ are eigenvalues of the 1D electron wave function and k [nm^{-1}] decays constant and it is related to the work functions of the sample and the tip respectively. As a consequence, tunneling current is highly localized between the last atom of the tip apex and the sample, which serves as a probe of Local Density of States (LDOS) of the investigated sample, assuming, that density of states of the tip is constant. Experiment is conducted such, that the tip is moved above the sample in raster mode. The control

of the tip position with the piezoelectric motors while current is measured, allows to probe the topography of the investigated sample. Experiments with STM can be performed in two different modes either in constant current mode, while the scanning distance is adjusted to keep the current constant or constant-distance. The STM has proved to be very powerful technique for studying or manipulating on-surface systems, especially in the case, when those systems have lack of periodicity and diffraction methods can't be used. No matter, which operation mode is used, topographic images always reflect a convolution of the electronic structure of the tip and surface. It is worth to mention, that extraction of quantitative information about the respective properties can be rather challenging. On the other hand, a direct and unambiguous investigation of the electronic surface structure and properties, or its potential energy landscape, can be obtained in a straightforward manner by spectroscopic operation.

1.3.2 Theoretical Description of the Tunneling Process

The tunneling process is described by a variety of different theoretical models, two of which will be briefly described here. The first is a simple time-independent 1D model. Despite its approximate character, this model is very useful, as it can be solved analytically and leads to the fundamental dependencies of the tunneling current. The second model takes all three dimensions into account, as well as the electronic structure of the tip and sample.

Simple 1D model

In a first approximation, the tunneling junction can be described as a one dimensional and time independent system. The electron is approximated as a free electron with energy E, separated by a potential barrier of height Φ and thickness d. The stationary Schrödinger equation for the electron wave function Ψ in the tip, the sample, and the barrier has to be solved:

$$\left(\frac{\hbar^2}{2m_e}\Delta + V\left(r\right)\right)\Psi = E\Psi \tag{1.3}$$

where m_e is the electron mass, and V(r) the potential describing the barrier with height Φ and width d and E energy of the electron. The exact solution for these wave functions can be found by using a plane wave approach for Ψ of the three regions - tip (I), vacuum (II), and sample (III). Fig. 1.2

$$\psi_1 = e^{ikz} + A \cdot e^{-ikz}$$

$$\psi_2 = B \cdot e^{i\kappa z} + C \cdot e^{-i\kappa z}$$

$$\psi_3 = D \cdot e^{ikz}$$

with $k = \dfrac{\sqrt{2m_eE}}{\hbar}$ and $\kappa = \dfrac{\sqrt{2m_e(\Phi - E)}}{\hbar}$

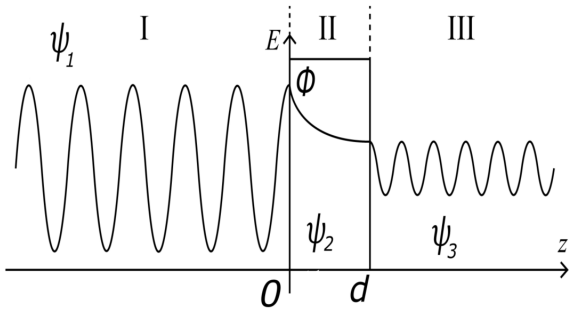

Figure 1.2: *One dimensional potential barrier with energy* Φ *and width d. A particle that is traveling from the left to the right is described by three wave functions* ψ*:* ψ_1 *before, inside* ψ_2 *and* ψ_3 *after the barrier.*

By matching the amplitude and the first derivative at the boundaries of the different potential regions, the coefficients (A, B, C, D) can be determined [40]. Then we can define a transmission coefficient T by comparing the wave functions on both sides of the barrier:

$$T = \frac{|\psi_1|^2}{|\psi_3|^2} = \frac{A^2}{D^2} = \left[\frac{\left(\frac{k^2+\kappa^2}{2k\kappa} \right)^2 \sinh kd}{\kappa d} \right]^{-1} \tag{1.4}$$

which can be simplified for a high barrier potential compared to the energy of the electron $\Phi \gg E$, i.e., if $\kappa d \gg 1$

$$T \approx \frac{16k^2\kappa^2}{\left(k^2+\kappa^2\right)^2} \cdot e^{-2kd} \tag{1.5}$$

The number of tunneling electrons, which is basically tunneling current I_t, will be proportional to T. Therefore with the thickness of the barrier given by the tip height d, we find:

$$I_\infty T_\infty e^{-2kd} \tag{1.6}$$

This simple 1D model shows, that the tunneling current depends exponentially on the tip-sample distance d. This Exponential dependency is the underlying mechanism for the high vertical resolution of the STM technique.

The Tersoff-Hamman Model

The Tersoff-Hamman model can be extended by including the electronic structure of tip and sample and the three dimension of the problem. Tersoff and Hamann presented this more realistic model in the 1980s [41]. Their straight forward point was a first order perturbation theory model introduced by Bardeen [42]. In this model, tunneling

process is described by the tunneling matrix $M_{T,S}$ which represents the overlap of the wave functions of tip ψ_T and sample ψ_S.

The tunneling current for the general geometry can be written as:

$$I = \frac{2\pi e}{\hbar} \sum_{T,S} f\left(E_T\right)\left[1 - f\left(E_S + eV\right)\right]\left|M_{T,S}\right|^2 \delta\left(E_T - E_S\right) \tag{1.7}$$

Where $f(E)$ is the Fermi-Dirac distribution function and E_T and E_S are energies of the tip and substrate respectively. V is the applied bias voltage. In the limit of the low temperatures and voltages $e \cdot V \ll \Phi$, and Equation 1.7 can be simplified due to the fact that $f(E)$ becomes a step function with $f(E) = 1$ for $E < E_{Fermi}$. Then we can approximate the term $[1 - f(E_s + eV]$ as a step function, which yields:

$$I = \frac{2\pi}{\hbar} e^2 V \sum_{T,S} \left|M_{T,S}\right|^2 \delta\left(E_T - E_{Fermi}\right) \delta\left(E_S - E_{Fermi}\right) \tag{1.8}$$

the tunneling matrix element $M_{T,S}$ was shown by Bardeen [42] to be integrated over an arbitrary surface between tip and sample:

$$M_{T,S} = -\frac{\hbar^2}{2m} \int \left(\psi_T^* \overrightarrow{\nabla} \psi_S - \psi_S^* \overrightarrow{\nabla} \psi_T^*\right) d\overrightarrow{s} \tag{1.9}$$

In order to receive at quantitative tunneling currents it is necessary to define the wave functions for the sample and the tip. These should describe the geometry found in STM itself. The surface is described through the wave function parallel to the surface, consistent with Bloch's theorem. In the perpendicular direction it decays exponentially into the vacuum:

$$\psi_s = V_S^{-1/2} \sum_G a_G e^{\sqrt{\kappa^2 + \left|\overrightarrow{G} + \overrightarrow{k}\right|^2} z} \cdot e^{\left(i\left[\overrightarrow{k_{||}} + \overrightarrow{G}\right]\overrightarrow{x}\right)} \tag{1.10}$$

where $e^{\sqrt{\kappa^2 + \left|\overrightarrow{G} + \overrightarrow{k}\right|^2} z}$ is a exponential decay and $e^{\left(i\left[\overrightarrow{k_{||}} + \overrightarrow{G}\right]\overrightarrow{x}\right)}$ Bloch wave. $\overrightarrow{G}$ is a reciprocal lattice vector, $\kappa = \hbar^{-1}(2m\Phi)^{1/2}$ the decay length into the vacuum, $\overrightarrow{k_{||}}$ the wave vector of the surface wave, and V_S the normalization volume of the surface. First few coefficients a_G are typically of the order of unity. The tip is modeled as a spherical potential (see Fig. 1.3) at the point closed to the surface and the rest is arbitrary. According to the spherical *s-wave* function, which is used for the tip:

$$\psi_t = V_T^{-1/2} \kappa R e^{\kappa R} \frac{1}{\kappa\left|\overrightarrow{r} - \overrightarrow{r_0}\right|} e^{-\kappa\left|\overrightarrow{r} - \overrightarrow{r_0}\right|} \tag{1.11}$$

here, V_T is the normalization volume of the tip, R the tip radius, κ and Φ are the same constants as mentioned above. For simplicity sake both wave functions of tip and the sample, are assumed to be equal. With this model wave functions, it is easier to simplify tunneling matrix 1.9 to:

$$M_{T,S} = -\frac{\hbar^2}{2m} 4\pi k^{-1} V_T^{-1/2} k R e^{kR} \psi_S(\overrightarrow{r_0}) \tag{1.12}$$

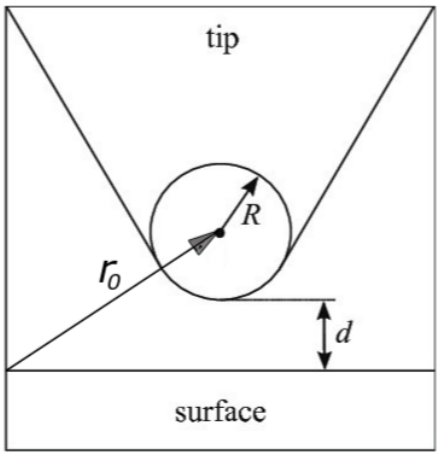

Figure 1.3: *STM tip model used to approximate the wave function in the Tersoff Hamann description. The center of the tip is at* $\overrightarrow{r_0}$ *with the assumed spherical geometry, R is the radius and d the distance to the surface.*

Equation 1.12 can be used to define the tunneling current giving:

$$I = \frac{32\pi^3 e}{\hbar k^4} V \Phi^2 R^2 e^{2kr} \frac{1}{V_T} \sum_{T,S} f\left|\psi_T\left(\overrightarrow{r_0}\right)\right|^2 \delta\left(E_T - E_{Fermi}\right) \delta\left(E_S - E_{Fermi}\right) \tag{1.13}$$

To simplify this expression we note that the local density of states for the tip and surface are defined as follows:

$$\rho_T(E) = \frac{1}{V_T} \sum_{T} \delta\left(E_T - E\right) \tag{1.14}$$

$$\rho_S(E, \overrightarrow{r_0}) = \sum_{S} f\left|\psi_S\left(\overrightarrow{r_0}\right)\right|^2 \delta\left(E_S - E\right) \tag{1.15}$$

the final expression for the tunneling current comes to:

$$I \propto V_T(E_{Fermi}) \rho_S(E_{Fermi}, \overrightarrow{r_0}) \tag{1.16}$$

Thus the current depends on the LDOS of the surface at the position of the tip $\overrightarrow{r_0}$ and Fermi energy E_{fermi}. This means, that STM images reflect the LDOS of the surface at the specific energy, rather than the position of the atoms. A more realistic description, a generalization of the Tersoff-Hofman model, defines the tunneling current by integrating over the states contribution to the I_t : the surface and tip DOS within the finite bias window. The dependence of the vacuum barrier on the tip-sample distance *d*, the energy *E* of each state, and the bias voltage V_{bias} are presented by a transmission coefficient *T(d, E, eV)* [43, 44, 45].

$$I \propto \int_{E_{Fermi}}^{E_{Fermi}+eV} \rho_S(E_{Fermi} - eV + \epsilon) \rho_T(E_{Fermi} + \epsilon) T(d, \epsilon, eV) d\epsilon \tag{1.17}$$

Therefore the main contributing factors to the tunneling current are: the DOS of the tip and the sample, and a transmission coefficient *T(d, E, eV)*. For small biases ρ_T and T can be assumed constant; the tunneling current would be proportional to ρ_S integrated from E_{Fermi} to the applied bias voltage $E_{Fermi}+V$. This model is still not a complete description of the tunneling process in an STM. Although in many standard situations it provides a reasonable qualitative picture. Some critical remarks have to be added nonetheless. The approximation of the tip as an s orbital is rather inaccurate, as in tungsten tips the d orbitals contribute to the major part of the tunneling current [46] Also, the interaction between tip and sample through microscopic chemical forces is not always negligible.

1.3.3 Scanning Tunneling Spectroscopy

The arrangement of the electrons in the sample is described in quantum mechanics as *"electron density"*. The electron density is function of both position and energy, and is formally described as LDOS, which is a function of energy. Spectroscopy, in its most general sense, refers to measurement of number of something which is function of energy. In particular, STS is used to measure the number of electrons as function of the electron energy (LDOS). The electron energy is set as electrical potential difference between sample and tip. Location normally is set by position of the tip. In Scanning Tunneling Spectroscopy (STS) the differential conductance dI_t/dV_t is recorded which is proportional to the LDOS of the sample at constant height following the Tersoff-Hammann model [37]

$$\frac{dI_t}{dVt}\alpha\rho\left(r, E_F + eV_b\right) \tag{1.18}$$

To obtain dI_t/dV_t, a small AC-voltage is applied between tip and sample, which modulates the tunneling current. Using a lock-in amplifier, the dI_t/dVt signal is directly recorded during the bias sweep Fig.1.4.

By positioning the tip over an object, the tunneling barrier described in Fig1.2 becomes a double barrier tunneling junction. In that case, one barrier is the vacuum between tip and molecule. When we speak about molecules at the surface, the closest to the Fermi energy E_{Fermi} are the Highest occupied molecular orbitals (HOMO) and the lowest unoccupied molecular orbitals (LUMO). By sweeping bias voltages to these energies, the molecular states are in resonance with the applied voltage which leads to a peak in the dI_t/dV_t signal. Thus specific electronic states of surfaces [37, 48, 49, 50], molecules, single atoms or molecular architectures can be investigated.

In particular, point spectroscopy is very powerful tool to probe the state of a surface and acquire interesting information besides the topography. In most cases, while performing point spectroscopy, the feedback loop is switched off and the voltage ramped while recording the response of various input signals.

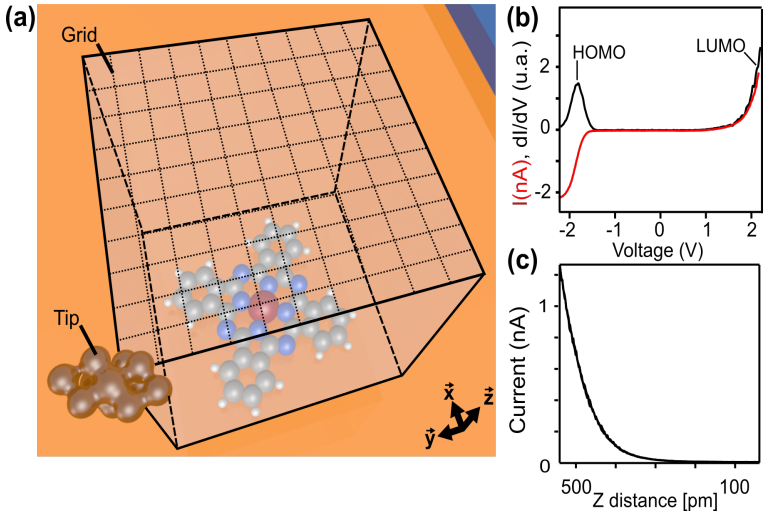

Figure 1.4: *Illustration of 3D-spectroscopic operation mode. Different spectroscopy methods* **b** $I_t(V)$ *and* **c** $I_t(z)$*.In* **b** *spectra refers to HOMO and LUMO. Figure adopted by permission of R. Pawlak from [47].*

Multidimensional Spectroscopy operation mode

An intriguing application of the STM lies in the possibility to spatially resolve the topography of subnanoscale systems. The technique can be combined with STS, mapping the spatial distribution of the features which are found. The basic method is to scan an area of interest and take the dI/dV intensity at each point of the scan Fig. 1.4. The resulting dI/dV map is to some extent an image of the spatial distribution of the state investigated. The speed of such an acquisition is normally limited by the settings of the lock-in amplifier and the pixel resolution of the dI/dV map. Depending on the size of the maps, the measurement time in experiments that are the part of this thesis was varied between 8-17 hours. To avoid the thermal drift in z direction the constant current mode is usually employed.

The interpretation of such dI/dV maps is however not trivial, because the topography of the samples has a strong influence on the height of the tip and can enhance or reduce certain features. In any case, the qualitative comparison of molecular states for similar molecules in different environments, as presented in later chapters, is not severely affected by topographic effects, therefore in this work no normalization techniques were used.

I(z) spectroscopy

Another common STM technique is Z spectroscopy – method developed by Vitali *et. al.* [51] By varying the tip-sample distance, the exponential distance dependence of the tunneling current can be probed Fig.1.4c Thus, the local potential barrier height can be extracted from the slope of the logarithmic $I_t(z)$-plot since the decay length κ depends on the work function at the tip position. The local potential height reveals information about the electronic alignment of a sample, e.g. of the charge transfer

between molecules and a metallic substrate [50]

1.3.4 Experimental setup for Microscopy methods

The experimental setup used in this work is a LT UHV STM (Scienta Omicron GmbH) operated with Nanonis electronics from SPECS. To achieve stable scanning conditions, the microscope is mounted in a UHV chamber and based on a liquid helium cryostat to work at temperatures ~ 5 K. The low operation temperatures are achieved by the use of a bath cryostat, made out of two tanks. The inner one holds up to 10 liters of liquid helium while the outer one is filled with liquid nitrogen. Both cooling stages have radiation shields that enclose the STM sample stage within. Using this method the sample can be cooled and measured for up to 60 h per refill of the helium deposit. The nitrogen tank lasts for approximately 36 h.

1.4 Surface Analysis II. Photoemission Spectroscopy

Photoelectron Spectroscopy (PES) is the most commonly used analytical technique to probe the electronic structure of the molecules Fig. 1.5, solids and surfaces. Furthermore, PES has widespread practical implications in various fields like surface chemistry or material science, and has significantly contributed to the understanding of fundamental principles in solid state physics. Historically the first experiments that revealed the interaction of light with matter, were performed by Heinrich Hertz and Wilhelm Hallwachs in 1887. These experiments demonstrated that negative charge – the electron had not been discovered yet – can be removed from a solid when its surface is irradiated by ultraviolet light, whereas no discharge was observed for positive charge. In one of the most famous publications in 1905, Einstein introduced the concept of the photon and deduced the relation between the photon energy – hν and the maximum kinetic energy of the emitted electrons, i.e. fundamental *photoelectric effect* [52], in which electron initially in a state with binding energy E_i absorbs a photon of energy $\hbar\omega$ and leaves the solid with kinetic energy:

$$E_{r\cdot i} = h\nu - \Phi_S \tag{1.19}$$

where $\Phi_s = E_{vacuum} - E_{Fermi}$ is the work function of the material. The necessary conditions for detecting the escaping elastic electron are:
- velocity of electrons should be directed towards the outer surface
- the energy of the photon is sufficient to allow the electron to escape from the solid, i.e. $\hbar\omega = E_i + \phi$
- the electron doesn't lose energy in collisions with other electrons on its way to the surface.

Typical PES instruments use helium gas sources of UV light, with photon energy up to 21.2 eV (corresponding to wavelength 23.7 nm). The photoelectrons that actually escaped into the vacuum are collected, energy resolved, slightly retarded and counted, which results in a spectrum of electron intensity as a function of the measured kinetic energy. Because binding energy values are more readily applied and understood, the

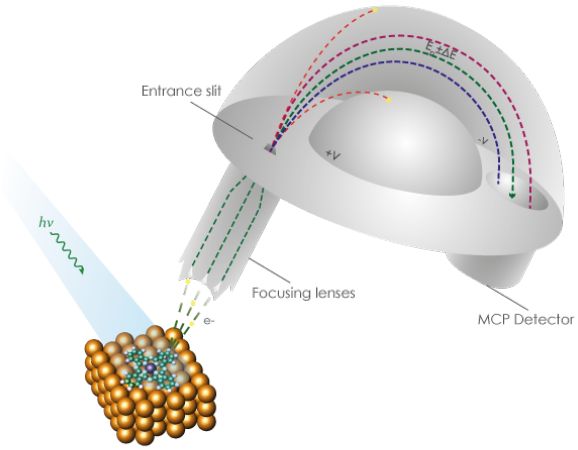

Figure 1.5: *Schematic drawing of a hemispherical electron energy analyzer during PES measurement. The photoelectrons are focused onto the entrance slit by the electrostatic lens system. Electrostatic fields within the sphere are established to only allow electrons of a given energy to arrive at the micro channel plate detector (MCP).*

kinetic energy values, which are source dependent, are converted into binding energy values, which are source independent. This is achieved by applying Einstein's relation:

$$E_k = h\nu - E_B \tag{1.20}$$

The hν term of this equation is due to the energy (frequency) of the UV light that bombards the sample. Photoemission spectra are also measured using synchrotron radiation sources.

1.4.1 Synchrotron Radiation

Synchrotron radiation is the name given to the radiation which occurs when charged particles are accelerated in a curved path or orbit. Classically, any charged particle which moves in a curved path or is accelerated in a straight-line path will emit electromagnetic radiation. Various names are given to this radiation in different contexts. For example, when it occurs upon electron impact with a solid metal target in an x-ray tube, it is called *"brehmsstrahlung"* radiation. Particularly, in the application to circular particle accelerators like synchrotrons, where charged particles are accelerated to very high speeds, the radiation is referred to as synchrotron radiation light. This radiated energy is proportional to the fourth power of the particle speed and is inversely proportional to the square of the radius of the path. It becomes the limiting factor on the final energy of particles accelerated in electron synchrotrons like the SLS at Paul Scherrer Institute. In other contexts like the detector arrays in accelerators, it can be

detected and used as an aid to analyzing the products of the scattering event. Synchrotron radiation characteristically is highly polarized and continuous. Its intensity and frequency are directly related to the strength of the magnetic field and the energy of the charged particles affected by the field. Accordingly, the stronger the magnetic field and the higher the energy of the particles, the greater the intensity and frequency of the emitted radiation.

1.4.2 X-Ray Photoelectron Spectroscopy

Depending on the energy of the photons used in the photoemission process, the techniques are usually divided into UV and X-ray techniques. When weakly bounded electrons are emitted, In the first case, we are talking about Ultraviolet Photoelectron Spectroscopy (UPS), where mostly loosely bound (valent) electrons are emitted and can give us information about electron distribution around Fermi level and their interaction with adsorbates [53, 54]. In addition, due to angular momentum conservation principle, parallel momentum of these electrons is conserved upon photoemission, and is easily related to emission angle in the variation of UPS that is named Angle-Resolved Photoemission Spectroscopy (ARPES) and is used in mapping the band structure of materials. If the X-rays are used, we are talking about X-ray Photoelectron Spectroscopy (XPS), where mostly core electrons are probed, carrying the information about chemical environment of the emitting atoms. Old name of this method is Electron Spectroscopy for Chemical Analysis (ESCA), an analytical technique to study the electronic structure and its dynamics in atoms and molecules [55, 56]. Detecting electrons that are ejected from higher orbitals to conserve energy during electron transitions is called Auger Electron Spectroscopy (AES).

Referring back to the schematic diagram of the photoemission process shown in Fig.1.6, wich represents XPS case, one can see, that the photoemission spectrum $I(E_k)$ is a fingerprint of the of the DOS in the probed material. Besides the peaks, due to elastic photoelectrons, there is a number of additional features in XPS spectrum, like continuous background of inelastic secondary electrons, Auger peaks, and peaks due to plasmon losses.

1.4.3 Angle Resolved Photoelectron Spectroscopy

Angle Resolved Photoelectron Spectroscopy (ARPES) is a powerful tool to directly probe the electronic structure of materials, which has been broadly used in the research of condensed matter physics. It plays an important role in unraveling the mechanism of many exotic phenomena in high-temperature superconductors, graphene, topological insulators, and many other advanced materials. The energy of the electron inside the solid can be obtained by usage of the photoelectron spectroscopy Fig. 1.7 – the core electrons will have lower kinetic energy than the valence electrons when absorbing the same photon energy.

Continuous efforts have been made over a hundred years, which finally enable the accurate measurement of the energy and momentum of photoeletrons. Combining the information of energy, momentum, and spin, one can have the full description of the

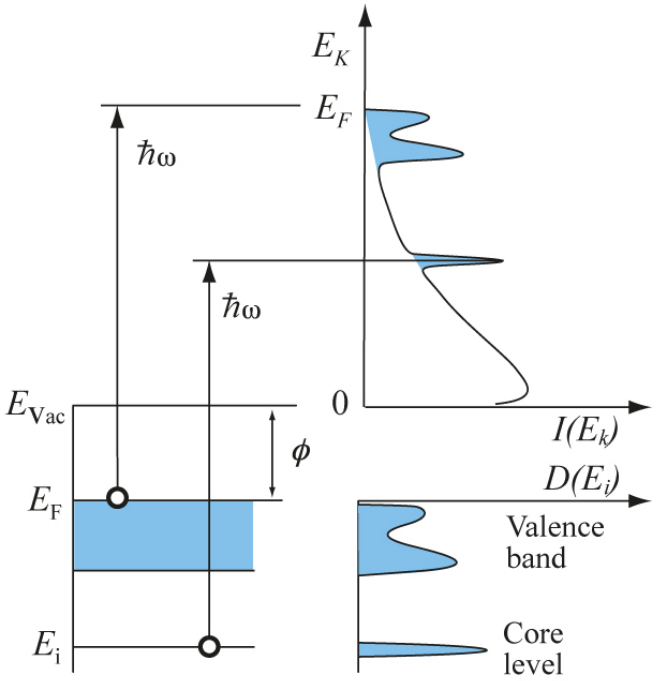

Figure 1.6: Schematic illustration of photoemission. *The correspondence between the density of occupied states $D(E_i)$ is the solid and angle-integrated photoemission spectrum $I(E_k)$ is shown. The peaks of the elastic photoelectrons are superposed on the continuous background of inelastic secondary electrons [37].*

electronic states in the material. In principle, the momentum of the electrons can also be obtained – different momentum electron will escape at the different angles from the surface of a material. However, since the electrons are being projected through the surface, the momentum perpendicular to the surface is not conserved. Therefore, angle-resolved photoemission is ideal for 2D materials where the principle momentum directions of interest are parallel to the surface. In practice, the electrons ejected from the material are collected by hemispherical detector in which lens voltages direct the electrons onto a two-dimensional multi-channel plate. The sample and the detector are kept in an UHV conditions in order to minimize surface contamination. Light sources are either synchrotron radiation at $\sim$ 20–200 eV, or plasma Helium discharge at 21.22 eV.

ARPES vs occupied states

ARPES measures photoelectrons which are ejected from the initial states to the final states after absorbing the incident photons. In other words, ARPES measures electronic states occupied by electrons, but not the unoccupied states. On another hand, to measure unoccupied states, one need to use inverse photoemission, in which low-energy electrons re directed at the sample surface and coupled with unoccupied states. At zero temperature, if the energy resolution of the system is infinite, then the measured electronic states should show sudden cutoff in the shape of the step function. This is

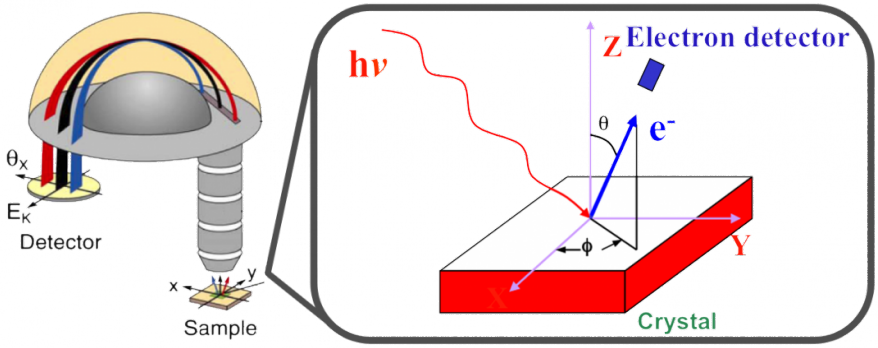

Figure 1.7: Schematic ARPES explanation. *The angular distribution of the kinetic energy of the electrons leaving the sample is measured and recalculated to energy vs momentum.*

called Fermi cutoff, and the corresponding energy is E_{kin}, an energy reference for BE of the occupied electronic states. In real experiments, the Fermi cutoff is broadened by the temperature and energy resolution of the measurements. This can be used to check the T of the sample by the Fermi cutoff broadening when energy resolution is known.

Narrow lines of the surface states in ARPES

Nobel metals host special electronic states that have been understood as text book examples of Shockley states. The electronic structure of noble metal surfaces is composed of *d*-bands, which are occupied and highly-dispersive *sp*-bands that cross the Fermi level. In addition to these, surface state electrons are present at the surface in the form of 2D electron gas. Surface states have played an important role in fundamental condensed-matter physics for decades. Understanding surface states requires understanding what happens to the Hamiltonian of the system when we approach the surface, i.e. when the bulk material is suddenly interrupted. The existence of the surface itself implies symmetry breaking, caused by the termination of the infinite crystal by the surface, along the direction orthogonal to the surface. This can introduce new evanescent solutions to the Schrödinger equation in the projected bulk band gaps residing only at the surface. Bulk state can be described as an oscillating wave which exponentially decays into the vacuum as it reaches the surface. A surface state, on the other hand, resides at the material surface, decaying both into the vacuum and into the bulk. Therefore, for a surface state to exist, it must lie in an energy gap between the bulk bands, otherwise it is named a surface resonance. Prototypical examples are found at the Brillouin-zone center of the noble metal (111) surfaces. These Shockley states appear in a gap of projected bulk bands along the Γ-L line. On another hand electrons of the surface state behave like free electrons parallel to the surface and form 2DEG.

1.4.4 Comparison between STS and ARPES

The tunneling current detected by STM is the convolution of surface electronic and topographic landscapes. In order to measure the surface electronic states, it is necessary to deconvolute the electronic information from the topographic structure. This is accomplished through scanning tunneling spectroscopy. STS enables the local, energy-resolved investigation of a sample surface DOS by measuring the differential conductance (dI/dV), which is approximately proportional to the DOS. STS enables the local characterization of physical and electronic properties of conducting samples. Typically, a small AC modulation ($V_{rms} < 100$ mV at 1 kHz) is superimposed on the DC bias voltage while a lock-in amplifier records the first harmonic of the signal that is in phase with the modulation. Contrary to the ARPES, STS can probe both occupied and unoccupied states depending on the selected bias voltage polarity. In addition, it has the capability to investigate the electronic structure at the atomic scale, while simultaneously providing topographic information. Therefore, STS is perfectly suited to study adsorbates positioned on substrates and confinement effects of surface state electrons, providing a complementary approach to k-vector resolving photoemission spectroscopy techniques.

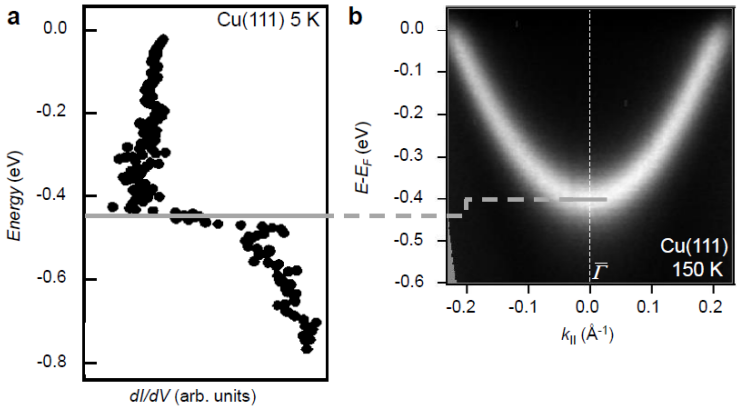

Figure 1.8: *STS vs ARPES Cu(111) surface state measurements. (a) Experimental dI/dV spectrum taken from the bare Cu(111) sample highlights the step-like character of the surface state [16]. (b) ARPES band structure of Cu(111) Shockley state shows its parabolic dispersion with a well-defined band bottom energy, effective mass and Fermi wave-vector (k_F).*

A comparison between STS and ARPES for the first time was done on Cu(111) by Crommie *et al.* [16]. They found a sharp increase of the differential conductance dI/dV signal at -0.45 V and explained this increase as electrons tunneling from the occupied surface state of Cu(111) into empty states of the tip Fig.1.8. Therefore, such a sharp increase of the dI/dV signal is recognized as the onset of the two-dimensional surface-state band of the noble metal (111) surfaces [Fig.1.8(a)]. Note that, apart from temperature induced variations on the onset energy of the surface state E_0, this is usually lower in STS measurements than ARPES by 5-10 meV because the electric

field induced by the presence of an STM tip affects the surface electronic structure, *via* the so-called Stark effect.

1.4.5 Photoelectron Diffraction

The analysis of the anisotropy in emission of a core level peak is also quite used in structural studies. In Photoelectron Diffraction (PhD), electrons due to the photoelectric effect are considered. The energy of the emitted electrons is a well-defined characteristic of the atom involved. If the adsorbed atoms on the substrate are being investigated, it can be directly determined at which atoms the initial *"input wave"* is generated. The elastic scattering of the wave from the *"emitted atom"* on the surrounding atoms is responsible for the anisotropy in the emission [57, 58]. In the experiment, angle-resolved photoelectron spectrometer is normally utilized to collect the data set. The evaluation of the surface structure proceeds through comparison of the experimental data with the result of the model calculations. The structure determination is more reliable when analyzing the high-energy ($\geqslant$ 400 eV) electrons emitted from core levels, for which case the emitted wave can be approximated by a spherical wave and the kinematic approach is justified [58, 59, 57].

Energy Scanned mode of Photoelectron Diffraction

The Energy Scanned mode of Photoelectron Diffraction (PhD) technique is widely used for the determination of surface adsorption structures [60, 61, 62]. The technique exploits the interference of the directly emitted component of the wavefield of photoelectrons emitted from the core level of an adsorbed atom with other components elastically scattered by surrounding (in particular substrate) atoms. The resultant intensity modulations provide information on the local scattering path differences and thus the local adsorption site. The first step of the method gives an approximate three-dimensional image of the dominant nearest neighbor scatters surrounding an emitter atom. In a second step this approximate structure is further refined using multiple scattering cluster calculations. Finally, a very recently developed procedure is employed in which the dynamics/displacements of the emitter atom are examined utilizing the Maximum Entropy Method.

Note, that PhD experiments represented in Chapter 5 were obtained in normal emission energy mode.

1.4.6 X-Ray Absorption Spectroscopy

X-Ray Absorption Spectroscopy (XAS) is a widely used technique for determining the local geometric and/or electronic structure of mater. As described before, each element has a defined energy of the core levels – so called, fingerprint of its nature. XAS is based on a similar physical effect as photoemission spectroscopy, i.e. excitation of electrons by photons. In the XAS experiment the absorption is measured as a function of a photon energy, thats why the method requires a tunnable source of X-rays. The experiment

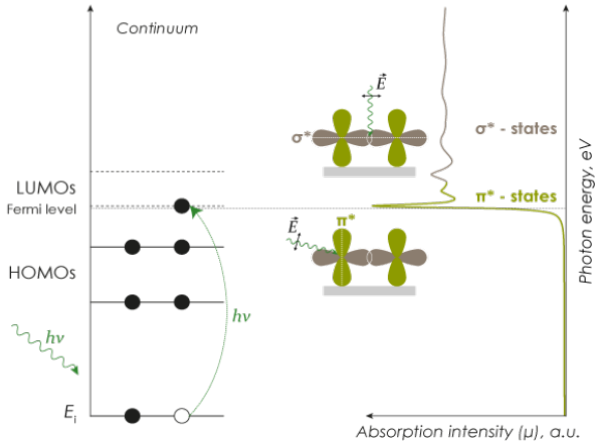

Figure 1.9: *Schematic representation of the X-ray absorption process. The left panel depicts the photo excitation of an electron into unoccupied molecular orbitals. The right panel shows the X-ray absorption spectrum as a function of excitation photon energy. It can be divided into sharp π^* and broad σ^* resonances.*

is usually performed at synchrotron radiation facilities, where we can tune the energy of x-rays towards the resonance condition. At the resonance, the electron from the core level is excited to the unoccupied states at the Fermi level. The resonance energy is given exactly by the binding energy of electron in the atom Fig.1.9. The excited electron follows the dipole selection rule ($\Delta = 1$) which means that an electron from s orbital can only be excited to p orbital, electron from p orbital to d or s, and so on . It is also possible, that an electron is transferred such that $\Delta l = 2$ is fulfilled (e.g. second order process), however, the cross-section of these processes is very small – less than 1 %. Specific transition has its own labeling, e.g. transition of an electron from 1s orbital to Fermi level is denotedas K-edge transition, and transition from 2s level – as L_1edge. Excitation of electrons from 2p orbital as $L_{3,2}$-edge transition. And it is worth to notice here, that two different subscripts at L edge corresponds to spin-orbit splitting of the final states.

An x-ray absorption spectrum is generally divided into 4 methods: *pre-edge* ($E < E_0$); *x-ray absorption near edge structure* (XANES), where the energy of the incident x-ray beam is $E = E_0 \pm 10$ eV; *near edge x-ray absorption fine structure* (NEXAFS), in the region between 10 eV up to 50 eV above the edge; and *extended x-ray absorption fine structure* (EXAFS), which starts approximately from 50 eV and continues up to 1000 eV above the edge. The minor features in the pre-edge region are usually due to the electron transitions from the core level to the higher unfilled or half-filled orbitals (e.g, $s \rightarrow p$, or $p \rightarrow d$). In the XANES region, transitions of core electrons to non-bound levels with close energy occur. Because of the high probability of such transition, a sudden raise of absorption is observed. In NEXAFS, the ejected photoelectrons have low kinetic energy ($E\text{-}E_0$ is small) and experience strong multiple scattering by the first and even higher coordinating shells. In the EXAFS region, the photoelectrons have high kinetic energy ($E–E_0$ is large), and single scattering by the nearest neighbouring

atoms normally dominates.

1.4.7 X-Ray Magnetic Circular Dichroism

In optics, the term *"dichroism"* refers to changes in the absorption of polarized light on passing through a material in two different directions. Since materials typically absorb one color of white light preferentially, the material appears with two different colors for the two light directions - it is *di-* – two- *chroic* – colored. Today, the term *dichroism* is used more generally to reflect the dependence of photon absorption of a material on polarization. The origin of the dichroism effect can be anisotropy in the charge or the spin in the material. XMCD is the difference between two X-ray absorption spectra obtained with circularly polarized X-rays of opposite polarization. XMCD also gives information about the magnetic state of the atoms. Core electrons are excited in the absorption process into empty states above the Fermi energy and thereby probe the electronic and magnetic properties of the empty valence levels. In the following we are concerned with the spectra of the magnetic $3d$ transition metal elements Fe, Co and Ni. Their magnetic properties are largely determined by the $3d$ valence electrons. X-ray absorption spectra are governed by dipole selection rules the d-shell properties are best probed by L-edge absorption studies ($2p$ to $3d$ transitions).

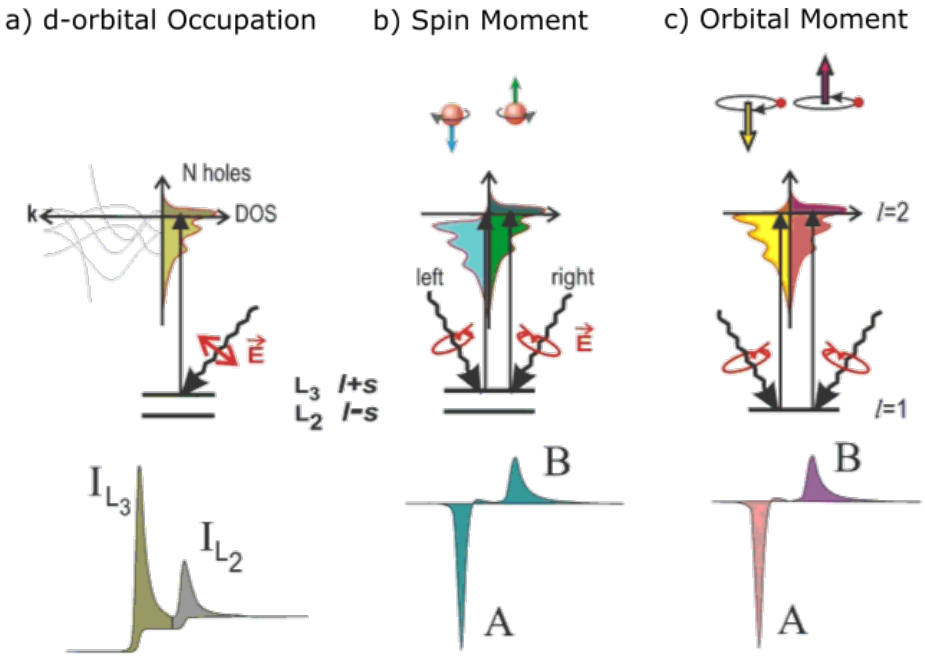

Figure 1.10: *Electronic transitions in conventional L-edge x-ray adsorption* ***a****, and XMCD* ***b,c****, illustrated in one-electron model. The transitions occur from the spin-orbit split 2p core shell to empty conduction band states. In conventional x-ray absorption the total transition intensity of two peaks is proportional to the number of d holes (first sum rule). By use of circularly polarized x-rays the spin moment* ***b*** *and orbital moment****c*** *can be determined from linear combinations of the dichroic difference intensities* ***A*** *and* ***B****, according to other sum rules.*

The L-edge x-ray absorption spectra of the transition metals and oxides are dominated by two main peaks separated by about 15 eV as shown in Fig.1.10. The two main peaks in the spectra arise from the spin orbit interaction of the $2p$ core shell and the total intensity of the peaks is proportional to the number of empty $3d$ valence states. The metal spectra mainly show two broad peaks, reflecting the width of the empty d-bands. The oxide spectra exhibit considerable fine structure, called multiplet structure.

The concept of XMCD spectroscopy, pioneered by Gisela Schütz *et al.* in 1987 [63], are illustrated in Fig. 1.10. The first x-ray absorption sum rule links the total intensity of the L_3 and L_2 resonances with the number N of empty d states (holes). The d valence shell can hold up to 10 electrons which are filled into band states up to the Fermi level and the number of filled states is therefore 10 – N. For a magnetic material the d shell has a spin moment which is given by the imbalance of *spin-up* and *spin-down* electrons or equivalently by the imbalance of *spin-up* and *spin-down* holes. In order to measure the difference in the number of d holes with up and down spin, we need to make the x-ray absorption process spin dependent. This is done by use of right or left circularly polarized photons which transfer their angular momentum to the excited photoelectron.

The photoelectron carries the transferred angular momentum as a spin or an angular momentum, or both (Stohr & Wu) [63]. If the photoelectron originates from a spin-orbit split level, e.g. the $p_{3/2}$ level (L_3 edge), the angular momentum of the photon can be transferred in part to the spin through the spin-orbit coupling. Right circular photons (RCP) transfer the opposite momentum to the electron, left circular photons (LCP) photons, and hence photoelectrons with opposite spins are created in the two cases. Since the $p_{3/2}$ (L_3) and $p_{1/2}$ (L_2) levels have opposite spin-orbit coupling, the spin polarization will be opposite at the two edges. In the absorption process, *"spin-up"* and *"spin-down"* are defined relative to the photon helicity or photon spin.

Since spin flips are forbidden in electric dipole transitions, spin-up (spin-down) photoelectrons from the p core shell can only be excited into spin-up (spin-down) d hole states. Hence the spin-split valence shell acts as a detector for the spin of the excited photoelectron and the transition intensity is simply proportional to the number of empty d states of a given spin. When the photon spin and the magnetization directions are perpendicular the resonance intensities at the L_3 and L_2 edges lie between those obtained for parallel and anti-parallel alignments.

The L_3 and L_2 resonance intensities and their differences for parallel and anti-parallel orientation of photon spin and magnetization directions are quantitatively related by sum rules to the number of d holes and the size of the spin and orbital magnetic moments. Angle dependent measurements in external magnetic fields give the anisotropies of the spin density and orbital moment [64].

1.4.8 Experimental setup for PES

All XPS experiments presented in this thesis have been performed in the Surface Science Laboratory at Paul Scherrer Institute (Villigen, Switzerland). The spectrometer includes a hemispherical analyzer and monochromatic X-ray source (Al Kα excitation,

hν = 1486,6 eV) for core-level spectroscopy. The electron BE calibration was done by setting up the Au $4f_{7/2}$ peak of a gold sample to 84.0 eV. The typical resolution of the system is FWHM = 0.25 eV at 20 eV pass energy.

ARPES measurements which are presented in the Chapter 4 and Chapter 3 were performed on a lab-based experimental setup equipped with a display type hemispherical analyzer *Phobios 150* with an energy/angle resolution of 40 mV/ 0.1 ° and non-monochromatized He source. Being the reported states so close to the Fermi energy, we had only contribution from the HeIα (21.22 eV) photon energy. All the present data were recorded at room temperature.

ARPES and PhD measurements which are presented in Chapter 2.1 and Chapter 5 were performed at the PEARL beamline at Swiss Light Source, PSI (Villigen, Switzerland) [65]. Essentially, beamline covers the photon energy range from 60 to 2000 eV. Experimental station is divided into three sub-systems: one (attached to the beamline) for the photoemission measurements, one for LT STM and one for *in situ* sample preparations. The photoemission station is designed as a state-of-the-art ARPES facility with a *Carving 2.0* six-axis manipulator and *Scienta EW 4000* hemispherical electron analyzer with two-dimensional detection. The entrance slit of the analyzer is oriented vertically (parallel to the main axis of rotation), in this operation, the symmetry of the differential photoemission cross section with the respect to the light polarization allows for a homogeneous illumination of the detector.

Magnetic measurements exploiting XAS and XMCD spectra presented in Chapter 5 and Chapter 6 were performed at the XTREME beamline, SLS located at PSI. XTREME beamline is equipped with one Apple II type undulator producing linearly and circularly polarized photons with maximum flux of 4.7×10^{12} photons/second. Optics of the beamline allows working in wide energy range from 150 eV up to 2000 eV, what corresponds to the 31^{st} harmonics. Experimental chamber at the beamline is equipped with pumped Helium cryostat, which allows measurements at T = 2 K. Experimental chamber is equipped with a vector magnet, which can produce magnetic field of strength 7 T along the beam direction or field of 2 T in the direction perpendicular to the beam in the plane of the synchrotron ring. Spectra measured at XTREME beamline were acquired in TEY mode and normalized to the flux intensity of the incoming beam [64].

1.5 Surface Analysis III. Theoretical Methods

In this section are introduced main modeling and theoretical methods that have been used through this thesis, *i.e.* the combined electron plane wave expansion (EPWE) and electron boundary elements method (EBEM), density functional theory (DFT). Note, that these calculations have been performed by close collaboration with theoretical groups.

1.5.1 Electron Boundary Elements Method and Electron Plane Wave Expansion method for Periodic Systems

The combined EPWE and EBEM [66, 28] have been developed by Prof. Dr. García de Abajo and represents a scalar variant of the electromagnetic PWE/BEM extensively used for solving Maxwell's equations and optical response for arbitrary shapes. It is based on Green's functions for finite geometries and electron plane wave expansion for periodic systems. For the band structure calculations, the particle-in-a-box model is extended to infinite 2D systems by defining an elementary cell and using periodic boundary conditions. Within the EPWE code, solutions of the Schrödinger equation are represented as a linear combination of plane waves and a satisfactory convergence is achieved with a basis set consisting of ~ 100 waves [28].

In the following, the EBEM/EPWE simulation procedure is explained step by step: for the simulations the first step is to parametrise the geometrical structure of the networks that will mimic the potential barriers that scatter the 2DEG. The complexity of the geometries can be simplified since the molecular electrostatic clouds, that are responsible for the potential barriers, are generally very smooth and relatively featureless. We choose the width and length of the straight beads to match the molecular width and the network dimensions. Note that this step of considering the scattering barrier geometry (length and width) as accurate as possible to the STM observations of the backbone dimensions is of key importance for a successful matching and understanding of confinement and coupling effects in such nanoporous systems. After this parametrisation, the V_{eff} and m^* parameters are iterated to fit the experimental data. With V_{eff} the scattering of the surface state with the molecular barriers is defined and both the band bottom ($\overline{\Gamma}$ point in ARPES and onset of bonding state in STS) and opening of the gaps are quantitatively determined. The effective mass parameter is inversely proportional to the dispersion of the band so the curvature, i.e. the top of the band is obtained. Note that changes in m^* do not alter significantly the energetic position of the band bottom of the first confined state (but it affects on the energetic position of the lower edge of the $\overline{M}$ point gap.

In this thesis the local electronic properties of nanoporous network such as LDOS for empty and filled environment were performed by using this method in collaboration with Dr. Ignacio Piquero-Zulaica (former Centro de Fisica de Materials, San Sebastian, Spain, now TU Munich, Germany) and Dr. Zakaria M. Abd El-Fattah (Al-Azhar University, Cairo, Egypt and ICFO-Institut de Ciencies Fotoniques, The Barcelona Institute of Science and Technology, Barcelona, Spain)

1.5.2 Density Functional Theory

The quantum mechanical wavefunction contains, in principle, all the information about a given system. For the case of a simple 2-D square potential or even a hydrogen atom we can solve the Schrödinger equation exactly in order to get the wavefunction of the system. We can then determine the allowed energy states of the syatem. Unfortunately

it is impossible to solve the Schrödinger equation for a N-body system. Evidently, we must include some approximations to render the problem soluble albeit tricky. In general, DFT is a method of obtaining an approximate solution to the Shroedinger equation of a many-body system. Whereas the many-body electronic wavefunction is a function of 3N variables (the coordinates of all N atoms in the system) the electron density is only a function of x, y, z – only three variables. In the context of computational materials science, *ab initio* (from first principles) DFT calculations allow the prediction and calculation of material behaviour on the basis of quantum mechanical considerations, without requiring higher order parameters such as fundamental material properties. In contemporary DFT techniques the electronic structure is evaluated using a potential acting on the system's electrons. This DFT potential is constructed as the sum of external potentials V_{ext}, which is determined solely by the structure and the elemental composition of the system, and an effective potential V_{eff}, which represents interelectronic interactions. Thus, a problem for a representative supercell of a material with n electrons can be studied as a set of n one-electron Schrödinger-like equations, which are also known as Kohn–Sham equations.

All DFT calculations presented in this thesis were performed in collaboration with Dr. Jorge Iribas Cerda (Instituto de Ciencia de Materiales de Madrid, Madrid, Spain) and Dr. Jonas Björk (Linköping University, Sweden).

2

A two-dimensional porphyrin based porous network assembled due to the electrostatic repulsion

Spontaneous self-assembled monolayers of organic-conjugated transition metal complexes on surfaces is a focus towards future device engineering and basic science. Huge amount of literature reports related to the first monolayer, reorganization and self-assembling processes are available in the scientific literature. This fact is contributed to the generally accepted opinion that structural and chemical properties of the first monolayer are the key parameters for controlled thin film growth. Metallo-supramolecular engineering on surfaces provides a powerful strategy towards low-dimensional coordination architectures with prospects for several application fields. Optical and magneto-electronic properties are intimately connected, and the accurate determination of electronic levels, excitation, and relaxation dynamics is mandatory for the optimization of electronic, photovoltaic, and opto-electronic devices. This chapter shows, that highly ordered two-dimensional network architecture can be obtained by self-assembly of octaethylporphyrines with selected metal center. Such molecular network emerge from the site-specific interactions between the central transition-metal ions of the building blocks and properties of the underlying substrate.

2.1 Introduction and motivation

Synthetic porphyrins and phthalocyanines are used in the phototherapy of cancer and in solar cells, through virtue of their unique photo-physical properties, and are versatile building blocks for the realization of molecular materials which exhibit various light-driven chemical reactions. In recent years, adsorbed coordination compounds have attracted considerable attention with respect to the controlled functionalization of the surfaces on the nanoscale. A multitechnique approach is necessary to extract and enlighten the interrelation between structural and electronic properties [67]. The fundamental understanding of molecular solid properties and the controlled ordering processes of organic architectures received paramount interest for their promising appli-

cations. The level of efforts placed on the study of transition metal complexes and their single layers on surfaces has grown steadily in last few decades [68]. Deposition of the large molecules onto surfaces leads to a high variety of possible interactions. In particular, apolar and neutral molecules are not expected to build up long-range interaction potentials, if they are not mediated by the underlying substrate, and in the most cases, attractive dispersion forces lead to nucleation in 2D or 3D condensates [69]. The bond strength spreads from very weak van der Waals interactions to non covalent or strong chemical bonding. Even in a weak-bonded molecular layers [70], the simple change of symmetry induced by adsorption and the induced dipoles can lead to modification of the molecular and metallic states, affecting the electronic structure at the interface [71, 72, 73, 74, 75]. To acquire the ability to design materials with selected properties requires a deep understanding of the proper molecular precursors characteristics used as building blocks and of the modifications induced when deposited in thin films. Important examples are supramolecular, two-dimensional metal-organic coordination networks [5] and planar metal complexes such as metalloporphyrins and metallophthalocyanines [76, 77, 78]. Quite often, applications require the organization of the metal complexes on a solid interface, whereby the interaction between the coordinated metal ion and the underlying surface can drastically affect the functional properties of the complexes themselves. The coordination networks are generally synthesized by *in situ* approach, which employs co-deposition of the metal and the ligand onto the surface [23, 79]. Normally, thin films of metalloporphyrins and phthalocyanines can often be prepared by *ex situ* metalation of the metal-free based macrocycle and subsequent vapor deposition of the intact complexes. Molecular crystalline materials can be altered by manipulating spin, electron transfer, proton transfer, molecular structure, and orientation, leading to dynamical switchable properties by external stimuli such as light, electric field, and temperature [80]. The precise control of the switching properties is the focus of recent frontier developments. For single layer, the dynamics study is still to be systematically understood due to the experimental difficulties. In the adsorbed state, the interacting atom from underlying substrate can occupy one of the axial sites and, as an additional ligand, influence the electronic structure of the metal center, which can bring to completely different resulting architecture formation, what will be discussed in the following paragraph. The weak lateral forces applied by surface upon physiosorption of the molecules and the charge transfer from the supporting substrate, allow the weak intermolecular forces in combination with electronic structure of the metal center to play a significant role in the formation of long-range order in the adsorbed phase. In the following paragraph it is shown that porphyrin based porous network can be self-assembled due to the dipole-dipole interaction mediated by strong site-specific interaction between metal ion and underlying substrate, combined with charge transfer, van der Waals interactions and electrostatic repulsion.

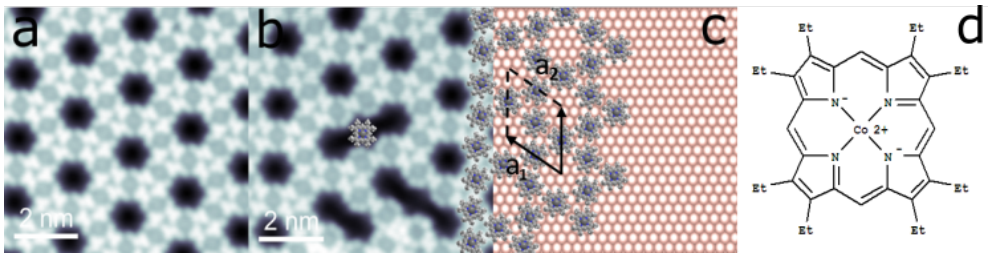

Figure 2.1: *STM topographic images of* ***a*** *self-assembled porphyrin based network on Cu(111) substrate.* ***b*** *same network with defects,* ***c*** *proposed model of the formed network. (STM details: 10×10 nm, 400 mV, 10 pA) and* ***d*** *chemical structure of the used CoOEP molecule.*

2.2 Results and Discussion

Transition metal complex at the noble surfaces

The adsorption of cobalt (II) octaethylporphyrin (CoOEP) on noble Cu(111) substrate was investigated by combination of STM, STS, XPS and ARPES, in order to achieve detailed mechanistic understanding of the surface chemical bond of coordinated metal ions. Previous studies of the related systems, especially cobalt (II) tetraphenylporphyrin (CoTPP) on Ag(111) [74] and CoOEP on Ag(111) and Au(111) substrates [74, 75], have revealed adsorption-induced changes of the oxidation state of the Co ion. These effects were attributed to a covalent interaction of the Co ion with the underlying substrate. However, recent studies showed that the porphyrin macrocycle of the adsorbed CoTPP undergoes a pronounced saddle-shape distortion, which could alter the electronic structure and provide an alternative explanation for the new valence state previously attributed to the formation of a surface coordinative bond [81]. In this work, was used Cobalt (II) Octaethylporphyrin molecules to fabricate 2D periodic array of coupled quantum dots, studied the manner of formation and influence of the underlying surface onto resulting architecture. The molecular layer was prepared by vapor deposition of the CoOEP molecules at ∼200°C onto the the atomically clean surface. The STM topography image in Fig.2.1 shows the formation of the porphyrin based porous network on Cu(111) substrate. Van der Waals repulsion between ethyl legs involving three molecules, as a result, each molecule repel with four neighbors, and all ethyl end groups are engaged in noncovalent bonding for the porous network structure. Here, the six-fold symmetry of the Cu(111) surface leads to the observed hexagonal pattern. STM was acquired in constant current mode with a bias voltage 400 mV and current 10 pA. At the given tunneling conditions, individual ethyl groups of the molecule are easily distinguishable from the Co ion, since they appear like protrusions. This contrast stems from an enhanced tunneling contribution of the HOMO and LUMO states of the molecule. At lower coverage CoOEP molecules spread out all over surface without creating any periodic pattern, which indicates repulsive behavior. The macrocycle adopts a moderate symmetric "crown" shape conformation, with all eight ethyl legs pointing up [82]. At higher coverages, extended domains of highly

regular hexagonal supramolecular porous networks were observed. We attribute this observation to the fact, that molecules don't form closed packed structure due to the repulsion between the ethyl groups Fig.2.1. The coverage-dependent intermolecular potential wells forming the molecular superlattices are combined with long-range interactions driven by the electrostatic repulsion between molecules. This suggests that local charges at the interface induced upon chemisorption cannot be fastly investigated in metalic surfaces. The self-assembled layer forms a hexagonal porous network with a lattice constant Fig.2.1 of 2.47 ± 0.05 nm, and the distance between Co ions 1.41 ± 0.05 nm, which is the typical arrangement for various porphyrin based networks. The molecular self-assembly here is likely to be driven by both van der Waals interactions and dipole-dipole interactions between metal ions and underlying surface. Evidently, the self-assembled molecular structures adapt to the available surface symmetry.

Identification of the reversible switching of the electronic interaction between Co ion and Cu surface

Vapor deposition of CoOEP molecules onto Cu(111) substrate at room temperature results in the formation of periodic porous molecular network, observed by means of STM (Fig.2.1). In order to investigate the nature of the resulting architecture, was probed chemical environment of C, N and Co for monolayer and multilayer coverage at the Cu(111) substrate by means of XPS. Interestingly, the Co $2p_{3/2}$ peak position for the Co ion in monolayer is 778.3 eV, which is closer to the position of a Co^0 species than to original Co^{2+}, although the nominal oxidation state of Co ion in CoOEP molecule is two. Comparison with Co $2p_{3/2}$ multilayer spectra, in which main peak is located at typical Co^{2+} position of 780 eV, suggests that this shift to lower binding energies is related to an electronic interaction of the Co ion with underlying Cu(111) substrate. The local interaction character between Co and Cu atoms implies substantial bonding strength and a large charge transfer between ion and surface. The charge transfer is expressed by a partial decrease of the electron density in the whole molecular plane. The result is a neutral state of the molecule. Also the charge transfer at the interface has a crucial influence on the magnetization of the CoOEP molecules. As it will be shown in Chapter 5 by means of XMCD measurements Fig.5.4(a), in the case of CoOEP on Cu(111) substrate the magnetization of the adsorbed molecules vanishes because of the absence of exchange field. Indeed the $3d$ orbitals of Cu are filled and only the $4s$ electrons interact with the molecule and screen the Co spin moment. Using x-rays of variable wavelength on the other hand, gives us opportunity to measure probabilities of transition from core levels to Fermi level given by absorption of x-rays when energy of photon matches that of given transition, ie. X-ray Absorption Spectroscopy. Both XPS and XAS surface sensitive techniques provide information about chemical composition of the material and valence state of the probed element. Notably, both XPS and XAS spectroscopies are capable of unraveling magnetic properties of probed systems when they are combined with usage of circularly polarized light.

Further investigation with XPS proved that the oxidation state of the Co ion is strongly influenced by Cu(111) substrate. The Co $2p_{3/2}$ core level exhibits a more

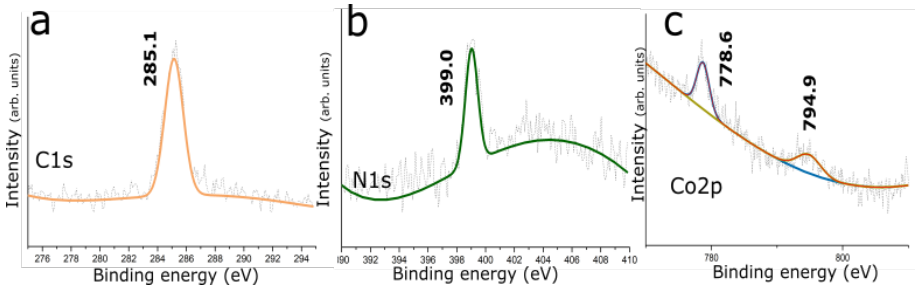

Figure 2.2: *The XPS data for single ML of CoOEP deposited onto Cu(111) substrate.* ***a*** *C1s spectra,* ***b*** *N1s spectra and* ***c*** *Co2p spectra.*

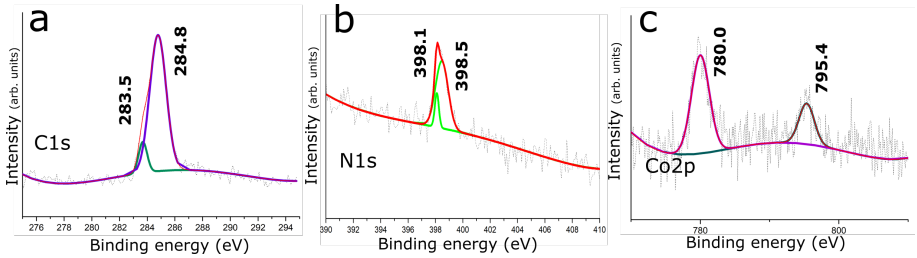

Figure 2.3: *The XPS data for multilayer of CoOEP deposited onto Cu(111) substrate.* ***a*** *C1s spectra,* ***b*** *N1s spectra and* ***c*** *Co2p spectra.*

complex line shape associated with the multiplet structure resulting from the open-shell character of the Co ion and is consistent with the earlier reports on similar porphyrins In the CoOEP multilayer, the Co 2p main peak appears at the typical Co^{2+} position – 780.0 eV and satellite at the higher BE, in agreement with the formal oxidation state of the ion. The satellite structure has been attributed to the open-shell character of the Co^{2+} ion with its d^7 electron configuration [83]. In the monolayer spectra, however, the Co 2p binding energy is lowered by 1.4 eV and the signal is thus shifted to a typical Co^0 position. This shift is much larger than the corresponding shifts of the C 1s and N 1s signals (0.1 and 0.5 eV), indicating that the Cu surface interacts more strongly with the Co ion than with other parts of the molecule. Considering possible initial state contributions, the reduced Co 2p BE suggests an increase of electron density at the Co ion, i.e. a partial reduction. To explain these findings, it was proposed that semi-occupied or vacant Co 3d orbitals (most likely the Co $3d_{z2}$) that extends in the axial direction overlap with electronic states of matching energy and symmetry of the Cu surface, resulting in the formation of new mixed states below E_{Fermi} [74, 81]. These states take up electrons from the Fermi sea of the Cu(111) surface. Therefore, this model provides a consistent explanation for the transfer of electron density from the substrate to the Co ion.

Electronic properties of the on-surface architecture at Cu(111)

On-surface architectures, like individual adsorbates (as in details described in Chapter 3) generally scatter electrons of the Shockley surface state. The areas enclosed

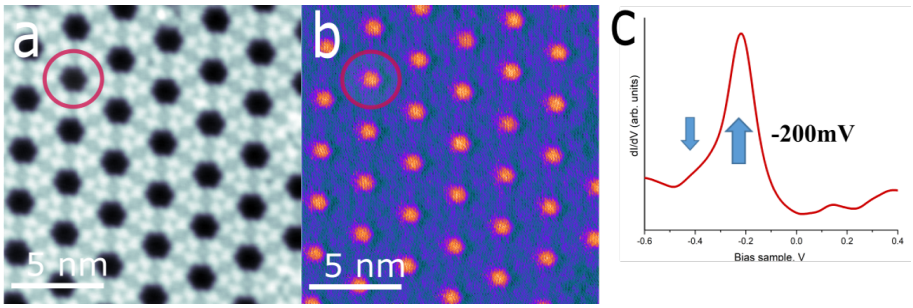

Figure 2.4: *Study of the electronic confinement of the surface state within the pores of the formed network corresponding to the array of 0D quantum dots.* ***a*** *STM topograph of the porous network 15×15 nm, 200 mV, 50 pA and* ***b*** *simultaneously recorded dI/dV map (lock-in: V_{rms}=16 mV, f=514 Hz).* ***c*** *STS spectra recorded in the middle of the pore and exhibits the presence of the confined state.*

by on-surface structures provide confinements which can in many cases, be viewed as quantum dots (QD) [14, 13, 36, 84]. The strength of such confinement depends on the arrangement of the neighboring units as well as on the confining barrier properties, especially on the interaction between the adsorbates and the surface states. For example, lately it has been demonstrated by the comparison of the confinement strength in quantum systems featuring the same arrangement, but being constructed from slightly different building blocks. The fabricated 2D periodic array of quantum units was designed by CoOEP building blocks self-assembled into a porous network utilizing strong van electrostatic strain. The first example of the confinement of the Shockley surface state by a honeycomb network prepared by molecular self-assembly was demonstrated by Lobo-Checa *et al.* [14]. Similar to DPDI network, CoOEP network also can confine the Shockley state. 2D dI/dV map simultaneously recorded with STM image Fig.2.4 and STS spectra acquired in the center of the pore revealed a new occupied electronic state at -200 mV, while typical spectra at the bare Cu substrate is characteristic -400 mV [85]. 2D dI/dV recorded at the energy of the newly founded electronic state showed that confinement is localized in the pores of the created network.

Complementary ARPES data taken for full monolayer of CoOEP network covering Cu(111) substrate Fig.2.5 showed the appearance of the new weakly dispersing electronic band below Fermi level. The bottom of the dispersive band was observed at -0.325 meV, which is in agreement with dI/dV spectra which has similar asymmetric shoulder at the same energy. The existence of a weakly dispersing band can be explained by the coupling of the neighboring quantum dot states enabled through the lossy scattering of the confined electrons at the boundaries of the pores. Similar forward scattering has been reported for 3deh-DPDI network.

Furthermore, we were not able to resolve any signature of a Kondo resonance on the CoOEP molecule by scanning tunneling spectroscopy experiments conducted with a metallic tip at the Cu(111) substrate. Observation of a Kondo signal is possible when the unpaired electron of the magnetic adsorbate is neither too weakly nor too strongly coupled to the substrate electron bath [86]. In our case, the CoOEP molecules adsorbed at the Au(111) substrate has shown magnetic signal, and a spin density clearly localized

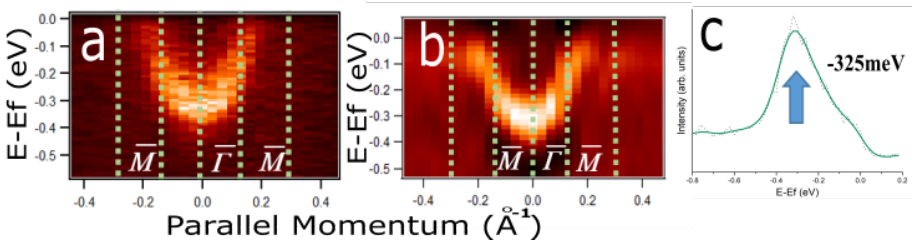

Figure 2.5: *Band dispersion resulting from the periodic influence of the porous network on the surface state studied with ARPES* ***a*** *raw data,* ***b*** *second derivative and* ***c*** *Normal emission spectra at 77 K showing the confined state, while the bottom of the surface state band was observed at -325 mV.*

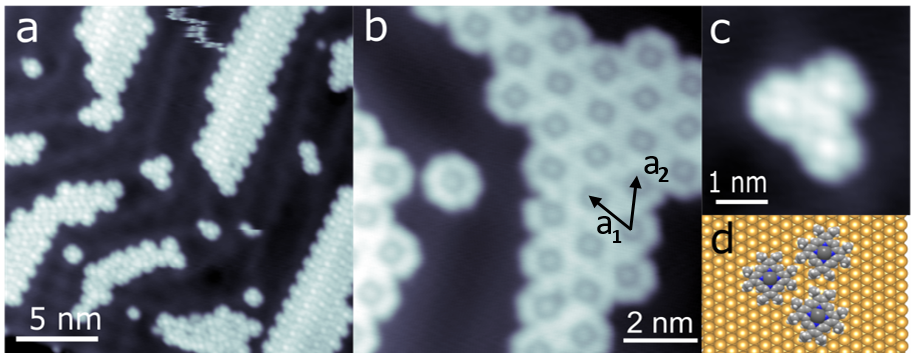

Figure 2.6: *The STM overview of the closed pack self-assembly formed by CoOEP molecules across the Au(111) substrate.*

on the half-filled $3d_{z2}$ orbital of the Co atom. However, upon adsorption, the $3d_{z2}$ orbital of the Co atom interacts strongly with the Cu(111) substrate leading to a complete quenching of the magnetic moment of the CoOEP. This assertion is in line with the previous studies that also report an absence of the magnetic properties of the molecule upon adsorption [81].

CoOEP at the Au(111) surface

To test, which influence has the underlying surface onto network formation, was performed an experiment with Au(111) substrate. Notably, CoOEP was found self-assembled into the closed packed structure Fig.2.6. The positions of the BE energy for Co2*p* XPS spectra in Fig.2.7 for monolayer (Fig.2.7a) and multilayer (Fig.2.7b) are the same. This means, that there is no charge transfer from metal ion to the underlying substrate in the case of Au supporting substrate. Also measured dI/dV spectra above the metal ion of the CoOEP molecule shows Kondo resonance. Obtained results confirm that role of the underlying substrate in this study is important for patterning metal surfaces with porous molecular networks a uniform change of the electronic surface properties.

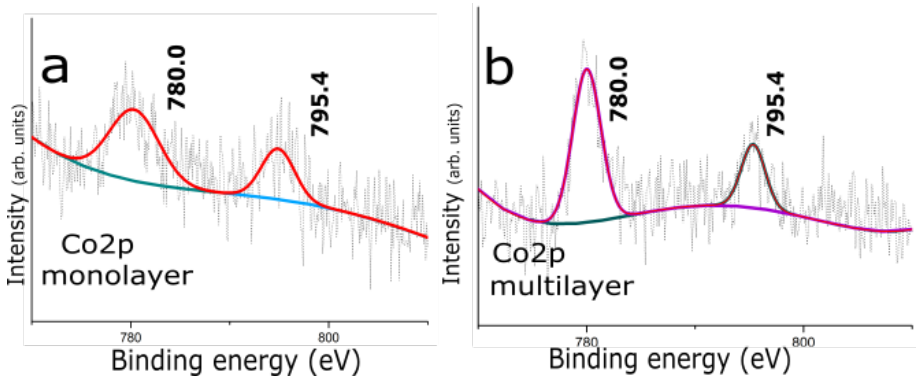

Figure 2.7: *XPS spectra of Co2p for* ***a*** *monolayer and* ***b*** *multilayer of CoOEP deposited onto Au(111) surface.*

2.3 Details of the experimental methods

Preparation procedures for all experiments were carried out at UHV conditions with the base pressure 3×10^{-10} mbar. The Cu substrate was prepared by repeated cycles of sputtering with Ar^+ ions at energy ∼2 keV, ion current ∼10 μA, and annealing to 450°C in order to achieve atomically clean and flat substrate with extended terraces. The purity of the substrate was verified by XPS and STM. The molecules were thermally sublimed from commercial nine cell evaporator (Kentax GmBH). The deposition rates were recorded by a quartz-crystal micro balance. The STM measurements were performed at helium temperatures with use of the Omicron LT-STM. The bias voltage in presented data is shown with respect to the sample, i.e. negative voltage corresponds to the occupied states of the sample. The STM micrographs were recorded in the constant current mode. The STS measurements were performed with a lock-in amplifier frequency of 514 Hz and V_{rms}=8 mV (zero-to-peak value). The condition of the tip was verified before and after acquisition of the STS spectrum by recording dI/dV spectra on the bare surface. XPS measurements were performed at RT with monochromatic Al-Kα X-Ray source. The resolution reaches a value ∼0.1 eV of full width half maximum (FWHM). The calibration of the energies was performed via reference measurements of a clean Au(111) crystal (Au $4f_{7/2}$=84.0 eV). The C1s and N1s and Co2p spectra were fitted with Gaussian profiles.

2.4 Conclusions

The binding energy of the Co $2p_{3/2}$ core-level peak was found to be 778.6 eV, which is more compatible with a Co^0 oxidation state (778.1 eV for Co metal [74]) than with the nominal oxidation state of +2 (780.0 eV for Co–TPP multilayer on silver [74]). This results from the pronounced different electronic environment between these systems (metal, molecular multilayer, and molecular monolayer on a metal). It can be mostly explained by the differing abilities of each system to screen the core hole left by the photoemission process and is consequently a final state effect, as observed on numerous

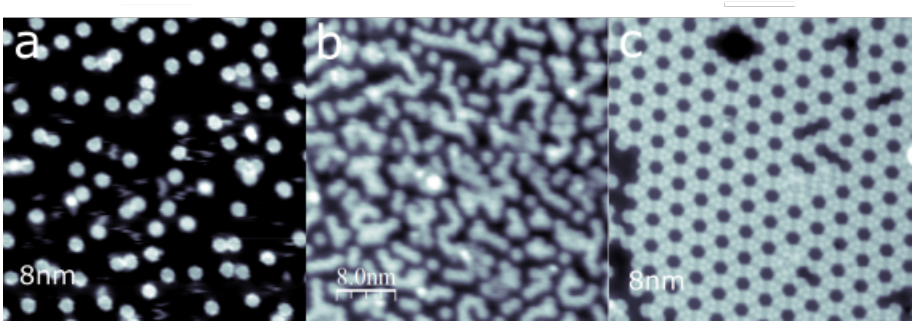

Figure 2.8: *The STM topography for different coverage dependent CoOEP network formation* ***a*** *0.1 ML – molecules are randomly distributed.* ***b*** *0.5 ML coverage and* ***c*** *formed network at 0.75 ML coverage.*

porphine-based species on various substrates. Such final states effects on the binding energy can dominate over the contribution from charge transfer. This is a strong reminder of the dangers to assigning an oxidation state by simple inspection of the binding energy. The significant overlap between the orbitals of the Co ions and the underlying substrate, implied by the charge transfer, suggests that the primary local interaction between the substrate and the molecule is through the Co atom. Thus, its adsorption height markedly below the macrocycle. It is therefore likely that the Co–P would exhibit a significant surface trans-effect [87, 88, 67, 89, 90]. For the Cu substrate, the magnetization of the Co ion of CoOEP is destroyed by the influence of the paramagnetic surface. The substrate 4*s* electrons magnetically screen the spin of Co atom. Like in Kondo physics, the interaction between the localized spin of Co and the itinerant spins of the substrate results on the zero spin state. Also it was shown, that due to the van der Waals strain and strong dipole-dipole interaction between Co ion and underlying surface we can easily achieve extended periodic porous network. The coupling of the confined states enabled through so-called lossy scattering resulted in the formation of the 2D band structure. This means, that by pattering metal surfaces with porous molecular networks a uniform change of the electronic surface properties may be achieved.

3

Effective determination of surface potential landscapes from metal-organic nanoporous overlayers

The results presented in the following chapter have been published in the New Journal of Physics. Figures are adopted with permission of co-authors [112].

The controlled adjustment of material's properties by modification on the atomic scale is a major goal of surface science. On the closed-packed faces of noble metals the surface-state electrons are well suited to monitor and influence the properties of the surface. Determining the scattering potential landscape for 2D molecular architectures provides a way to understanding fundamental quantum electron phenomena. 2D arrays of electronically coupled Quantum Dots fabricated on metallic surfaces, obtained via molecular self-assemblies, assure ultimate precision of each confining unit and long-range order. In particular, quantum states have always been related to a modification of the native surface states of the substrate material. In this chapter we study the effective determination of the surface states formed in a metal-organic nanoporous array. By combining several surface sensitive techniques together with the Electron Plane Wave Expansion (EPWE) simulations on metal-organic porous architecture grown at Cu(111) substrate, we demonstrate here the parametrization of the surface state environment.

3.1 Introduction and Motivation

Since organic molecules scatter surface electron waves, the extended regular structures that can be produced with molecular self-assembly allow the tunning of electronic properties not only locally, but surface wide [13]. With the reflectivity for the electron waves being finite, the leakage-induced electronic coupling between neighboring quantum dots results in dispersive bands [91]. The modeling of electron scattering by 2D arrays of organic and metal-organic nanoporous networks is often performed using EBEM/EPWE, which accounts for the local scattering response [28, 13, 5] and the

electronic band structures resulted from the Bloch-wave states generated from interdot coupling [14, 24, 92]. However, it is a semi empirical method, so some assumptions need to be made regarding the potential barrier strength, repulsive/attractive interaction and geometries, which often lead to arbitrary or non physical conditions. In particular, earlier published works use smaller molecular backbones than the actual molecular building blocks [13, 28] altered effective pore sizes [13, 92], attractive scattering potential regions at the metal sites in metal-organic systems [13, 28, 5] or effective masses m^* than the 2DEG reference [5, 24]. The main issue here is if such assumptions are necessary when simulating the electron confinement by 2D nanoporous networks. By studying in depth the interaction between the 3deh-DPDI nanoporous network [5, 24, 14, 31, 93, 33, 36, 94] and the Shockley state of Cu(111), we show that the parametrization of the surface potential landscape in metal-organic networks is often inaccurately modeled leading to incorrect scattering potentials. Based on a combination of STM/STS, ARPES in combination with EBEM/EPWE simulations, was demonstrated that both local confinement effects and interdot coupling induced electronic bands can be reproduced. This is achieved by starting from a realistic scattering geometry and then assigning repulsive scattering potentials to its barriers for both compounds of the network – molecules and coordinating adatoms. However, we require a 2DEG re-normalization that affects the effective mass m^* and energy reference (E_{ref}). Explanation for these changes is assigned to the alteration of the vacuum region upon network presence, which is known to partly define the Shockley state [95, 96]. This experimental-theory synergy enables us to capture the intricacies of the scattering potential landscape, and to reveal systematic modeling procedures.

Note that KPFM measurements used in this study have been performed by Dr. Shigeki Kawai from MANA/NIMS (Tsukuba, Japan), ARPES by Dr. Ignacio Piquero-Zulaica from CFM-CSIC (San Sebastian, Spain) EBEM/EPWE simulations by Dr. Zakaria M. Abd El-Fattah from Al-Azhar University (Egypt) and Dr. Ignacio Piquero-Zulaica (now TU Munich, Germany).

3.2 Results and Discussion

Assembly and properties of porous network

Chemistry and supramolecular chemistry at the surfaces [97, 98, 77, 99] have benefited significantly from high resolution of the STM and AFM micrographs. Supramolecular chemistry and coordination chemistry in general depend on the arrangement of molecules via a combination of predominantly non-covalent bonds. Fully saturated organic molecules in absence of functional groups often form simple patterns[100]. By chemical coordination of building blocks with deposited or thermally ejected adatoms from the substrate, planar Metal Organic Frameworks (pMOF's), on-surface coordination networks, or so called supramolecular networks [14, 25] can be formed. In on-surface chemistry, chemical reactivity also including coordination reactivity has been investigated by choosing the underlying substrate[26]. The role of the underlying surface in

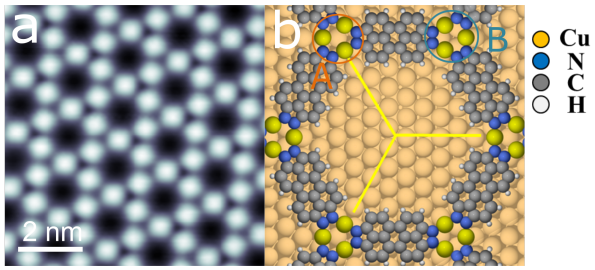

Figure 3.1: 3de-DPDI network on Cu(111). ***a*** *STM image of the long-range ordered metal-organic network. STM details I=10 pA, U=800 mV.* ***b*** *theoretical model of the single pore exhibiting the tree-fold symmetry due to the variations in the registry of the underlying substrate and metal coordination linkers.* ***A*** *and* ***B*** *representing inequivalent nodes of the pore.*

general is two-fold – the substrate is acting like a geometric support for the orientation of the monomers and during the formation of the polymer, and it often modifies reaction pathways and activation barriers in catalyzing the coupling reactions. Adatoms, steps or kinks and other possibly desirable defect sites may take a decisive role here. Notably, there is no report yet about periodic, extended 2D porous structures on non-metallic substrates which may act like host-guest systems for further studying of interactions [28]. Nevertheless, covalent bonded polymers [**?**], and strongly linked coordinated networks are required for the proposed studies at variable temperatures and with strongly adsorbing guest molecules to prevent the collapse of the host network. In on-surface (metal)-organic self-assembly the binding site and the conformation or the chirality of a building block depends very often on the surface molecular interaction as well as on the nearest neighbor interaction between the adsorbates [16, 101, 22].

The porous network that we studied here, is formed by DPDI (4,9 - diaminoperylene quinone-3, 10-diimine), which undergoes triple dehydrogenation process, when thermally sublimed onto Cu(111) and heated to 320°C. Resulting converted building blocks coordinate with ejected from the bulk Cu adatoms, and form long-range well ordered metal-organic nanoporous network [14, 101, 24]. As shown in Fig.3.1, the unit cell is composed of 3 molecules and 3 Cu adatoms and has periodicity of 25.5 Å. The model shown in Fig. 3.1(b) represents the three-fold symmetry of the network, which arises from the different registry of the Cu coordination atoms with respect t the surface: one type of Cu trimer, which forms the node (**A**) positioned above on top site, while the other node (**B**) surrounds a hollow site [101, 23].

Electronic properties of 2D metal-coordinated DPDI network: properties in local and periodic confinement

Periodic 2D arrays of quantum dots are the best probed by the complementary techniques such as STS [33] and ARPES [14, 84]. While STS accesses the *local* electronic structure of the quantum dots, and barriers between them, ARPES probes *cooperative* coherent Bloh waves interactions between the electrons in the array of quantum units. It reveals how the interplay between the electronic wave functions on such units give

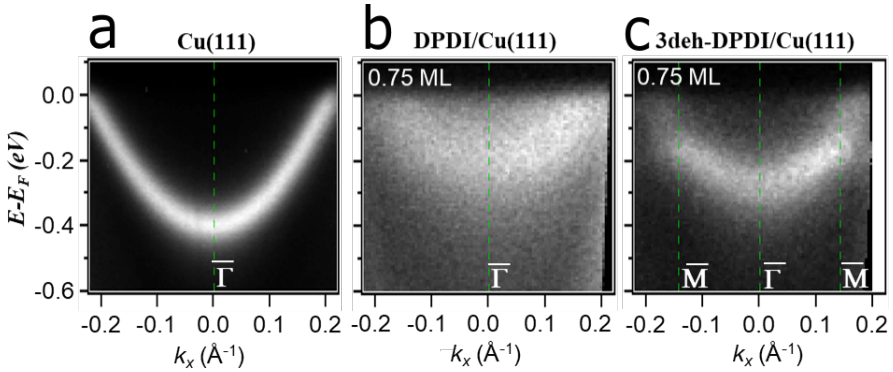

Figure 3.2: Electronic band structure formation of 3deh-DPDI network on Cu(111). ***a*** *Pristine surface state of Cu(111),* ***b*** *0.75 ML of native DPDI and* ***c*** *0.75 ML of 3deh-DPDI molecular network at the Cu(111) substrate. The band structure clearly evolves into shallow dispersive band for the n=1 PLS. Adopted from [112].*

rise to a well-defined band dispersing in energy and momentum, and with a certain effective mass, caries velocity. These properties are of fundamental interest for carrier mobility and ultimately for quantum devices and architectures. The evolution of electronic band formation Fig. 3.2 was characterized by choice of the appropriate molecular coverage before annealing Fig. 3.2b, and after, when highly robust and extended on-surface superstructure is formed [14]. Each pore of the extended network confines the 2DEG of the surface state, that can be described as 0D QD. Because of the imperfect *lossy* confinement, coupling of QD with their surrounding environment results in shallow dispersive electronic bands (Fig. 3.2c). By combining experimental STM/STS data with two simulations (Fig.3.3) obtained using the scattering geometry shown in models **a** and **g** and barrier potentials specified in table 3.1. In Figure 3.3 STM/STS row consists of a topographic image **d**, three *dI/dV* maps at constant height at different energies, which corresponds to first PLS -0.186 eV, 2PLS – 0.016 eV and 0.385 eV 4PLS **e** and four *dI/dV* spectra acquired at relevant positions of the unit cell **f**. All experimental data can be vertically compared to two EBEM/EPWE models: the top reproduces the one in ref.[5] and the bottom is a new one proposed in this work. The scattering geometries shown in **a** and **g** consist of three parts: Cu substrate area – red, molecules – rectangles in purple or light blue, and metal coordination regions – hexagons in green or violet/yellow. The corresponding potential values are indicated in Table 3.1. Experimental parameters: *dI/dV* maps and *dI/dV* spectra obtained from a grid spectroscopy measurement (35×30 points) with initial tip conditions 400 mV/70 pA and lock-in frequency 514 Hz; zero-to-peak amplitude: 8 mV. A smoothing of 30 mV is applied to each *dI/dV* map. The top row in Fig. 3.3 assumes the scattering geometry proposed in ref.[5], which is formed by hexagons at the Cu adatom coordination sites connected by molecular building blocks 5.5 $\AA$ wide. In proposed model the metal adatom regions are dominating spatially over the molecules and weakly resembles in STM topography. Using the 2DEG reference of E_{ref}=-440 mV at 5 K, and m^*=0.44 m_0, was found, that for simulations it was perfect match to represent n=1 PLS *dI/dV* map, but this agreement doesn't work for higher orders. For example,

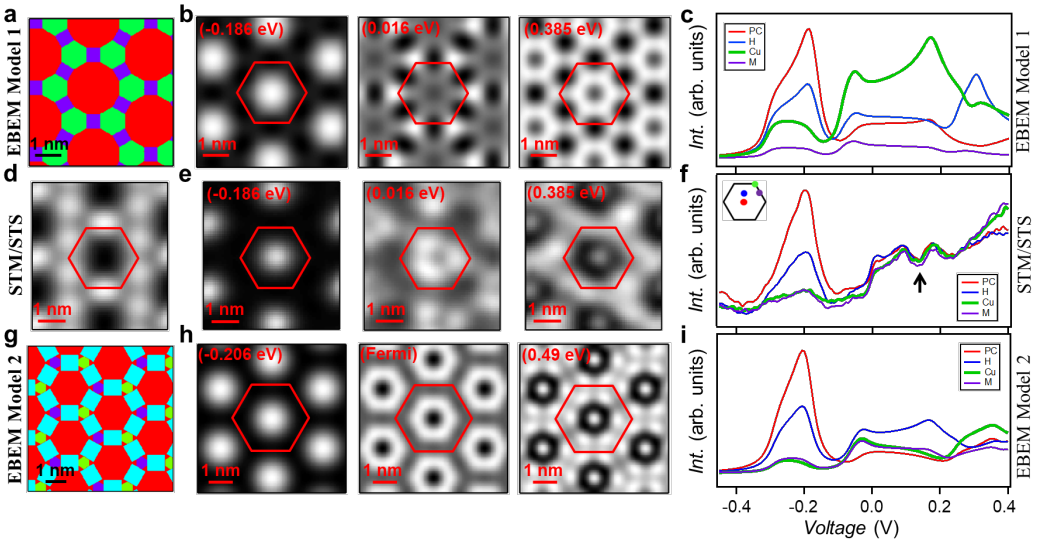

Figure 3.3: EBEM/EPWE simulated and experimental LDOS for 3deh-DPDI metal organic network. *The top* ***a-c*** *simulated data are reproduced from [5] and bottom simulated data* ***g-i*** *for optimized model [112] corresponding two different EBEM/EPWE simulations were used to compare to the experimental case shown in the central row* ***d-f****.*

.

one can note that the LDOS central intensity is reversed for the highest dI/dV map presented. Similarly, when comparing the dI/dV spectra at selected unit cell positions Fig. 3.3(c,f), was found that only the pore center spectrum acceptably matches te experimental curves, but the rest deviate strongly when bias transcends over -0.12 V. At the half way – H spectrum – the dominant peak at +0.32 V is experimentally absent. Secondly, for the metal center, two pronounced peaks are observed at -0.09 V and 0.18 V and show a drop of the intensity at the right side of the simulation, which are absent in the experimental data. In particular, the strong localization at the Cu atoms for the 0.18 V state, with LDOS as large as the fundamental n=1 PLS, is farthest from experiment, indicating nonphysical potential assignment for this region.

The pronounced disagreement between experiment and EPWE model generated with the parameters proposed in [5] requires the reconsideration of the scattering potential and geometries in this simulations. Based on previously reported high resolution AFM and STM works [102, 33] and the network model of Figure 3.1 (b), the scattering geometry was represented by realistic dominant repulsive nature of the molecules, instead of the metal coordination nodes. This leads to the molecular size of 9×8 $\AA$ in lateral size and much smaller metal coordination regions that realistically fill the space left between molecules. We find that using E_{Ref} = -440 meV (for 5 K) and $m^* = 0.49$ m_0, which notably overcomes the pristine surface state of underlying Cu substrate, together with homogeneous repulsive barriers 3.1, we can finely capture most details of the experimental LDOS and dI/dV spectra. Note that these are not just arbitrary values, but the result of ARPES and STS experimental data. These parameters turn

	V_{mol} (meV)	V_{met} (meV)	E_{Ref} (meV)	m^*/ m_0
Model 1 ref.[5]	1500	-100	-440	0.44
model 2	390	390	-440	0.49
model 3	390	440 (green) 340 (purpule)	-440	0.49

Table 3.1: *EPWE potential parameters used in the models discussed before.* V_{mol} *refers tospace occupied by the molecule and* V_{met} *to the metal coordination centers, which are respectively described as purple and blue rectangles, green or violet/yellow hexagons in Fig. 3.3* ***a*** *and* ***g****.*

.

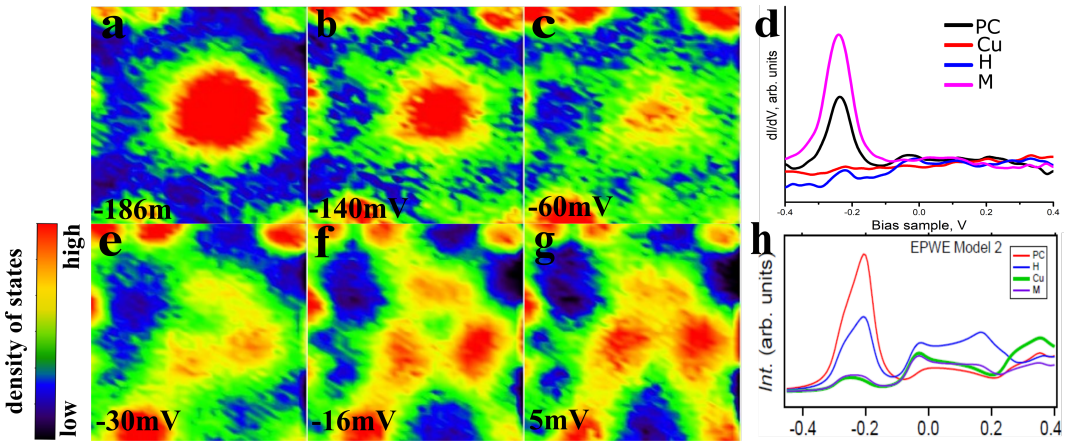

Figure 3.4: LDOS of the 3deh-DPDI network on Cu(111). ***(a-c, e-g)*** *dI/dV slices at the corresponding energies of the single pore metal-organic network exhibiting the three-fold symmetry of the nodes. STS details I=350 pA,* V_{vmrs}*=8 mV.* ***(d)*** *experimental point spectroscopy of the single pore,* ***(h)*** *simulated dI/dV curves.*

out to be crucial for pushing to lower energies the higher order confined states. For the more quantitative investigation of the repulsive scattering potential for both molecule backbone and metal node STS was performed *dI/dV* maps Fig. 3.4 recorded at 5 K (lock-in: V_{rms}=8 mV, 514 Hz) Initial parameters V=80 mV, I=350 pA. The *dI/dV* spectra represented in Fig. 3.4 Note, that the n=1 PLS peak is observed at the Fig.3.4 **d** were extracted from a set of 64×64 normalized point spectra. The spectroscopic conductance maps **a-c, e-g** are displayed as measured without convolution or high pass filtering. The automated procedure for taking a set of measurements takes from 10 to 20 h. The eigenstates can be tuned by choosing the appropriate length of the linking molecule. The bias voltages of the characteristic features (n=1 and n=2) of the DPDI network is represented in Fig.3.4**a** and **f**.

The LDOS simulation shown in Figure 3.5 displays a six-fold symmetry that contradicts previous experimental findings reporting the existence of two structurally different adatom coordination sites within the network. This difference is explained as a variation of the registry with the substrate, where the three metal adatoms bridging the molecules of the network arrange either surrounding a three-fold hollow site or a

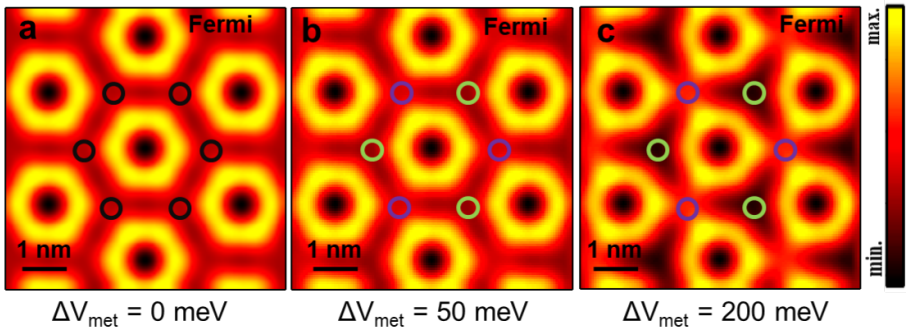

Figure 3.5: LDOS of the 3deh-DPDI network on Cu(111) simulated with EPWE. *The LDOS asymmetry can be simulated with EPWE as a perturbation of the scattering potential.*

.

Cu atom of the substrate . This subtle variation shows up in the AFM acquired with a CO functionalized tip **??** and in the dI/dV maps whenever the intensity shifts away from the pore center, as is the case of n=2 PLS Fig 3.4. It is worthy to note that, this is the first experimental observation of the triangular shape of n=2 PLS, although they were predicted for hexagonal lattices with three-fold symmetry.

The LDOS asymmetry can be simulated with usage of EBEM/EPWE as a perturbation of the scattering potential. In particular, **a** shows the unperturbed hexagonal case when ΔV_{met}= 0 eV, whereas **b** and **c** introduces potential variations of ΔV_{met}= 50 meV and ΔV_{met}= 200 meV, respectively. The green metal coordination position has a higher potential value than the violet one and, correspondingly due to the triple symmetry of the pore, the distortion becomes stronger the larger the difference between the two sites is.

Discussion

The combination of surface sensitive techniques such as spectroscopies and EBEM/EPWE simulation has produced two relevant results. First, the metal coordination sites exhibit repulsive scattering potential character compatible with the presence of three-fold symmetry in the higher energy states. Second, a mass re-normalization of the 2DEG occurs upon presence of the network on the Cu(111) surface. These findings are compatible with the ARPES data shown in Fig. 3.6. This situation corresponds to the one in which 3deh-DPDI network completely saturates the surface and no trace of the Cu SS is observed. This straightforward evidence for confirmation of the fact that the 2DEG re-normalization is correct since both the simulated band structure and the isoenergetic cuts fit exceptionally well to the experimental data when using the scattering parameters indicated in Model 2 of Table 3.1. In Figure 3.6, the second derivative of the experimental data exhibits the expected shallow dispersive bands of organic QD arrays. The lower energy band corresponding to n=1 PLS has a 80 meV bandwidth and shifts $\sim$ 150 meV towards E_{Fermi} with respect to the pristine Cu surface state and increases m^* to $\sim$ 0.58 m_0. This effective mass is higher than the 2DEG

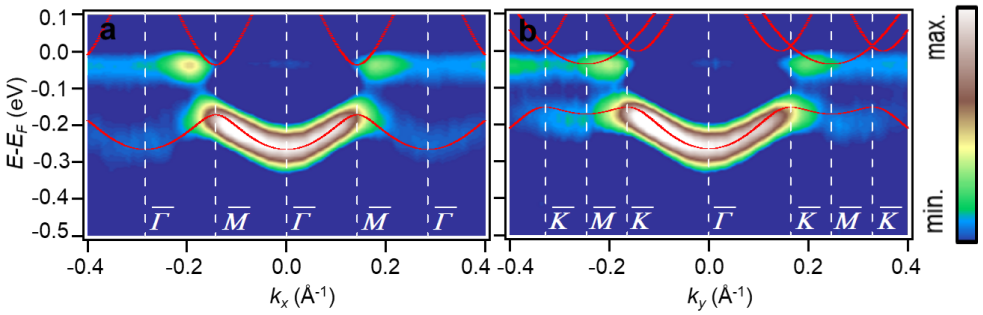

Figure 3.6: Energy dispersion maps for the two high symmetry directions $\overline{\Gamma M}$ and $\overline{\Gamma K}$. *The colorplot represent second derivative of the intensity to show the weak details with respect to the energy and parallel momentum.*

reference as a result of the confinement induced by the nanoporous network [5], which is certainly substantial from the prominent energy gap (120 ± 30 meV) detected at the zone boundaries – $\overline{M}$ point, separating the n=1 and n=2 PLS bands.

The high quality of the obtained network allows to observe faint replica bands in adjoining Brillouin zones. Simulated EBEM/EPWE bands using the scattering potentials of model 2 Fig.3.1 are superimposed as red lines onto the experimental data and match perfectly both high symmetry directions. Comparison of the experimental **a** and simulated **b** isoenergetic cuts at k_x and k_y obtained at the energy -0.24 eV, lower edge of the $\overline{M}$ point -0.13 eV, inside the gap -0.07 eV and at the Fermi level. As a reference, the metal-organic network induced hexagonal SBZ is superimposed onto the second derivative data.

As a reference, the metal-organic network induced hexagonal Brillouin zones is superimposed onto the second derivative data. ARPES parameters hν=21.22 eV, T_s = 10 K for 3.6 and T_s = 150 K for 3.7. Notably, the three-fold symmetry observed in the simulated and experimental LDOS for the n=2 PLS is absent in the Fermi surface map of Fig. 3.7. Instead, all isoenergetic cuts k_x and k_y exhibit six-fold symmetry (hexagonal shape) that diverges from the circular and isotropic pristine Cu surface state. It could be argued that due to the averaging character of ARPES, probed area contains, with equal probability, network patches with **A** and **B** metal coordination regions at equivalent pore sites 60° relative rotations. Nonetheless, the primary reason behind is the conservation of time reversal symmetry, which requires E(k) = E(-k). Hence, isoenergetic cuts should appear as six-fold even if a single three-fold symmetric 3deh-DPDI network domain was present on the surface. This is in agreement with other three-fold symmetric surface structures such as Ag/Cu(111) superlattices, where the band structure also appears as six-fold symmetric. Using the scattering parameters of both model 2 and model 3 in Table 3.1, the electronic band structure agrees with the band structure dispersion, gap size and isoenergetic shapes experimentally observed. Thus, the nice agreement between theory and experiment supports and validates the repulsive scattering character assigned for molecules and metals, as well as the imposed re-normalization of the 2DEG reference.

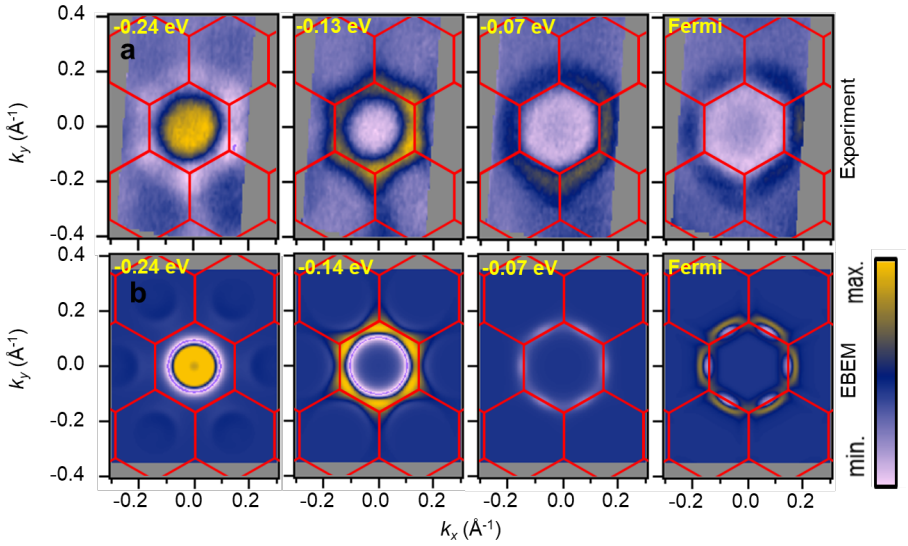

Figure 3.7: Comparison of experimental and simulated Brillouin zones. *Experimental* ***a*** *and simulated* ***b*** *isoenergetic cuts at k_x and k_y obtained at the energy -0.24 eV.*

3.3 Details of the experimental methods

To avoid contributions from the Shockley surface state of bare Cu(111) to the ARPES signal, it was crucial to achieve a homogeneous Cu-coordinated 3deh-DPDI network completely covering the surface. Therefore, DPDI was sublimated onto Cu(111) held at RT in a wedge geometry (producing a coverage gradient) in the proximity of the optimal coverage ($\sim$ 0,75 ML) and then annealed to 250°C until a sharp and intense signal emerging from the n=1 PLS was visible in the ARPES channelplate detector. The annealing step is crucial for conversion of the DPDI molecules into 3deh-DPDI molecules that will create the Cu-coordinated network [14, 101]. All dI/dV spectra were recorded with open-feedback loop. The dI/dV data presented in this chapter were extracted from the grid spectroscopy measurements, in which an area of 5.45 $\times$ 4.3 nm^2 was mapped by acquisition of dI/dV spectra above each point with the resolution of 35 points $\times$ 30 points. The initial tip conditions amounted to 400 mV/70 pA (lock-in frequency: 514 Hz; zero-to-peak amplitude: 8 mV). The value of the initial voltage was chosen such that no contribution from quantum dot states or network backbone is present. Under this conditions, normalization could be performed by setting the same dI/dV value at the set point energy for all other spectra. In this way artifacts originating from local surface potential variations are minimized.

3.4 Conclusions

The overall agreement between the measured and the simulated shapes of the resonances substantiates that the difference between the eigenstates of a purely hexagonal QD array and our system originates by an effective repulsive potential of both - molec-

ular building blocks and metal nodes. Our results prove that an appropriate EBEM/EPWE simulation of the electron confinement by QD arrays should be achieved by combination of STM/STS and ARPES experimental data and using realistic geometries of the overlayer before defining the strength of the scattering potential barriers. Moreover, the 2DEG reference requires certain flexibility, especially in m^*, in agreement to previous work [14]. The 2DEG reference changes upon the growth of the organic overlayer. The resulting *lossy* confinement depends on the detailed potential landscape exerted by the nanoporous network on the 2DEG, defining the interpore coupling and producing new electronic bands separated by gaps at zone boundaries. In conclusion, we have shown that it is possible to obtain the scattering potential landscape exerted by a nanoporous metal-organic overlayer onto a 2DEG and determine the relevant confinement details and interaction effects. This is achieved by combining semi-empirical EBEM/EPWE simulations with local and averaging electronic experimental techniques such as STM/STS, AFM, KPFM and ARPES. It is shown that the scattering potential must be parameterized as realistically as possible to the network geometry while providing flexibility to the 2DEG, which requires a slight energy and/or mass re-normalization due to the interactions between overlayer and substrate. Following other works, we provide a tentative upper limit to the repulsive scattering magnitude of the molecules for related systems. We also find that slight perturbations in the scattering potential at the metal sites are responsible for the deformation of the confined states, which show up as three-fold. This work confirms that the confined 2DEG is sensitive to existing subtle interactions of the overlayer with the substrate and corroborates the surface state re-normalization, which provides consistency to the results obtained by these semi-empirical simulations.

4

Pillow effect upon pore filling by organic adsorbates in an extended quantum box array

Addressable quantum system with defined architectures provide unique platforms to investigate the degree of electronic coupling between their units [103, 104]. Self-assembled on-surface porous networks are used to realize arrays of coupled quantum dots [14, 84]. Controlled modification of the electronic properties of such quantum units and the inter-unit coupling is desired for further applications. Comparative studies upon presence of guest-adsorbed molecules should lead to conclusive information on the conformation, electronic structure and intercoupling modification of such quantum dot arrays. In this chapter was realized goal by adsorbing electron donor Zinc Octaethylporphyrin (ZnOEP) molecules [105] inside metal-organic porous network [23]. Using complementary surface sensitive techniques in combination with theoretical simulations, we show that quantum states inside the porous network can be modified, affecting the partially confined state energy and interdot coupling, by the *"nano-pillow effect"*. In view of the charge injection at the metal-organic interface, this Pauli repulsion effect dominates even in the case of presence of the electron donor molecules. These studies pave the way for future light re-emission by the adsorbed porphyrins as well as the miniaturization of highly integrated molecular electronic devices.

4.1 Introduction and motivation

The control of material properties for technological applications has always been of prime interest on material science. One key element in building modern quantum electronic devices is the use of self-assembled architectures. For organic compounds this spontaneous organization can be achieved by modifying the molecular endgroups in order to achieve different type of inter-molecular interactions. The electronic properties of organics in contact with metal substrates depend on the alignment of the electronic levels and bands at the metal-organic interface and resulting hybridization of states, as

well as the charge transfer to or from adsorbates. The *"pillow"* effect, which originates from common energy level alignment of the metal and organic energy states, whereby electron long-range interactions are obtained using an expansion in the metal-organic overlap. Origin of the *"pillow"* effect goes back to the repulsive exchange, so called Pauli interactions. Simpler, *"pillow"* or *"push back effect"* is triggered by presence of the molecule close to the metallic surface, when molecule reduces the spilling out local potential of the work function. Only few experimental and theoretical studies about single molecules adsorbed at the metallic surfaces, pointed presence of the *"pillow"* effect [106, 107, 53, 108].

Of particular interest are organic nanoporous networks, as their pores can be viewed like single quantum box (QB) as they confine the surface electrons from the substrate [14, 36, 20, 109, 13, 28, 110, 34, 24]. The strength of such QB confinement depends on the geometry and periodicity of the network as well as on the confining barrier potential generated by its components – molecules and ion centers [24, 26, 111, 112]. It has been demonstrated that identical arrangements using different building blocks (i.e. non-metallated vs metallated porphyrin) can lead to differences in the confinement by changing the barrier strength [113]. Moreover, adsorbing atomic guests onto the pores modifies the QB electronic structure [31, 36, 35]. However, only few studies exist of the interaction that big organic molecules, in particular with an extended π-electron system, have on the pore confinement [114].Experimental research has proven that the properties of the anode, specifically anode/hole transport layer topography plays major role in the efficiency, performance and the lifetime of light emitting OFET devices. In the past, so called common vacuum level approximation, which dates back to Mott and Schottky, has been used to predict the relative position of electronic states at the metal-organic interfaces. In particular, porphyrins are an important class of organic building blocks that readily self-organize on the metallic surfaces. Because of the chemical and optoelectronic properties of porphyrins, they serve as excellent candidates for wide usage in electronic devices such as solar cells and sensors. Further investigation is still necessary to unravel the interplay between the electronic and geometric structure of the complex metal-organic structures on solid substrates, in particular the influence of the molecule-confinement interaction and the intercoupling between QBs.

Towards the investigation of complex multi material surface templated host-guest on surface architectures, and in particular their electronic and mechanic properties, we present the results concerning presence of the *"nano pillow effect"* at the metal-organic interface. In particular, this investigation was realized in the case of presence of the *lossy* confinement (localized and delocalized parts) inside the pore, which directly interacting with adsorbed porphyrin [107]. Here we report, that the surface potential difference of up to 1 eV is responsible to the site-selective immobilization of the metal-organic pattern. In this work we used self-assembly of molecules to fabricate 2D periodic array of coupled quantum units [14, 23] as the template and we studied *"nano pillow effect"* in averaging and local manner in combination with EPWE/EBEM theoretical methods, presence of the quantum dot intercoupling effect through the confining barrier can be modified by presence of the adsorbates.

4.2 Results and Discussion

Architecture of the 2D array

We employ highly ordered stable Cu-coordinated, 3-deh 4,9-diaminoperylene quinone-3,10-diimine (3deh-DPDI) hexagonal porous network grown on Cu(111) [23] as a template Fig.4.1a. The electronic Shockley state of the underlying noble surface is confined in the pores, resulting in modified states that leak into neighboring pores and generate a distinct band structure [14] Fig.4.1b. As a guest adsorbates we used ZnOEP molecules, which are known as an electron donor and due to its optical properties. ZnOEP has highly conjugated π-electronic structures, and they are strong absorbers of light in visible spectra, and can re-emit light upon excitation. Because the porphyrin macrocycle has a nearly planar geometry, it likely lies flat on a surface and provides a sustained foundation for any potential surface supported by two-dimensional network. In particular, ZnOEP was observed to adsorb with its porphine ring parallel and in direct contact with the underlying substrate and perfectly fitting the metal-organic pore [114]. Experimental STM topographs shows that all the 8 ethyl substituents of the porphyrin stay in an *"all up"* or in *"crown"* configuration, instead of the packing seen in the crystal structure [115]. Also, important to note here is that most of the electronic features come from organic macrocycle, because the influence of Zn central atom is modest.

Fingerprint of the adsorbates onto quantum dot array electronic structure acquired by ARPES

To unravel the electronic structure, we performed Angle-Resolved Photoemission Spectroscopy (ARPES) measurements. This averaging technique provides direct access to the occupied band structure of the system. ARPES probes the intercoupling between the confined electrons in the array of quantum units, and shows how the interplay between the electronic wave functions in such units gives rise to a well-defined band dispersing in energy and momentum, and with a certain effective mass. These properties are of fundamental interest for carrier mobility and ultimately for quantum devices and architectures. ARPES has been successfully used to probe quantum confinement in different materials and can even give an accurate description of many-body interactions [116].

By use of ARPES we characterized the organic network in two cases: first completely empty Fig.4.1a, and second when the pores are filled with ZnOEP molecules Fig.4.1b. These molecules were observed to adsorb in the porous structure [114] with its porphine ring parallel and in the direct contact with the pore state. Evolution of the electronic band registered by ARPES in both cases provide evidence for the partial localization and coupling of the QBs [14, 101]. ARPES measurements were performed on a lab-based experimental setup equipped with non-monochromatized He lamp, where the gas pressure was tuned to maximize the He I_α ($h\nu = 21.22$ eV) signal. Using these conditions, we did not observe any original Cu bulk bands contribution from other

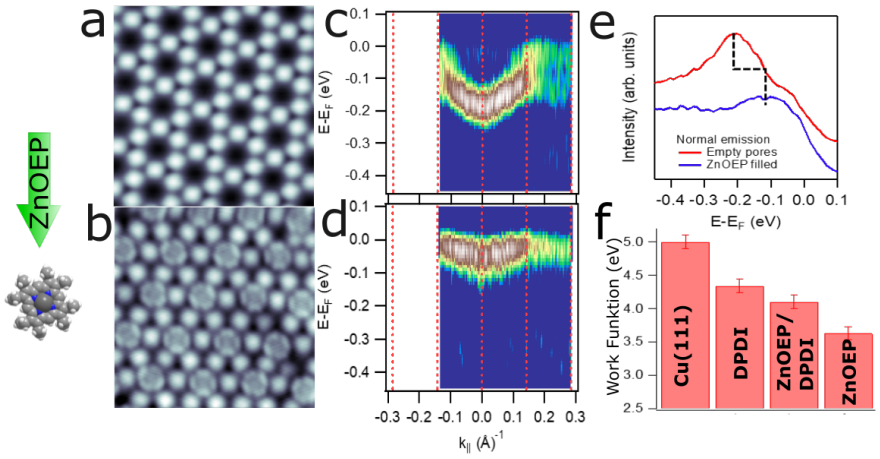

Figure 4.1: Electronic modification of the 2DEG partially localized state by ZnOEP adsorption across the DPDI network. ***a, b*** *STM images of the empty and occupied by ZnOEP network (STM details: 10 × 10 nm^2, 400 mV, 50 pA). 2nd derivative of the ARPES experimental spectral function close to the* $(\overline{\Gamma M})$ *high symmetry direction acquired for the empty* ***c****, and ZnOEP filled network* ***d****, respectively.* ***e*** *normal emission energy distribution curves* $(k|| = 0)$ *showing a clear shift of the partially localized state ∼130 meV towards Fermi level.* ***f*** *experimental work function variations from the different surface terminations as obtained by photoemission and charge transfer maps.*

.

excitation lines (satelites) in the limited spectral region reported here. All the present data were recorded at room temperature. The corresponding raw Fig.4.1 and second derivative ARPES data are present in Fig.4.1c-d, respectively.

The spectral distribution at the fundamental energy (Gamma point) of the vacant network has its maximum at 220 ± 10 mV binding energy (BE). When the network is filled with ZnOEP we observe a 120 meV energy shift towards the Fermi level, since the fundamental energy moves to -100 meV. The shift towards lower BE of the spatial component upon presence of the ZnOEP across the network, as measured by ARPES, addresses to ∼130 mV. This is better observed from the normal emission energy distribution curves subtracted from ARPES data in Fig.4.1e. We interpret this energy shift as the result of the Pauli repulsion between the confined electronic state and the ZnOEP molecule, similar to the recently reported shift of the QBs toward lower BE caused by the Xe adsorption across the DPDI network [101]. Shift in the partially localized state ∼120 mV towards Fermi Level is concomitant with a reduction of the work function due to the presence of the ZnOEP molecules across the network [**??**]. Of course, the electronic properties of the adsorbed molecules are modified by interaction with the substrate. In particular, charge transfer between the substrate and molecule modifies the molecular band gap Fig.4.8. Nevertheless, the existence of the work function at the material surface is natural. As for the photoemission process alone, the WF refers to material work function which is the energy a photoelectron needs to pay if it moves from the Fermi level of the material to the vacuum level. In

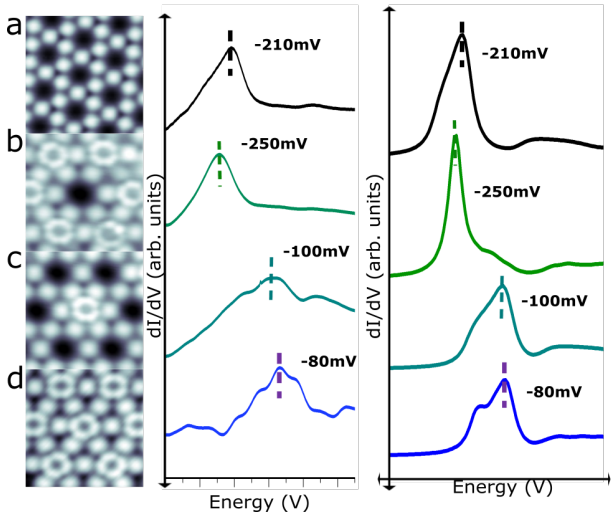

Figure 4.2: ***Evolution of the electronic state of one particular QB modified by its neighboring environment.*** *The left column shows the topographic images with all possibilities (STM details: 6×6 nm, 50 pA, 400 meV):* ***a*** *all pores are empty,* ***b)*** *empty pore surrounded by filled pores,* ***c*** *filled pore surrounded by empty ones, and* ***d*** *all guest filled pores. On the right column the corresponding dI/dV specters recorded at the center pores are shown indicating their maxima energy values (Initial parameters: 800 meV, 200 pA).*

our studying, we observed, that in the case of fully occupied quantum dot array with ZnOEP, common WF of the metal-organic architecture is reduced up to 1 eV (Fig.4.1f)

QB electronic structure acquired by STS

To investigate locally the influence of the adsorbates on the local level upon the electronic states, we employed Scanning Tunneling Microscopy/Spectroscopy. However, since STM is a local technique, the different contributions between filled and empty pores can be studied. In other words, we can investigate the influence of the surrounding environment onto the confined surface state we generated different configuration of the filled and empty QBs. Representative experimental and simulated dI/dV spectra and STM data are presented in Fig.4.2. All experimental dI/dV spectra (middle column) were recorded with open feedback loop and with metallic tip and then normalized for better visual comparison. The dI/dV data presented in Fig.4.2 was obtained from grid spectroscopy spectra of an area of 2.5×2.5 nm mapped by acquisition of the dI/dV spectra above each point with the resolution of the 64×64 dots. As described in detail in Ref [117] a normalization could be performed by using the same current/energy setpoint for all dI/dV spectra. In this way artefacts originating from local work function variations are minimized. In the first test-case Fig.4.2, we have native DPDI network, and dI/dV curve has its maximum at the 210±10 mV BE. In the second test-case Fig. 4.2, we have empty pore surrounded by occupied by ZnOEP pores. The dI/dV signal was obtained at higher BE exhibiting a sharp peak with

full width at half maximum around ∼50 mV.This downwards energy shift can be explained by first order perturbation theory: the interaction of the electronic states of one quantum array with states of the neighboring systems leads to the stabilization of the isolated state [101]. The electronic coupling between present electronic states strongly depends on the overlap of the *lossy* confinement, which is reduced here by the state energy mismatch between the empty pore and the surrounding occupied environment. Moving on to the third test-case of the single filled pore surrounded by empty environment (4.2(c)) exhibits a QBs peak at the slightly higher BE ∼100 mV and full width at half maximum around ∼170 mV wider than the the Fig.4.2c peak is wider than Fig.4.2(d) because we have a leak from the unoccupied states into that particular pore Fig.4.2. The QBs modified by porphyrins are perfectly agreeing with what we detected by ARPES. The observed energetic adjustments of the dI/dV peaks which characteristically depends on the neighboring environment provides significant evidence that these peaks are not derived from molecular orbitals. In ARPES data the energy positions of the corresponding quantum dot states are found to be farther from the Fermi energy than in STS data. These differences are likely related to the technical aspects of each technique. ARPES averages over the whole illuminated region, losing its local character, and probes the coherent part of the electron wave function, whereas STS is a local technique also sensitive to the non-coherent part [118]. This gives rise to the fundamental divergence between these two techniques: ARPES is k-selective, whereas STS integrates over k-space. As a result, ARPES can quantify the minimum energy value of the quantum box state, whereas in STS a large fraction of the projected DOS (convoluted with tip LDOS) contributes to the observed dI/dV line shape. In this way, the STS energy maximum shifts towards the bandwidth center (towards the E_F) as compared to the ARPES result.

To explain shape and broadening of single dI/dV for all different cases, we turn to simulating the electronic properties for all previously mentioned configuration cases described in Fig.4.2 using EBEM/EPWE. The combined EPWE and EBEM [66, 28] represents a scalar variant of the electromagnetic PWE/BEM extensively used for solving Maxwell's equations and optical response for arbitrary shapes. In this studying the local electronic properties of nanoporous networks such as LDOS at a single pore are performed by using this method. The Schrödinger equation for electrons experiencing an effective potential V for instance when surface electrons encounter a molecular barrier in a hexagonal molecular nanoporous network. For the simulations the first step is to parameterize the geometrical structure of the networks that will mimic the potential barriers that scatter the 2DEG. Parameters used for simulation are represented in table 4.1. First was simulated the electronic structure of the 3deh-DPDI metal-organic network on Cu(111). As in this studying we are interested mainly in the n=1 PLS and in the pore center spectra, following model in Chapter 3, [112] we parameterize the scattering potential landscape of the network and assign both molecules and Cu adatoms in coordination a common repulsive scattering amplitude 4.1. The original Cu surface state is also taken into consideration. The LDOS at the center of the pore (right column in Fig.4.2) matches the peak shape and energy of the n=1 PLS. To simulate the Pauli repulsion effect produced by ZnOEP adsorbates on the confined

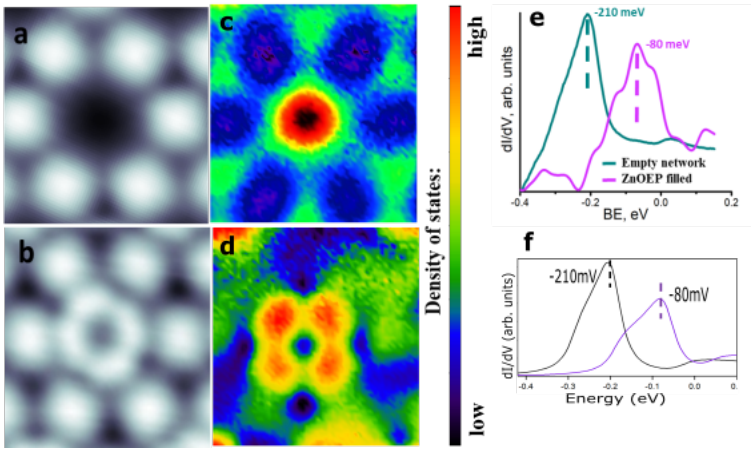

Figure 4.3: *STM topographic images of* ***a*** *a vacant single pore of the network and* ***b*** *a pore occupied by an adsorbed ZnOEP molecule (STM details: 2.5×2.5 nm^2 , 400 meV, 50 pA) and their corresponding acquired conductance maps* ***c, d*** *recorded at 5 K (lock-in: V_{rms} =8 mV, 514 Hz) Initial parameters V=80 mV, I=300 pA. Note that a modification of the barrier transmission probability is observed by the three-fold symmetry of the pore and guest molecule, causing the "nano-pillow" effect.* ***e*** *Comparison of the STS spectra subtracted from grid spectroscopy, in the empty pore middle (green) and above the metal center (pink) of the guest ZnOEP. The shift from -210 meV to -80 meV, can be attributed to the presence of the adsorbate inside the pore.* ***f*** *Simulated dI/dV spectra for corresponding cases.*

Configuration	m*/ m_0	V_{pore} (meV)	$V_{network}$ (meV)	E_{Ref} (meV)
pores empty	0.49	0	390	-440
pores filled	0.49	150	390	-440

Table 4.1: *EPWE potential parameters used for the empty and filled with ZnOEP network.*

state, we increased the potential inside the pore by 150 meV Table 4.1 so that the resulting dI/dV (violet curve) matches the experimental shift ($\sim$ 130 mV) measured with ARPES and STS 4.1 4.2. A small increase in coupling, which represents by the asymmetry of the curve is detected since the molecular barrier now represents a smaller effective scattering potential $V_{network}$=240 meV than the empty network. This is in agreement with the slight increase in the peak width detected in Fig.4.2

For the structural and electronic properties analysis of the system, a closer inspection of the metal-organic surface structure is essential. Each pore of the network possesses three-fold symmetry because of the inequivalence of its nodes, where three adatoms are accommodated in each vertex, that interact with the nitrogen functional groups on the ends of the molecules. STM topographic resolution and the spectroscopic capability provide a unique way to unravel the formation of the potential barrier. As it was studied by DFT calculations in ref. [33, 23, 102], nodes have different configuration when positioned above a hollow surface site hand nodes which are positioned above

on-top site of the surface atom [33]. Notably, in our studying we didn't observe any WF modification for different nodes in the presented conductance map for the empty pore Fig.4.3c, but due to the presence of the adsorbed porphyrin Fig.4.3d,we can see clear charge redistribution in the confining molecule-metal barriers, which follows triple symmetry of the nodes. Due to this modification, we investigated the local possibility of the transmission barrier modification via their interaction with present adsorbates. Also, from conductance map of the occupied pore we can see, that imaged ethyl groups despite that fact, that density of states is concentrated on the porphine core. The complex interplay between the electronic and geometric structure of represented molecules adsorbed on solid substrates, in particular the influence of the molecule-network and molecule-confinement interaction as well as the resulting electrical conductions and modifying transmission barrier probability through molecular complex. The observed energetic adjustment (upshifts) of the dI/dV evidences that we have interdot coupling between occupied pores which modifies their electronic states. This penetration into the barrier [SI 3.4] and the electronic interaction of the neighboring pores, is critically dependent on the core structure of the barrier itself in combination with the surface electronic states. In our example, both the metal-organic framework and the adsorbate affect the underlying electronic state differently and both moderate the lateral coupling between neighboring quantum boxes.

Comparison of the influence onto QDs of the free based H_2OEP and ZnEOP adsorbates

ZnOEP has four-fold molecular symmetry and rectangular shape. It was observed in previous study that molecule fits into the nanocavities formed by DPDI network [114]. At the presented data we see, that all 8 ethyl groups point upwards upon adsorption inside the network, i.e. the porphine core has maximum contact to the substrate i.e. confinement/adsorbate interaction. Due to the sterically allowed rotations of the ethyl groups around single C-C bonds connected to the porphine ring, *"crown"* shape is the most energetically favorable. The non-bonding interaction between chemically inert alkyl groups shows small influence of the adsorption configuration onto density of states. To investigate, if HOMO LUMO states of the molecule has influence onto the shape of presented dI/dV curves in this chapter, we calculated molecular states of ZnOEP in the gas phase Fig.4.4. As it is shown, the HOMO-LUMO gap is 6.71 eV, and main contribution onto the confinement-adsorbate interaction comes from the porphin molecular ring.

To test, if the metal ion of the molecular adsorbate has influence onto confinement-adsorbate interaction, was performed experiment with filling the network by metal free H_2OEP. The STM topographic images of Fig.4.5(a) a vacant single pore of the network and Fig.4.5(b) a pore occupied by an adsorbed H_2OEP molecule (STM details: 2.5×2.5 nm^2 , 400 meV, 50 pA) and their corresponding acquired conductance maps **c, d** recorded at 5 K (lock-in: V_{rms} =8 mV, 514 Hz). Initial parameters V=80 mV, I=300 pA. Notable, that a modification of the barrier transmission probability was not observed due to the presence of guest molecule. Fig.4.5(e) Comparison of the STS

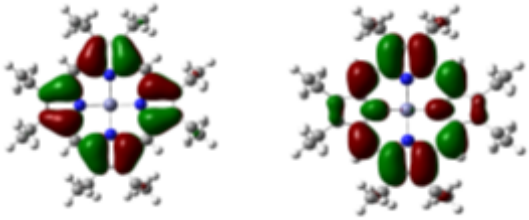

Figure 4.4: *Calculated density of states of the ZnOEP molecule in the gas phase. All ethyl legs point up. States close HOMO (left) and LUMO (right) show no dependence on the ethyl group orientation and energy gap is* δ E_{gap} *=6.71 eV.*

spectra subtracted from grid spectroscopy, in the empty pore middle (green) and above the metal center (pink) of the guest ZnOEP. The shift from -210 meV to -70 meV, can be attributed to the presence of the adsorbate inside the pore. Fig.4.5(f) dI/dV spectra for corresponding cases.

In contrast to ZnOEP, while H_2OEP is adsorbed across the DPDI network, very slight barrier trasnmission probability change was observed in the range of -70 $\sim$ -60 meV. Also it is visible, that main contribution to the confinement-adsorbate interaction comes from the molecular core. Interestingly, the quenched by H_2OEP confinement dI/dV peak was detected approximately at the same energy position as for ZnOEP.

4.3 Conclusions

In summary, we studied the interaction between a partially confined state and a molecular guest adsorbate. Empty and occupied quantum dots are electronically coupled and due to the presence of guest molecule. The observed energy shift when the pores are occupied by ZnOEP we assign it t an electrostatic repulsion commonly known as *"nano pillow effect"* which also causes modification of the transmission probability across the network barriers or the interdot coupling. Notably, molecular adsorbates, i.e. ZnOEP, show dramatic change in the transmission probability across the barriers. These results suggest that a wide range of quantum arrays formed from functional molecular building blocks can be fabricated and in combination with different adsorbates provide a rich playground for modification of the quantum dots properties.

4.4 Details of the experimental methods

Sample preparation

Samples were prepared and investigated in two ultra-high vacuum systems with base pressure bellow 1×10^{-10} mbar. The surface of Cu(111) was prepared by multiple cycles of Ar^+ ion sputtering at 2 keV, followed by annealing at 800 K. The surface order and cleanliness were monitored by STM/LEED and photoelectron spectroscopy.

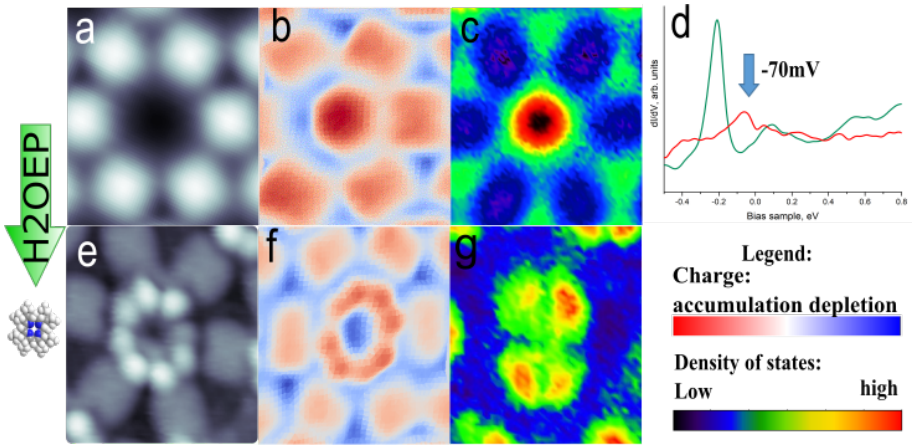

Figure 4.5: *STM topographic images of* ***a*** *a vacant single pore of the network and* ***b*** *a pore occupied by an adsorbed H_2OEP molecule (STM details: 2.5×2.5 nm^2 , 400 meV, 50 pA) and their corresponding acquired conductance maps* ***c, d*** *recorded at 5 K.* ***d*** *Comparison of the STS spectra subtracted from grid spectroscopy, in the empty pore middle (green) and above the metal center (red) of the guest H_2OEP. The shift from -210 meV to -70 meV, can be attributed to the presence of the adsorbate inside the pore.*

The DPDI molecules were thermally sublimed with ∼ 250°C onto the surface with the use of the nine-cell commercial evaporator (Kentax, GmBH, Germany), at a rate about 0.5ML/Min , monitored by a quartz microbalance, resulting in an average coverage in the submonolayer range up to a full molecular layer. After deposition, the sample was annealed to ∼300°C in order to convert native DPDI into 3deh-DPDI, which in combination with Cu thermally ejected from the substrate adatoms lead to growing of highly ordered porous network. ZnOEP molecules (commercially available from MERCK former Sigma-Aldrich) were thermally sublimed at ∼ 200°C onto the sample kept at RT.

ARPES raw data and second derivative

The ARPES measurements were performed on lab-based experimental setup equipped with a display type hemispherical analyzer (*Phobios 150*) with an energy/angle resolution of 40 meV/0.1° and monochromatized Helium source ($h\nu$= 21.22 eV). To avoid contribution from the Shockley surface state of the bare Cu(111) to the ARPES signal it was crucial to achieve homogeneous Cu-Coordinated network completely covering the surface. Therefore, DPDI molecules were thermally sublimed onto Cu(111) clean substrate held at RT, and then annealed until the sharp and intense signal emerging from the partial localization of the QB state as in 3 Fig.3.2, was visible in the ARPES chanelplate detector [23, 26].

The deposition of the ZnOEP experiment was started immediately when sample reached RT temperature. Fig.4.6 shows a comparison between the raw data and the 2nd derivative of the photoemission intensity. The latter is used to highlight weak

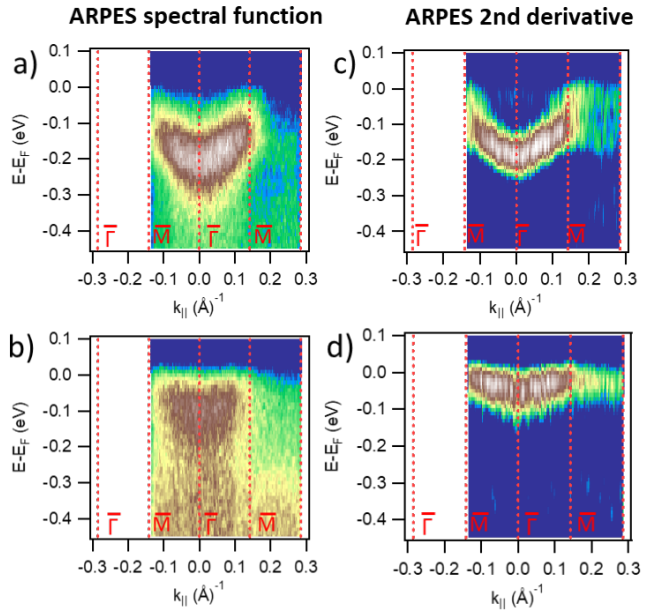

[h]

Figure 4.6: *ARPES raw data a and* ***c*** *ARPES raw experimental spectral function acquired for the empty and filled network respectively (**b, d**).*

details of the band structure. In ARPES data the energy position of the corresponding QB states are found to be slightly farther from Fermi energy than in STS. This difference is explained by technical aspects of each technique.

STM/STS measurements and data processing

All STM measurements were performed with Omicron LT-STM, operated at 4.2 K at ultrahigh vacuum conditions. In the STM the bias voltage is applied to the tip. The bias voltages given in manuscript and Supplementary Information referred to the grounded tip. Data were taken in constant current mode with $Pt-Ir$ tips (90 % Pt and 10 % Ir), prepared by mechanical cutting followed by cycle of sputtering and controlled quality in the bare Cu(111) surface. STM images reported in this paragraph were recorded with such prepared metallic tip. The STM images and simultaneously acquired dI/dV and I(z) maps shown in the Fig.4.2a-f were measured with -80 mV/300 pA (for dI/dV) 1 V/300 pA respectively, and with lock-in frequency of 514 Hz and V_{rms}=8 mV. STS spectra were normalized, due to the strong quenching effect. The STM data were processed with the WSxM software. For better comparability of the data the color histograms of STM images were adjusted. Low-Pass filter was used to reduce the noise. Data were acquired in constant current mode.

The dI/dV presented in Fig.4.3 are extracted from the grid spectroscopy experiments, in which area 2.5 × 2.5 nm of empty/occupied pores was mapped by acquisition of dI/dV spectra above each point with the resolution of 64 ×64 points. The initial tip conditions are 400 mV, 50 pA, and their corresponding acquired charge transfer maps lock-in: V_{rms}=8 mV, 514 Hz, I=300 pA, U=1 V. Conductance maps display dI/dV

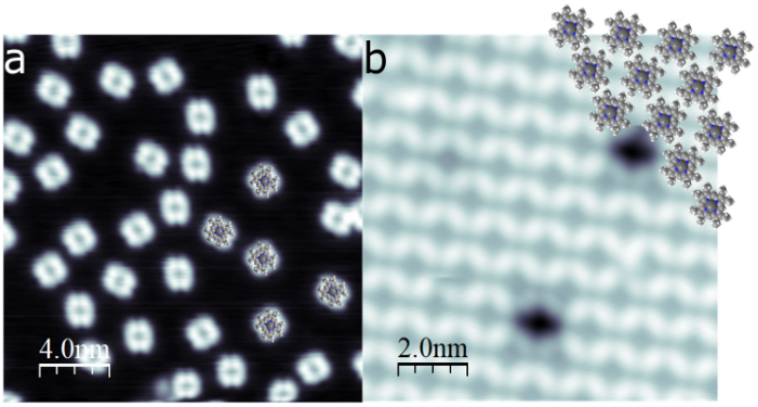

Figure 4.7: *ZnOEP across the bare Cu111 surface a free ZnOEP molecules on the bare Cu111 surface.*

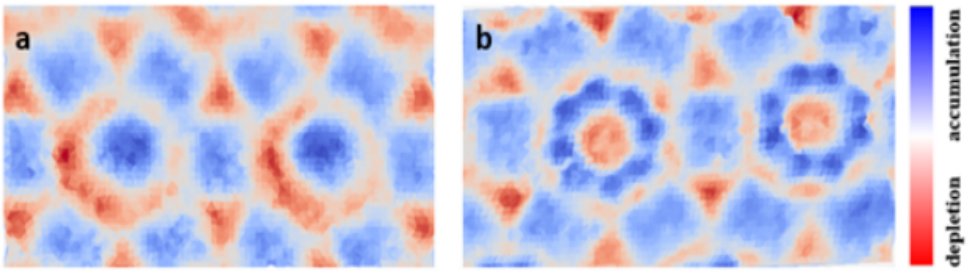

Figure 4.8: *Charge transfer maps of a a vacant pore and* ***b*** *occupied pores by an adsorbed ZnOEP molecule. (lock-in:* V_{mrs}*=8 mV, 514 Hz, I=500 pA, U=1 V, Size 3,5 × 6* nm^2*).*

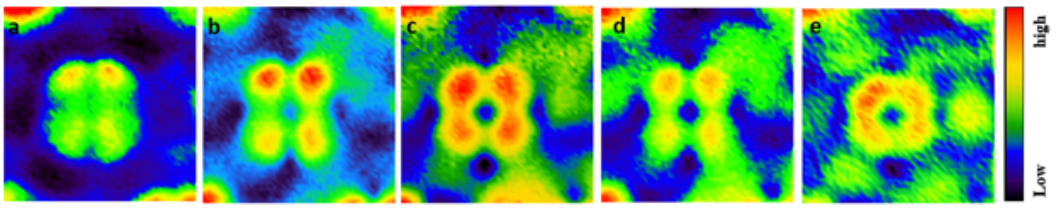

Figure 4.9: *Conductance 2D maps of the occupied by ZnOEP molecule pores subtracted from the 3D matrix at* ***a*** *1 mV* ***b*** *70 mV* ***c*** *88 mV* ***d*** *111 mV and* ***e*** *125 mV (lock-in:* V_{rms}*=8 mV, 514 Hz, I=500 pA, U=1 V size: 3.5 × 6* nm^2*).*

maps recorded at 5 K with lock-in: V_{rms} =8 mV, 514 Hz Initial parameters V=80 mV, I=300 pA. Fig.4.9 represents energy *slices* with different parameters, subtracted from the same grid spectroscopy experiments. Note that a modification of the barrier transmission probability is observed by the three-fold symmetry of the pore and guest molecule, causing the "nano-pillow" effect.

5

Magnetic imprint from the periodically distributed molecular adsorbates with selected metal centers

Dimensionality is one of the most important factors influencing the magnetic properties of matter. Imposing lateral confinement onto spin-bearing systems results in new size-effects, such as larger orbital magnetic moment, oscillation of the magnetic anisotropy energy or steering of the magnetization axis [119, 120]. However, the mechanisms that dictate the behavior of the magnetic signal upon alteration of the electronic environment are still highly unexplored. In this chapter is presented an experiment, where effect that modify the substrate electronic states upon the generation of a porous networks on the Cu(111) surface has on the magnetic signal of the selected metal centers embedded in organic molecular adsorbates. In particular, was probed magnetic anisotropy of *d*-shell transition metal centers of molecular adsorbates inside an extended 2D metal-organic architecture that is known to alter the Shockley state [14, 26] of Cu(111). For this purpose, X-ray Magnetic Circular Dichroism (XMCD) experiments were performed at low temperatures and in strong variable magnetic fields. Study combines multiple surface sensitive techniques such as STM/STS, X-ray photoelectron spectroscopy (XPS), Angle Resolved Photoelectron Spectroscopy (ARPES), Photoelectron Diffraction (PhD) and Density Functional Theoretical calculations (DFT). These results differ from previous models of hybrid metal-organic systems and provide a consistent description of their magnetic moments and Kondo physics in terms of spin and orbital multiplicity.

5.1 Magnetism at the nanoscale

The past decade has witnessed a dramatic increase of detailed information about surfaces, overlayers, and interfaces due to the development and refinement of surface sensitive experimental techniques. In particular, magnetic surfaces and multilayer systems continue to attract considerable interest both from a fundamental and applied point of view. The reduced dimensionality in these systems gives rise to a novel mag-

netic phenomena not observed in a bulk materials. Artificially structured magnetic materials with reduced dimensionality are of major importance in current storage and sensor technology [121] and have led to revolutionary changes in many areas of microelectronics.

Extensive research has been undertaken in the last decade to study hybrid systems combining metal and molecular layers for the design of novel magnetic devices [122]. Compounds that incorporate one or more local spins into an organic framework integrate a wide spectrum of magnetic properties with additional and sometime exotic electronic functionalities, such as Kondo physics and Coloumb blockade effect, giant negative magnetization [123] and site-specific control of the magnetic anisotropy [119]. The understanding of these complexes would be greatly improved by insight into their microscopic magnetic behavior, in particular, by the accurate determination of their spin and orbital moments as well as their anisotropies. This is of crucial importance when metal-organic molecules are interfaced with a magnetic or nonmagnetic metal as part of a hybrid layer since both their electronic and magnetic susceptibilities may differ significantly from those of the bulk compounds.

Molecules belonging to the metal-phthalocyanine and porphyrin family represent archetypal metal-organic semiconductors that display excellent chemical stability and film growth properties. Their planar macrocyclic structure can accommodate large variety of metal ions at their center, giving rise to many interesting magnetic phenomena, ranging from paramagnetism (Mn, Fe, Co, Cu) to one-dimensional Heisenberg and single molecule magnet behavior [124], as well as exchange coupling to metal and metal-molecular layers [125, 126]. Recent STM studies, however, have shown that the magnetic moment of metal based phthalocyanines deposited onto nonmagnetic metallic substrates is very often screened through the Kondo interaction [127, 128, 129, 130, 76] or even completely quenched by hybridization. Thus, in the interface regime, the physical properties of MePc appear to be dominated by the interaction with metal states, significantly reducing their magnetic response and usefulness for future applications. Because of its open d-shell, isolated transition-metal ions possess large magnetic moments governed by Hund's rules. The reduced coordination of atoms at surfaces of bulk systems or small clusters leads to smaller interactions among atoms and thus a narrowing of the local densities of states. The resulting electronic structures of the surface atoms approach the atomic limit where magnetism is favored. Intense studies of the surfaces and multilayer systems of magnetic transition metal ions have indeed confirmed such surface enhanced magnetism [131, 132, 133, 134]. Transition metal porphyrines and their derivatives represent a well-known class of the molecules with organic semiconducting properties in the bulk and broad spectrum of applications that includes field-effect transistors, gas sensors and photovoltaic cells [135, 136, 137]. Due to their relatively simple and robust structure as well as versatile chemistry, transition metal porphyrines have assumed the role of a model system to study the interaction of metal-organic complexes with metal underlying surfaces. Their flat adsorption geometry facilitates the bonding of both central TM ion and organic ligands to the substrate, while their capability to coordinate many different metal atoms allows for a systematic investigation of their magnetic properties [138, 77, 74, 139]. The interaction of octaethylporphyrines with metallic and non-metallic surfaces has been studied by

many techniques, including STM, UPS, XPS, XAS and DFT. In particular, investigation of the magnetic properties of molecules in general was focused on transition metal phthalocyanines and porphyrins with selected metal ion i.e. Mn [140, 141], Fe [142, 143, 144, 145], and Co [77, 146, 143, 147] for which it was shown that adsorption on the metallic substrate tends to quench the magnetic moment of the TM ion. In addition to such investigations is the implicit assumption that the magnetic properties of TMPc at the surfaces depend almost exclusively on the ground state of the TM ion itself, the competition between *d*-*d* electron correlation and covalency, that is, the transfer of charge between the *d*-orbitals and delocalized ligand states. Some subtle variations are encountered across the transition metals. Filling the *d* orbitals is not as straightforward as the *s* and *p* orbitals. If to refer back to the crystal theory, in the case when we know the relative energies of *d* orbitals in transition metal complex, we have to worry about how these orbitals are filled according to the Hund's rule. Degenerate in the case of the octahedral d^7 complexes Fig. 5.1 (Co^{2+} example) occurs the problem of two different configurations - *high-spin*, because it contains one unpaired electron, and *low-spin* because it contains three unpaired electrons. For octahedral d^8 Fig. 5.1 (Ni^{2+} example) complexes, there is only one way to write satisfactory configurations. The amount of energy required to pair electrons in the t_{2g} orbitals of an octahedral complex is more or less constant. The amount of energy needed to excite an electron into the higher energy (e_g) orbitals, however, depends on the value of δ_0 for the complex. As a result, we expect to find low-spin complexes among metal ions and ligands that lie towards the high-field end of the spectrochemical series. High-spin complexes are expected among metal ions and ligands that lie toward the low-field end of these series. In particular, charge transfer affects the magnetization of such TM ions, their coupling through the indirect exchange path, as well as the conductivity of important classes of materials. Recent studies of Mugarza *et. al* [148] has highlighted the possibility of inducing a magnetic moment delocalized over the phthalocyanine ligand, which affects the spin degeneracy and symmetry of the molecular ground state as well as the electrical conductance measured at different sites within the same molecule. Indeed, a growing number of experiments indicates that the organic ligand directly affects the magnetism and transport properties of metal-organic complexes [149, 150, 151, 152].

The interaction of such molecules with solid interfaces governs the self-assembly of supramolecular layers as well as electronic and magnetic properties of metal-organic architectures [148, 153] and single molecule devices. The large variety of organic and metal-organic complexes, combined with the possibility of tuning magnetic properties and electronic ground state of different complexes withing the same family of molecules, make such systems incredibly attractive for future applications. However, as was discussed in Chapter 2, electronic interactions of adsorbed molecules with the solid interface may induce charge transfer, distort the ligand field, and tune electron-electron correlation effects via screening and hybridization. The intricate interplay between all these processes is far from being understood.

Worth to notice, that only few related experimental studies exploring magnetism and ferromagnetic coupling in the self-assembled metal-organic networks have been published, but these were never addressed under the presence of molecular adsorbates

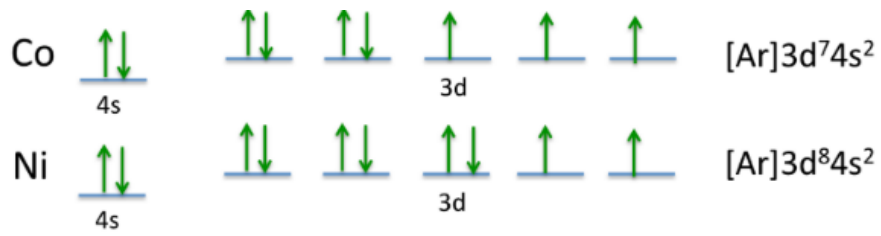

Figure 5.1: *Electronic configuration of the 3d shell of the selected transition metal ions Co upper row and Ni lower row.*

[129]. Detailed model describing adsorbate-confinement mechanism has been earlier developed for single atoms [154, 35, 101, 84, 155] and discussed in Chapter 4 for molecular adsorbate. However, few such models exist at present for big organic molecules, particularly with an extended π-electron system and selected spin center. The interplay between the electronic and geometric structure of the complex metal-organic structures on solid substrates, in particular the influence of the molecule-confinement interaction as well as the resulting electrical conduction and electron transfer through the confining barrier have not been yet fully explored. Indeed, very few related works dealing with their resulting magnetism can be found to date. In the previously mentioned studies, the magnetic anisotropy was enhanced by the linking metal adatoms that show splitting the d-levels of metal linkers by coordination to specifically selected organic ligands. Moreover, in one of these cases the magnetic moment of isolated Ni atoms was recovered by their coordination to TCNQ molecules [156]. Thereby the use of distinct metal-organic on-surface architecture in combination with magnetic adsorbates embedded in the selected molecular guests will provide with versatile systems where the effect that confined surface electrons have on the magnetic signal can be studied in details.

5.2 Results and Discussion

In this chapter was investigated the effect that laterally confined quantum well states have upon the magnetic signal of metal ions of the hosted adsorbates inside the pores of a metal-organic network. These porous on-surface architectures are known to confine the surface states at the pores, generating a periodic array of quantum dots. The selected molecular porous network is formed from the precursor 4,9-diaminoperylene quinone-3,10-dimine (DPDI) that undergoes a surface reaction with thermally activated substrate adatoms. Using this unique nanoporous system, we show the impact of the specific confinement/adsorbate interaction, which can significantly influence magnetic properties of the metal ion from the chosen molecular adsorbate. Here we present a comprehensive study of two different CoOEP and NiOEP molecular adsorbates hosted by DPDI network in order to shed light on the mechanism that lead to changes of transition metal ion magnetic properties due to the network presence. Combination of the Scanning Tunneling Spectroscopy (STS) with X-Ray Magnetic Circular Dischroism (XMCD), Photoelectron Diffraction (PhD) and DFT theoretical

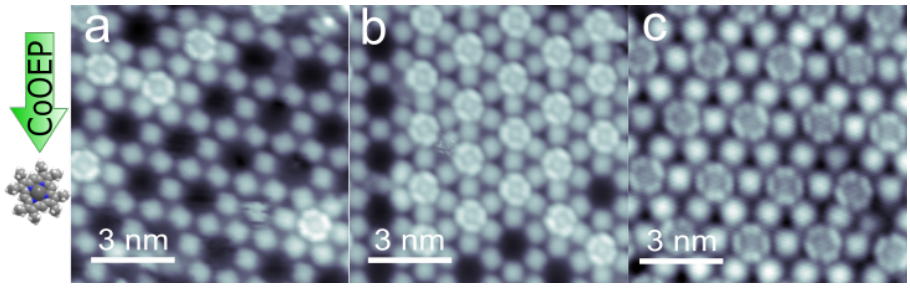

Figure 5.2: *Adsorbate coverage evolution STM topographic images of* ***a-c*** *CoOEP molecules hosted by DPDI network. (STM details: 10×10 nm, 800 mV, 10 pA).*

methods allows to elucidate the charge transfer, hybridization, and correlation at the adsorbate/quantum confinement interface on the magnetic properties. On the basis of its architecture and properties, which were discussed in details in Chapter 3 and Chapter 4, the electronic properties of network itself depends on the electronic levels, bands and resulting hybridization of states.

CoOEP adsorbed across the DPDI network

The first chosen molecular adsorbate was CoOEP Fig.5.2. Notably in original ground state Co metal ion has a d^7 configuration and oxidation state 2^+, which was already mentioned in Chapter 2. The adsorption evolution of CoOEP across the network has been studied by STM. Their topographic appearance already reflect difference from previously mentioned ZnOEP (Chapter 4). The transition metal ion appears as protrusion in CoOEP and as depression in ZnOEP.

To investigate how changes initial quantum confinement due to the molecular adsorbate presence, we used STM/STS techniques providing site specific *"local"* information on the effect of the CoOEP adsorption. Summarizing dI/dV spectra and STM topographs represented in Fig.2.1, all dI/dV spectra were recorded with open feedback loop and with metallic tip. The dI/dV data presented in Fig.2.1(g) were compared to subtracted from the grid spectroscopy spectra presented in Fig.5.3(e,f). Notably, the influence of the CoOEP molecular adsorbed by means of both STS and ARPES has shown similar mechanical and electronic properties as it was discussed in details in case of ZnOEP (Chapter 4). ARPES data presented in the table 5.3 has shown the energy for the chosen configurations are found to be further from the Fermi energy, and bottom of the dispersive band for fully filled DPDI network by molecular CoOEP adsorbates was found at 0.165 eV. In ARPES data the energy positions of the corresponding quantum box states are found to be farther from the Fermi energy than in STS data. These differences are likely related to the technical aspects of each technique. In particular, ARPES averages over the whole illuminated region, losing its local character, and probes the coherent part of the electron wave function, STS is a local technique also sensitive to the non-coherent part. As a result, ARPES can quantify the minimum energy value of the quantum unit state, whereas in STS a large fraction of the projected DOS (convoluted with tip LDOS) contributes to the observed

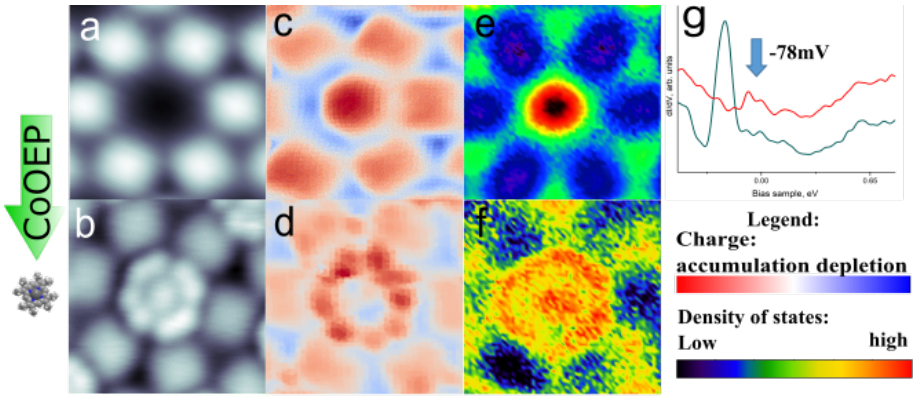

Figure 5.3: *STM topographic images of* ***a*** *a vacant single pore of the DPDI network and* ***b*** *pore occupied by an adsorbed CoOEP molecule (STM details: 2.5 × 2.5 nm^2, 800 meV, 50 pA) and their corresponding acquired charge transfer maps (****c, d****) (lock-in: V_{rms} = 8 mV, 514 Hz, I = 400 pA, U = 1 V).* ***e*** *and* ***f*** *display dI/dV maps recorded at 5 K (lock-in: V_{rms} = 8 mV, 514 Hz, I = 300 pA, U = 70 mV).* ***g*** *comparison of the STS spectra subtracted from grid spectroscopy, in the empty and occupied pore. The shift from -210 meV to -70 meV, can be attributed to the presence of the adsorbate inside the pore.*

dI/dV line shape. In this way, the STS energy maximum shifts towards the bandwidth center as compared to the ARPES result. This results are very similar for previously mentioned ZnOEP molecular adsorbate. From the conductance map represented in Fig.2.1(f) of the occupied pore, we can see that imaged molecular adsorbate despite that fact, that density of states is homogeneously distributed across the molecular core and transition metal ion. The complex interaction between the electronic and geometric structure of the represented molecules adsorbed on solid substrates, in particular the influence of the molecule-network and molecule-confinement intercoupling as well as the resulting electrical conduction and the charge transfer. The observed energetic adjustment and asymmetry of the dI/dV peaks, together with observed typical contrast which follows triple symmetry of the pore, indicates interdot coupling in full agreement with studying presented in Chapter 4.

Controlling spins of Co ion by electronic environment

X-ray absorption spectra of the circularly polarized synchrotron light with opposite helicities – μ^+ and μ^- are presented in Fig.5.4. Case Fig.5.4(a) represents CoOEP adsorbed across the bare Cu(111) surface, which was discussed in details in Chapter 2. In cases represented in Fig.5.4(b,c) CoOEP molecular adsorbate hosted by DPDI network. Taking into account previously mentioned oxidation reduction of the TM ions at the bare Cu(111) substrate (Chapter 2), Co ions preserve different physical properties which they have in an isolated phase, despite the interaction between the CoOEP and the Cu(111) substrate. DFT calculations reveal to 2^+ valency and the *low spin* state of the Co ions for molecules in the gas phase [152]. Following this observation

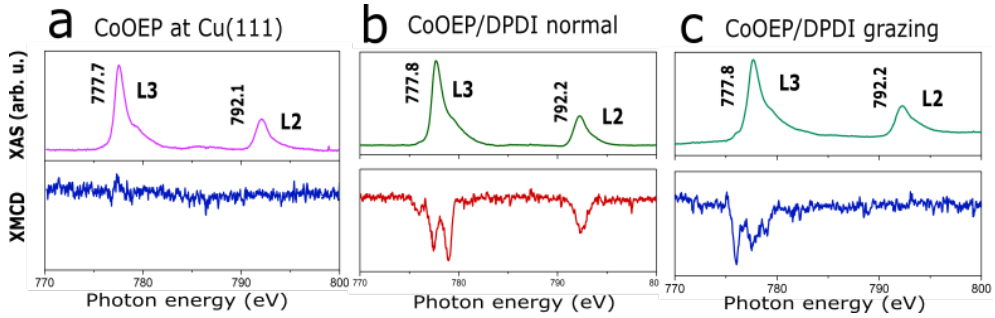

Figure 5.4: *XAS of CoOEP/Cu(111)* ***a****, CoOEP/DPDI/Cu(111) (note, that for both normal and grazing incidents spectra are similar)* ***b*** *in normal and* ***c*** *grazing incident of the incoming synchrotron light. The changes in the spectra point to a charge transfer to the Co ion and a hybridization at the interface. The corresponding dichroic spectra clearly demonstrate and induced magnetic moment in the molecular spin systems. Background subtracted XAS and XMCD, together with normal incidence spectra simulated with multiplet calculations.*

and considering the angular dependence at the energetic position between the fine structure components of the Co L_3 edge – XAS signal appear at ∼777.7 eV, suggesting considerable electronic interaction of the central metal ion with the axial surface-ligand. This clearly shows that supporting substrate quenches the (super)exchange interaction responsible for the antiferromagnetic coupling between the molecule TM ion and the axial surface ligand. This behaviour is observed irrespective of the native oxidation state (Chapter 2), and indicates clear evidence that the magnetization of the Co in CoOEP adsorbed across the Cu(111) substrate is switched off. We assign the *off* state of the molecular spin to the pairing of the initially unpaired spin supplied by the underlying substrate. Means, an assignment of the empty orbitals accessed by excitation of the $2p$ core-level electrons can be quantitatively made. According to ligand field theory, the $3d$ orbitals of the Co ions transform as a_{1g} (d_{z^2}), b_{1g} ($d_{x^2-y^2}$), b_{2g} (d_{xy}), and e_g ($d_{yz,xz}$) in a C_{4v} symmetry, which is expected for planar adsorbed CoOEP molecules. According to DFT calculations for isolated CoOEP [152], the b_{1g} ($d_{x^2-y^2}$)) state is highest in energy and completely empty. It can therefore be related to the energetically higher lying broad peak with a maximum at 779.5 eV, whereas the a_{1g} (d_{z^2}) state is half filled and can be related to the narrow peak at 777.7 eV. However, the e_g ($d_{yz,xz}$) and a_{1g} (d_{z^2}) states could also together carry one hole if to take into account mentioned before multiplet calculations. Furthermore, when CoOEP molecules are adsorbed across the DPDI network, the astonishing presence of a finite Co XMCD signal proves on one hand a net $3d$ magnetic moment localized on the Co ions and on the other hand an unexpected magnetic coupling between the quantum confinement and the Co ions. Co $L_{2,3}$ XAS of CoOEP hosted by DPDI network shows almost the same line shape as the one for the Co at the bare Cu(111) surface, indicating electronic coupling between the TM ions and the quantum confinement, whereas for Cu(111), Ag(110) and Ag(111) interactions were reported [152, 74], to partially reduce the Co^{2+} ions.

In the dichroic spectra Fig.5.4(b,c), magnetic molecule show a magnetization, as characterized by the three peaks at the L_3 edge and one peak at the L_2 with 776.0 eV, 777.5 eV, 779.0 eV and 792.2 eV respectively. Similar shape of the XAS was reported for single Co atoms and CoTPP molecules adsorbed across graphene surface [157, 158]. The isotropic Co L_3 edge XAS spectra, measured at the magic angle of 35° grazing incidence (Fig. 5.4(c)), has a main peak at 777.7 eV and L_2 at 792.3 eV, corresponding dichroic spectra has main peaks at the same energy positions as for normal incident. XMCD signals match each other in size and positions, but in case of the normal incidence the orbital moment of Co ions is dominating significantly, while in grazing it is almost vanished.

By employing the XMCD spin sum rule on the Co dichroic spectrum measured at 2 K and in 7 T magnetic field, an effective spin moment of $m_s = (0.11 \pm 0.01)\ \mu_B$ and $m_{S+7D} = (0.02 \pm 0.01)\ \mu_B$ for normal and $m_s = (0.06 \pm 0.01)\ \mu_B$ and $m_{S+7D} = (0.07 \pm 0.01)\ \mu_B$ were obtained. The effective spin magnetic moment fits to a low-spin S=1/2 configuration of the Co ions. The XA spectrum as well as XMCD spectra exhibit a particular finestructure at the Co L_3 edge, which by comparison to the CoPc bulk measurements is consistent with a antiferromagnetic coupling (AFM) between CoOEP in contact with present quantum confinement is clearly identified by the negative sign of the L_3 and L_2 dichroic signals in the representative spectra. Such similar AFM coupling was observed for single adsorbed molecules at the different interfaces [159, 160, 125]. Following numerical calculations based on the density functional theory, and our experimental observation this coupling occurs by superexchange through Co ions in combination with N and C atoms of the porphine core and present quantum confinement [161, 86, 162]. XAS experiments were aquired in total electron yield mode recording the sample drain current as a function of photon energy, while monitoring the incoming beam intensities by the total electron yield of a freshly evaporated gold grid. Measurements were taken at XTREME beamline at the Swiss Light Source in PSI, Villigen. Furthermore, the XAS were normalized to the corresponding spectra measured of the clean substrate and scaled to 1 in pre-edge energy region. The photon energy resolution was set to . Typical photon flux densities at the sample of about 10^{12} $s^{-1}cm^{-2}$ were used to prevent radiation damage, which can be excluded here from the comparison of spectra taken immediately after sample preparation and at later times. The X-rays propagation vector and magnetic field vector are in both cases collinear.

NiOEP adsorbed across the DPDI network

Second chosen molecular adsorbate was NiOEP Fig.5.5. In comparison to the Co, Ni ion has a d^8 configuration and ground state of the molecule in the gas phase is 2^+. To check if electronic and mechanic properties of the proposed metal-organic network differ due to the presence of NiOEP adsorbate, was employed STM and STS measurements. The dI/dV data presented in Fig.5.5(g) were compared to subtracted from the grid spectroscopy spectra presented in Fig.5.3(e,f). Notably, the influence of the NiOEP adsorbate has shown similar mechanical and electronic properties as it was mentioned for ZnOEP and CoOEP before. ARPES data presented in the table 5.2 has shown the energy for the chosen configurations are found to be further from

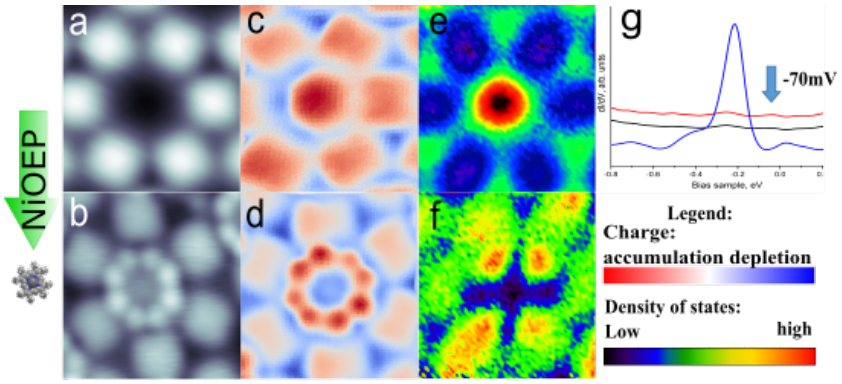

Figure 5.5: *STM topographic images of* ***a*** *a vacant single pore of the DPDI network and* ***b*** *pore occupied by an adsorbed NiOEP molecule (STM details: 2.5 × 2.5 nm², 800 meV, 50 pA) and their corresponding acuired charge transfer maps (**c, d**) (lock-in: V_{rms} = 8 mV, 514 Hz, I = 400 pA, U = 1 V).* ***e*** *and* ***f*** *display dI/dV maps recorded at 5 K (lock-in: V_{rms} = 8 mV, 514 Hz, I = 300 pA, U = 70 mV).* ***g*** *comparison of the STS spectra subtracted from grid spectroscopy, in the empty and occupied pore. The shift from -210 meV to -70 meV, can be attributed to the presence of the adsorbate inside the pore.*

the Fermi energy, and bottom of the dispersive band for fully occupied DPDI network was found at 0.140 eV. Same as before, these differences in STS spectra and ARPES data are related to the technical aspects of the techniques. This observation is very similar for previously mentioned systems (Chapter 4 and CoOEP case). Furthermore, proposed system was investigated on the local level by means of STS (Fig.5.5(d,f)). From the conductance map represented in Fig.5.5(f) of the occupied pore, we can see that imaged adsorbate despite that fact, that density of states is almost vanished on the porhine core but concentrated on the ethyl groups of the molecule.

Controlling spins of Ni ion by electronic environment

Referring back to the crystal field theory for four coordinated Ni^{2+} complexes a detailed calculation has been made for tetragonal and tetrahedral symmetry [163]. However these spanned a limited range of parameters and could only be applied to a general discussion of the correlation of magnetic moment and structure. One set of results that are immediately available from the calculated energies are the minimum field strengths necessary for a change in the magnetic moment of the Ni^{2+} ion. A change in magnetic moment from the free ion value would then be the result of nothing more than an electrostatic interaction in excess of this specified magnitude. No abrupt change in the nature of the interaction, nor in the symmetry of the molecule need be postulated, and no a priory correlation of magnetic moment and structure can be made. This approach is in sharp contrast to the standard correlations between bond type, magnetic moment, and structure which resulted from the valence bond approach applied to the problem of complex molecules. A search of the literature revealed however, that such correlations had not been proven, either theoretically by independent energy and bond

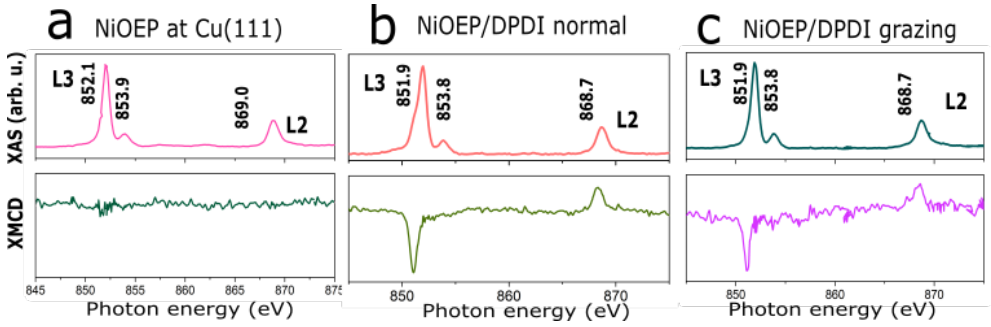

Figure 5.6: *XAS of NiOEP/Cu(111), notably, grazing and normal incidents looks the same* ***a****, NiOEP/DPDI/Cu(111)* ***b*** *in normal and* ***c*** *grazing incident. The corresponding dichroic spectra clearly demonstrate and induced magnetic moment in the system.*

type calculations, nor experimentally by proofs of structure for pertinent compounds. The ligand field picture offers one plausible interpretation of the magnetic moments of Ni^{2+} complexes. The electron configuration for the ground electronic state of a weakly tetragonal Ni^{2+} complex can be written as $t_{2g}^6 e_g^2$, the addition of the eights electron results in a partially filled d shell. The crystal field stabilization energy is zero. The presence of the two electrons in the unfavorable e_g state exactly balances the stabilization resulting from the six electrons in the t_{2g} level. Thus we see that even for a rigorously square planar Ni^{2+} complex it is possible to have a paramagnetic ground state. This situation is entirely analogous to that which gives rise to the low-spin complexes and S = 0.

The electronic and magnetic properties in both cases while NiOEP is adsorbed at the bare surface and across the network was investigated by element-specific X-ray absorption spectroscopy (XAS) and X-ray magnetic circular dichroism (XMCD) measurements (Fig.5.6). Concerning control of the magnetic moment and axial coordination, only off-switching and spin tuning have been established so far [87, 120]. Also this set was incomplete since the spin-off $\rightarrow$ spin on case of the single molecules was missing. Switching the spin in molecular adsorbates by presence of quantum confinement to the on-state is more difficult than switching it off. An addition obstacle in realization of this process can come from the possibility that underlying electronic structure can modify the spin states. For $3d$ transition metals, the absorption cross-section at the L_3 and L_2 edges ($2p \rightarrow 3d$ electronic transitions) provides element-specific information on the magnetization of the surface adsorbed transition-metal molecular complexes. For native NiOEP at the Cu(111), the absence of an XMCD signal demonstrates that the adsorption of the molecules on the bare surface alone does not induce a magnetic dipole moment in the Ni^{2+} central ion (Figure 5.6(a)). The presence of the DPDI network, however, results in a clear XMCD signal evidencing the presence of a magnetic moment on the Ni (Fig. 5.6(b, c)). The $spin - on$ state is characterized by a AFM coupling to the substrate as indicated by the negative sign of the dichroic spectra. Such coupling for paramagnetic porphyrins and phthalocyanines in contact with paramagnetic substrates has been observed earlier and studied in detail [159, 160].

The magnetic signature in the sequential processes that is, the switching between the molecular $spin - off$ and $spin - on$ states occurs in the presence of the quantum confinement and its exchange interaction with the central metal ion of the molecule.

In the same manner as before, by employing the XMCD spin sum rule on the Ni XMCD results obtained at 2 K and in 7 T magnetic field, an effective spin moment of $m_s = (0.07 \pm 0.01)\ \mu_B$ and $m_{S+7D} = (0.47 \pm 0.01)\ \mu_B$ for normal incidence were obtained. our-coordinated Ni^{2+} complexes are usually in the low-spin (S=0) state. Ni^{2+} ions with a coordination number of five (square pyramidal) or six (octahedral) are usually paramagnetic high-spin (S=1) species. However, the nature of the quantum confinement is similar to chemical ligand, that is, whether it acts as σ donor or as π acceptor. Presented XAS results confirms that fact, the effective spin magnetic moment fits to a high-spin S=1 configuration of the Ni ions. The XA spectrum as well as XMCD spectra exhibit a particular finestructure at the Ni L_3 edge, which by comparison to the CoPc bulk measurements is consistent with a antiferromagnetic coupling (AFM) between NiOEP in contact with present quantum confinement is clearly identified by the negative sign of the L_3 and L_2 dichroic signals in the representative spectra. Such similar AFM coupling was observed for single adsorbed molecules at the different interfaces [159, 160, 125]. Following numerical calculations based on the density functional theory, and our experimental observation this coupling occurs by superexchange through Ni ions in combination with N and C atoms of the porphine core and present quantum confinement [161, 86, 162].

Measuring adsorbate-substrate distance in the selected systems

The strong correlation between the magnetic moment tuning and adsorption on metal surfaces, with molecules and axial ligand forming local bonds to individual atoms withing a metal substrate, have been established over many years of studying. The recently proposed "surface trans-effect" appears to be a further manifestation of this analogous behavior [87, 90, 131], but so far the tru nature of the modified molecule-metal surface bonding has been unclear. In the scientific literature is available studyings, where by use of X-ray standing waves, we demonstrate that ligation of ammonia and water to iron phthalocyanine (FePc) on Ag(111) increases the adsorption height of the central Fe atom; dispersion corrected density functional theory calculations accurately model this structural effect [90]. In particular, the local bonding of molecules to metal substrates has been found to commonly reflect the local atomic, rather than delocalized metallic, character of the surface [87, 164, **?**] Recently, spectroscopic measurements on the adsorption of planar metallo-complexes on metal surfaces have been interpreted as evidence for one further example of this analogue behaviour, namely the "trans-effect" in metal coordination chemistry [87, 120]. Here we provide quantitative structural measurements that clearly demonstrate that this surface induced trans-effect does indeed occur in studied system.

The presence of the magnetic moment in TM ions of molecular adsorbates hosted by DPDI network determins different adsorption hight. The TM ion is expected to be pulled up from porphyrin plane in z axis, if to take into account *trans* effect. To determine the adsorbate TM-substrate distance d_{TM-S} between the TM ion of

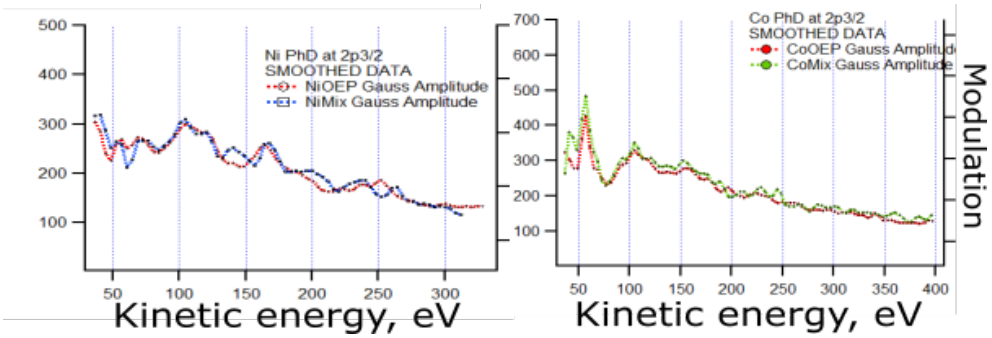

Figure 5.7: *One dimensional modulation functions extracted from the experimental data at NE for selected systems.*

Table 5.1: *Summary for d_{TM-S} simulated 1D modulation at NE.*

experiment	d_{TM-S} Å	distance
NiOEP/DPDI	bridge	3.24
NiOEP/bare	top	2.21
CoOEP/DPDI	fcc	2.49
CoOEP/bare	fcc	2.55

the molecular adsorbate and the underlying substrate, the Photoelectron Diffraction (PhD) intensity modulation of the metal $2p_{3/2}$ peaks was measured as a function of the electron energy and simulated numerically using specific cluster code EDAC. In the simulations several structural and non-structural parameters are optimized using a particle swarm global search algorithm, which minimizes the R-factor. The optimized parameters are the adsorbate-surface distance d_{TM-S}, the possibly relaxed distance between the TM and neighboring nitrogen and carbon atoms, the size of the cluster, the crystal structure of the surface and the amplitude of the modulation function. The measured modulation function was normalized and Fig. 5.7 shows a line profile $\chi(\mathrm{E}_{kin})$. The corresponding simulations are shown in the table 5.1. R-factor results from over 10000 calculated configurations as a function of d_{TM-S}, the main parameter of interest. Represented data shows strong dependence of the adsorption parameter where the minimum R-factor designes the best fit value, and the width of the distribution can be used to estimate adsorption difference for central metal ion of the molecule adsorbed across the bare Cu(111) and across the DPDI network.

5.3 Conclusions

This work shows the interplay between the spin and orbital degrees of freedom in systems at the border of metal ions atoms of the molecular adsorbates and present quantum confinement. As such, it provides microscopic understanding of materials with perpendicular magnetic anisotropy, which are required for further downscaling of spintronic devices. Despite the very large magnetic anisotropy, the coupling of d-electrons

of the transition metal ion to the environment makes the spin lifetime of transition metal atoms very sensitive to perturbations caused by the ligand field and scattering from conduction electrons. Judging from the knowledge accumulated on magnetic properties switching or tuning and this work, CoOEP/DPDI and NiOEP/DPDI represent a very favorable combination for the miniaturization of magnetic data storage devices beyond the present technological limits. On a more fundamental note, this results show that the combination of STS and XAS is extremely powerful to describe the many-body interactions. Up to this moment only *spin-on* $\rightarrow$ *spin-off* switches and *spin tuning* had been established, but a *spin-on* switching was missing. This operation is realized in case of the low-spin d^8 Ni^{2+} and converted to the Ni^{3+} complex with its high spin state by the combination of the charge transfer and quantum confinement/adsorbate interaction. The paramagnetic Cu bare surface quenches magnetic moment of the NiOEP and CoOEP complexes, but by presence of the organo-metallic DPDI network, i.e. electronic barrier, this system presents $spin - on$ switch. In conclusion, was demonstrated how the magnetic properties of Co and Ni ions of molecular adsorbates hosted across the metal-organic network can be tailored by choosing the appropriate electronic environment. In particular, the complex interplay between the $3d$ orbitals and the quantum confinement, modified by the underlying substrate, can generate significant magnetic moments and perpendicular magnetic anisotropy in Co and Ni atoms, two fundamental requirements for information storage devices. Axial coordination between quantum confinement and molecular adsorbate can also be used to control magnetic anisotropy as well as the strength and sign of the exchange interaction. The complexity of the obtained results asks for theoretical investigations which may capture the complex interaction of the molecular adsorbates with a present quantum confinement. This approach is able to provide benchmark results for first principle calculations to be assessed and improved towards the more accurate prediction of the properties of nanostructures.

Details of the experimental methods

It is well known that both the electron density and the local density of the surface states near the Fermi level energy play a critical role in determining the STM image [165]. STM imaging of electronegative or electropositive elements, for example can result in the observation of anomalous heights [153]. Another classic example is the observation of the dangling bonds on the silicon surface [166]. It is clear in the present case that the occupancy of the d-orbitals is playing a significant role in the STM image. In the presented chapter being recorded with the same parameters, Co^{2+} is acting as a conductor, while Ni^{2+} is not.

ARPES and PhD measurements which are presented in this chapter were performed at the PEARL beamline at Swiss Light Source, PSI (Villigen, Switzerland) [65]. Essentially, beamline covers the photon energy range from 60 to 2000 eV. Experimental end station is divided into three sub-systems: one (attached to the beamline) for the photoemission measurements, one for LT-STM and one for *in situ* sample preparations. The photoemission station is designed as a state-of-the-art ARPES facility with

Table 5.2: *Summary for electronic structure bulk bands and Fermi energy found for studied systems.*

	SS bottom, eV	molecular states, eV	
DPDI	0.260		1.4
CoOEP	0.325	0.8	1.68
CoOEP/DPDI	0.165	0.83	1.69
NiOEP	0.335		1.02
NiOEP/DPDI	0.140	0.54	1.02

a *Carving 2.0* six-axis manipulator and *Scienta EW 4000* hemispherical electron analyzer with two-dimensional detection. The entrance slit of the analyzer is oriented vertically (parallel to the main axis of rotation), in this operation, the symmetry of the differential photoemission cross section with the respect to the light polarization allows for a homogeneous illumination of the detector. All presented spectra were recorded at ∼100K, and in normal emission mode.

Magnetic measurements exploiting XAS and XMCD spectra presented in were performed at the XTREME beamline, SLS located at PSI. XTREME end station is equipped with one Apple II type undulator producing linearly and circularly polarized photons with maximum flux of 4.7×10^{12} photons/second. Optics of the beamline allows working in wide energy range from 150 eV up to 2000 eV, what corresponds to the 31^{st} harmonics. Experimental chamber at the beamline is equipped with pumped Helium cryostat, which allows measurements at T = 2 K. Experimental chamber is equipped with a vector magnet, which can produce magnetic field of strength 7 T along the beam direction. Spectra measured at XTREME beamline were acquired in TEY mode and normalized to the flux intensity of the incoming beam [64]. Circularly and linearly polarized XAS measurements at Co and Ni $L_{2,3}$ absorption edges were performed in the total electron yield (TEY) mode. The base pressure in the measurement chamber was 1.0×10^{-10} mbar, and the temperature was always kept at the minimum reachable value, i.e., 2 K. The external magnetic field B (always parallel to the incident photon beam) was applied either at grazing incidence i.e., at an angle $\Theta = 70^\circ$ with respect to the surface normal – see Fig. 1.10 or at normal incidence ($\Theta = 0^\circ$). To avoid sample degradation induced by the synchrotron radiation, was employed a reduced beam intensity and carefully monitored for possible changes in the XAS spectra. We also took care to minimize the radiation dose, exploiting the whole sample surface changing regularly the irradiated sample region. The XMCD spectra are defined as the difference between the XAS spectra taken with the helicity of the incident photon anti-parallel and parallel to the external field normalized to the height of the XAS edge.

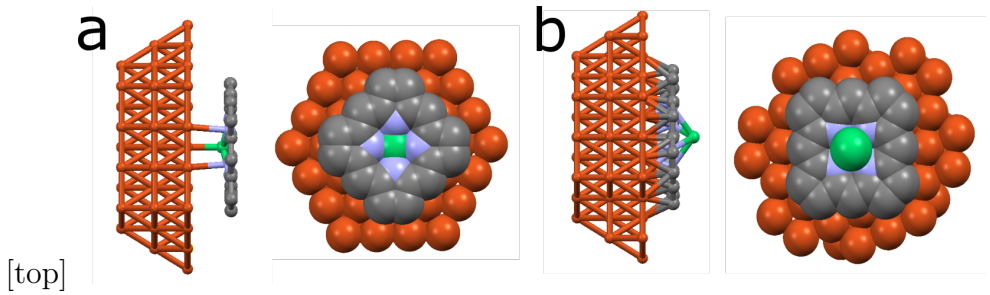

Figure 5.8: *Optimized DFT models used in numerical simulations of PhD energy scanned mode for* ***a*** *adsorbed at the bare surface and* ***b*** *inside the pore.*

6 Magnetically anisotropic trigonal prismatic manganese complexes at noble surfaces

Innumerable molecules can be considered as interesting for organic based electronic devices coming along with similar high diversity of chemical structures and associated properties. Targeting the goal to control displacements and electronic states of the molecules at the surface, the interplay between molecules and underlying substrate has to be understood. Magnetic properties have traditionally been associated with infinite solids, such as bulk metals, or infinite inorganic polymeric solids of variable dimensionality. For an understanding the mechanism of the modification due to the mutual influence between a molecule and a surface in close proximity towards each other, at first one needs to know the general characteristics of the initial molecule and the surface. In contrast to much studied commercially available planar transition-metal phthalocyanines and porphyrins [76, 87, 167, 149] shown comparative investigation of crystal growth of on-surface assembly *in situ* between Au (111) acting as an underlying substrate and novel Mn complex with thriagonal prismatic geometry, which in crystalline bulk samples exhibit unusual magnetic properties.

6.1 Introduction and Motivation

The last decade has seen a remarkable growth in the number of paramagnetic metal complexes deposited on varied crystalline substrates. Both magnetic and non-magnetic interactions have been investigated at the metal substrate interface. The majority of reports of the magnetic properties of surface-deposited paramagnetic molecules on metal substrates have used planar neutral molecules. Recently, the successful sublimation of the 7-coordinate [Er(trensal)] compound demonstrated that it was possible to self-assemble complexes with complex geometries on metallic substrates and that surface magnetic interactions could be successfully probed [168] in contrast to the commercially available planar transition-metal phthalocyanines and porphyrins [76, 87, 167, 149], we have prepared Mn complexes with triagonal prismatic geometry exhibiting unusual magnetic properties in the bulk crystalline samples. The complexes

comprise an ionic compound with both an organic anion and an organic cation i.e. a completely different chemical architecture which can be deposited by sublimation. The novelty of this ionic system motivates to study the surface supported chemical recombination and interactions of the highly anisotropic manganese complexes described in This chapter.

6.2 Results and Discussion

The molecular structure of the manganese complex $[Mn(3\text{-}OEe\text{-}sal)_2pip]BPh_4$ studied in this work is presented in Fig.6.9(b). The structural details of the metal complexes, in particular the coordination environment of the metal ions, are sensitive to the kind of $3d$ metal ion involved. According to single-crystal x-ray diffraction each Mn^{2+} ion is situated in a distorted thriagonal prismatic N_4O_2 coordination sphere. The magnetic properties of the polycrystalline samples were determinated between 10 K and 250 K. The χT values of these latter complexes typically show an increase in their magnetic moment up to temperatures as high as 250 K. At lower temperatures, e.g. at 10 K this value rises almost to impressive 6 cm^3 mol^{-1} K. This suggests a strong concerted magnetic response to external magnetic fields. The magnitude of the observed effects suggests that the ions in the aligned crystalline form exhibit an easy axis for magnetization. This concerted response was sufficiently strong that single crystals could be attracted to a neodymium magnet after brief cooling in a liquid nitrogen bath. The cationic metal-ligand assembly is charge-balanced in the crystal by a polyatomic counter-anion. Our preliminary work demonstrates that sublimation of mono- and multilayers of positively charged thriagonal prismatic Mn metal-organic complexes on non-magnetic Au(111) and Cu(111) substrate is possible with preservation of molecular integrity. The molecular monolayers were investigated systematically with a combination of STM and XPS.

Molecular geometries and synthesis of the manganese complexes

Note that chemical synthesis of the compounds used in this study have been performed by Vibe Boel Jakobsen from University college Dublin (Dublin, Ireland).
The manganese triagonal prismatic complexes were synthesized by the following receipt:
• $[Mn(3\text{-}OEe\text{-}sal)_2pip]BPh_4$ to a well stirred solution of 1,4-bis(3-aminopropyl) piperazine (1 mmol, 0.205 mL) in 50:50 solution of acetonitrile/ethanol ratio (20 mL), 3-ethoxysalicylaldehyde (2 mmol, 0.332 g) was added forming a yellow solution, which was stirred for 15 min. Solid manganese 3^+ chloride hexahydrate (1 mmol) in 50:50 acetonitrile/ethanol (10 mL) was added to the solution resulting in a black liquid followed by ammonium tetrafluoroborate (1 mmol), stirred for 15 min before gravity filtered. Large dark green crystals of suitable quality for X-ray crystallography were formed upon slow diffusion of diethylether into the solvent. Yield = 5 %. Non planar Mn-based molecular complex was obtained as dark green cubic crystal after evaporation of the metal-acetonitrile solution of the complex at the room tempera-

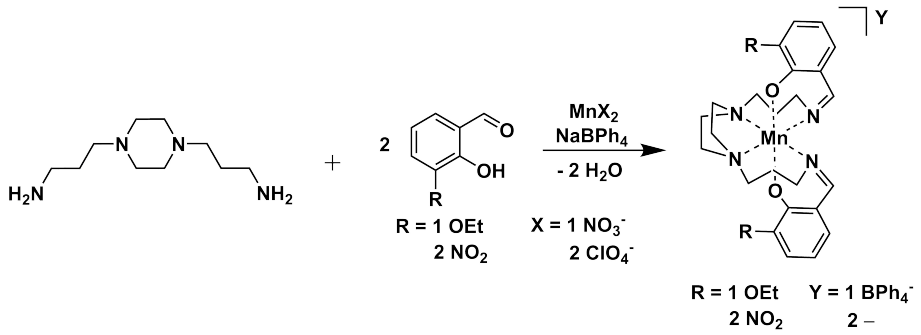

Figure 6.1: *Synthesis of Mn(3-OEe-sal)$_2$pip BPh_4 and Mn(3-ON_2-sal)$_2$pip complexes.*

ture. The compound chrysalises with distinct manganese cation and BPh_4 anion 7,265 $\mathring{A}$ apart, in the asymmetric unit. The molecular structure of the complex is shown in the Fig.**??**. The geometry around each manganese centre is octahedral with two tridentate ligands in a facial arrangement with two trans-phenolate (O2–Mn1–O2), trans-amine (N2–Mn1–N2) and trans-imine (N1–Mn1–N1) donors. Packing interactions were therefore examined in order to investigate the effects of hydrogen bonding or other types of connectivity in driving an asymmetric or symmetric Jahn–Teller-like distortions [169, 170]. The asymmetric units of complex comprise one full occupancy cation and one full occupancy anion. Theory element ratio for $C_{52}H_{58}BN_4O_4Mn$ is: C 71.89, H 6.73, N 6.45 in calculated theory and C 71.92, H 6.67, N 6.41 estimated from experiment.

• Mn(3-ON_2-sal)$_2$pip: to a solution of 3-nitrosalicylaldehyde (0.200 g, 0.1 mmol) in 10 ml 1:1 ethanol/ acetonitrile ratio, 1,4-bis(3-aminopropyl)piperazine (0.334 g, 2 mmol) in 10 ml 1:1 ethanol/acetonitrile ratio was added to give a yellow coloured solution which was stirred for 10 min. A solution of manganese 2^+ perchlorate hydrate (0.254 g, 1 mmol) in 5 ml 1:1 ethanol/acetonitrile was added into the Schiff base ligand solution resulting in the formation of a clear green solution which was stirred for 15 min and then left undisturbed. After 4 h of slow evaporation of the solvent orange needle crystals of suitable quality for single crystal X-ray diffraction had formed. Yield (88.3 mg, 16.0 %). Elemental analysis for $C_{24}H_{28}N_6O_6Mn$ shows C 52.28, H 5.04, N 15.19 in calculated theory and C 52.27, H 5.12, N 15.24 ratio, which was estimated experimentally. Finally, both crystals show octahedral packing motif where two basal planes are slightly offset. This pattern of parallel planes persist through the whole crystal. One explanation for the magnetic response is that there is an easy plane and the spins on every ion line up with the applied field in a single domain sample.

Molecular complexes at the Au(111) surface

Non covalent self-assembly of molecular units on metallic surfaces is now a well-established route for growing an extensive range of atomically well-defined nanostructures [171, 172]. This approach is extremely versatile, and the design of the product can, in principle, be controlled by the molecular precursors, the temperature, and selection of the supporting surface. At this point, there are several challenges, including

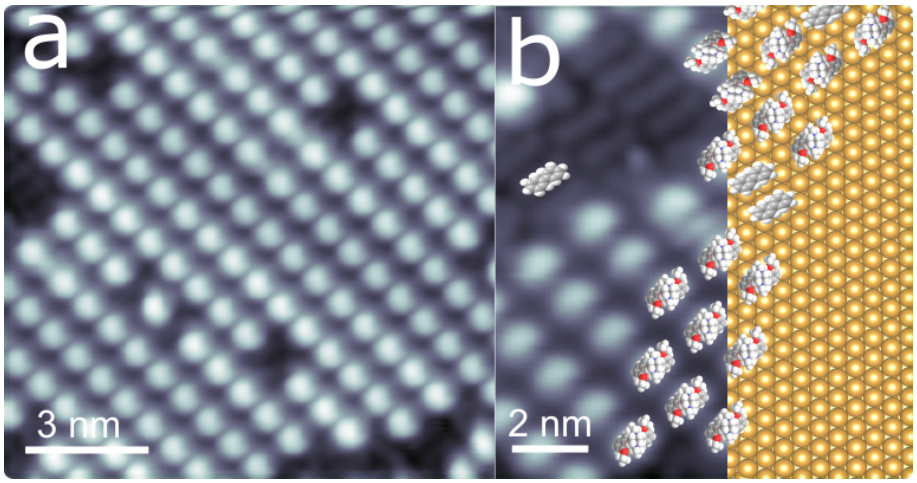

Figure 6.2: *Manganese ionic complex at the Au(111) surface.* ***a*** *overview of the closed pack structure,* ***b*** *observed deffect which consists of two monolayers and proposed model. STM details: 400 mV, 10 pA.*

scaling-up production of high quality nanostructures, characterizing the results in bulk and discovering new molecular precursors, which often involves significant amounts of trials and errors. Here, is shown for the first time self-assembly of manganese triagonal prismatic complexes at the surface investigated by combination of STM, XPS and XAS. The STM experiments were performed using LT-STM operated at 5 K and in ultra high vacuum conditions ($p = 1 \times 10^{-10}$ mbar). Clean and atomically flat Au(111) substrate was prepared *in situ* followed by deposition of sublimation of the molecules at $\sim 120°$. Two different adsorption configuration of the manganese complex were found (see Fig.6.2 and Fig. 6.5). Notably, Fig.6.2(a) shows closed pack structure of the molecules, which is following herringbone reconstruction of the underlying Au(111) substrate. Nevertheless, this structure has defects, and closer overview presented in Fig.6.2(b) shows, that proposed prismatic structure of the manganese complex was recombined while reached the surface.

The principle of recombination of halogen-based covalent self-assembly on surfaces was for the first time demonstrated on Au(111) by Grill and coworkers [173, 174], who used the tetraphenylporphyrin molecule with specific hydrogen atoms replaced by bromine. Since bromine atoms split off at lower temperatures than their hydrogen counterparts, unsaturated carbon atoms at predefined positions are generated, enabling coupling into covalent dimers, chains, and smaller 2D structures. First principles studies of adsorption of different amine- or thiolate- terminated molecules at the Au(111) have been reported. It was predicted, that ammonia is adsorbed at the top site. Phenylthiolate is attached to the bridge site and the phenyl ring is strongly tilted with respect to the Au surface [175, 176]. Despite active research, the exact bonding structure of self-assembled thiolates on the Au(111) surface is still an actively debated issue [175, **?**]. Less is known about amine adsorption on the Au surface. Therefore, a comparative study of adsorption of amines and thiolates on Au surfaces in the context of electron transport calculations is necessary.

In order to investigate if recombination process in manganese complex has similar phenomena as in previously mentioned cases, XPS technique was employed. The represented spectra Fig. 6.3 shows elemental composition of the complex, which fully agrees with theoretical estimation. But it is worth to notice, that sign of the B1s was not observed in XPS not for the monolayer, neither for multilayer. This we assign to the second step of the recombination process in manganese thriagonal prismatic molecule, in particular deboronation of the BPh_4. XPS was used to estimate the coverage of the manganese compound and to verify the stoichiometry after deposition. Also by XPS, the element-specific chemical environment (analysis of C1s, O1s, N1s and expected B1s signatures) was tracked. A monochromatized Al Kα X-ray source was used. The instrumental setup gives a full width at half-maximum (FWHM) of 1.0 eV. The energy calibration was performed using a Au(111) reference. All XPS data were obtained at RT, and the spectra were recorded in normal emission unless stated otherwise.

Tetraphenylborates are often studied in organometallic chemistry because of their favorable solubility in non-polar solvents and their crystallinity. The tetraphenylborate anion BPh_4^- is often used as a weakly coordinating anion in coordination chemistry. In some cases the phenyl rings of the BPh_4^- anion have been reported to interact with the metal center. The anion is often used to stabilize unsolved cationic complexes that would normally not be isolable [177, 178, 179]. However, there are a small number of examples of the tetraphenylborate anion reacting on the formation of complexes. Similarly, sodium tetraphenylborate has been used to isolate complexes containing dinitrogen ligands. Although BPh_4^- can be considered to be a stable countering in many reactions, the B–C bonds in BPh_4^- can also be cleaved to liberate benzene under strongly acidic and/or forcing conditions of temperature. These reactions can result in the formation of diphenyl- and triphenylborates. There are several possible mechanisms for the observed methanolysis of tetraphenylborate and the formation of biphenyl. Although phenyl fracture due to protic acids can be discounted in this case, phenyl group transfer from BPh_4^- to metal centers is well known and could initiate the formation of dimethoxydiphenylborate. Alternatively, the radical decomposition of tetraphenylborate to give biphenyl, after oxidation, and borate derivatives perhaps provides the most likely mechanistic pathway in this case. A possible mechanism is outlined in Fig. 6.4. As a result, the diphenyl adsorbs above the three-Au triangle on the Au(111) surface in planar mode Fig. 6.2 [174].

Due to the surface driven deboronation of the BPh_4^-, as a result we have by-product of decomposition, biphenyl, within the lattice assembled into the closed-pack structure, which is following herringbone reconstruction of the underlying Au(111) substrate. Furthermore, cation part of the manganese thriagonal prismatic complex - $Mn(3-OEe-sal)_2$pip$^+$ reassembles on top of the biphenyl layer also in the closed-pack manner Fig. 6.2(a). As it was mentioned before, two different assemblies of the manganese complex coexist at the Au(111) surface. And in the case of absence of the biphenyl assembly, which acts as insulating layer, $Mn(3-OEe-sal)_2$pip adsorbs into Kagome lattice Fug. 6.5. The coordination self-assembly of a series of peripheral bromo-phenyl and pyridyl substituted porphyrins with Fe was studied on Ag(111) surface and graphene [180, 181, 182]. in our case, the $Mn(3-OEe-sal)_2$pip is func-

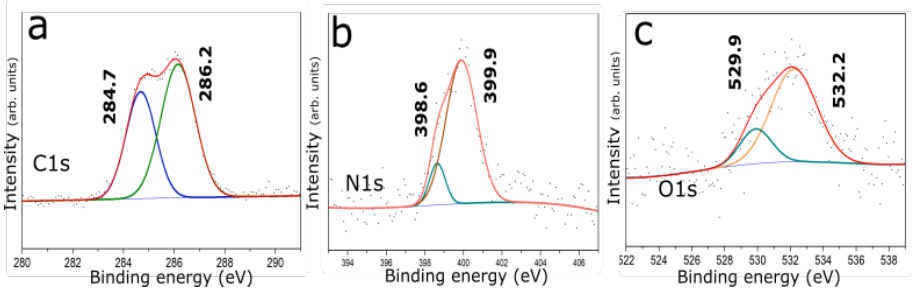

Figure 6.3: *XPS spectra for monolayer of manganese complex at the Au(111) substrate. Corresponding spectra for C1s, N1s and O1s elements.*

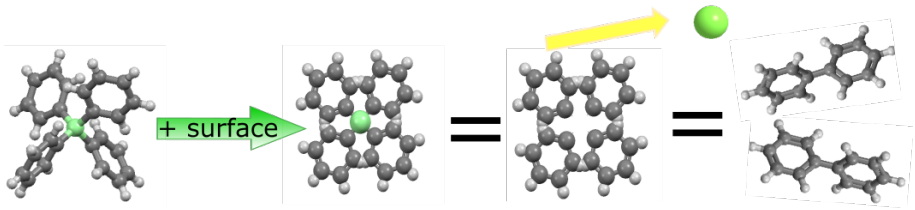

Figure 6.4: *Proposed model for recombination of the BPh_4.*

tionalized with two OEt groups generate discrete rosette and extended chiral Kagome framework structures. From the high resolution image shown in Fig. 6.5, the lattice constant of the hexagonal unit is determined to be 3.13 ± 0.05 nm (between centers of neighboring cavities). The hexagon unit consists of six molecules. Three adjacent molecules are linked through their terminal OEt groups in a three-fold binding mode. Each molecule, which displays a two-lobe submolecular feature, connects with four neighboring porphyrin molecules in a corner-to-corner manner, thus constructing the hexagonal lattice. Most probably, by varying the central metal ion of the molecule affords Kagome lattices with tunable molecular spins, providing ideal 2D model systems for studying spin frustration.

A Kagome lattice is a geometric arrangement consisting of interconnected triangles and hexagons. This structure has been of interest because of its relevance in terms of novel physical properties related with geometrically frustrated magnetism. However, natural Kagome structures are very rare. In represented studying Kagome lattice have been synthesized through supramolecular assembly after several steps of recombination, which exhibit interesting electronic and magnetic properties at room temperature. We assume, that presented Kagome lattice was fabricated due to the van der Waals interactions between OEt groups of the building block. Notably, as it is shown in Fig. 6.5(c), weakly bonded Kagome lattice is able to confine surface electrons. dI/dV spectra was recorded in the middle of nanocavity. Energy position of the present quantum confinement was observed at -230 meV below Fermi level. STM details: 800 mV, 50 pA, lock-in: V_{rms} = 16 mV, 514 Hz, I = 400 pA, U = 800 mV. Interestingly, it was difficult to get any submolecular-resolution STM topographs revealing the molecular orbitals of Mn complex. Which suggests that self-organized diphenyl pattern can act as a buffer layer and efficiently decouple the molecules from the metal substrate, pre-

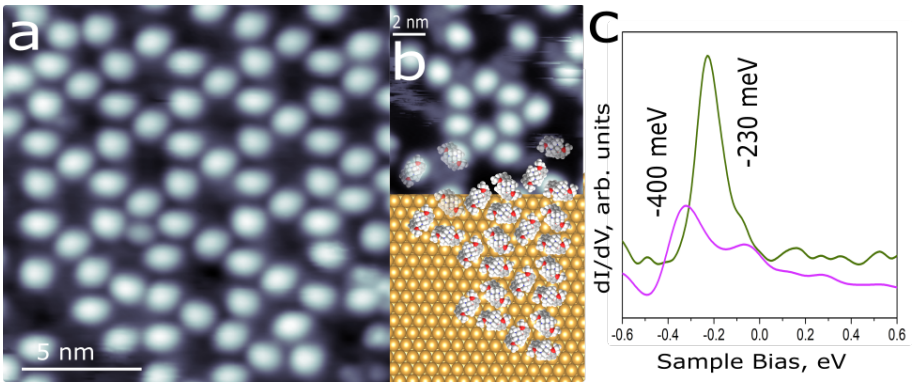

Figure 6.5: *Manganese ionic complex at the Au(111) surface.* ***a*** *overview of the Kagome pattern assembly,* ***b*** *Single chiral pore,* ***c*** *dI/dV spectra recorded at the center of the pore (green line) in comparison with present surface state of the Au(111) (pink line). STM details: 400 mV, 10 pA, lock-in: 16 mV, 514 Hz.*

serving the intrinsic electronic properties of the molecules. This is highly desirable for investigating spin properties of Kagome lattices, as it is known that electronic coupling between molecules and the metal substrates upon which they directly lie can lead to complete or partial quenching of the molecular spins [87].

Surface driven recombination of the manganese triangular prismatic complex

In order to investigate the possibility of the Au substrate to promote an on-surface Mn(3-OEe-sal)$_2$pip BPh_4^- transformation into two separated molecules BPh_4^- and Mn(3-OEe-sal)$_2$pip on a differently reactive surface, we have chosen a Cu(111) substrate. The STM topography of the manganese compound confirmed theory of the two-step recombination of the proposed ionic salt Fig. 6.6. After thermal deposition of the molecules, in the STM images we did not observe any stable patterns. Keeping the sample at RT over night and further cooling down to 5 K allowed us to visualize single Mn(3-OEe-sal)$_2$pip as well as secondary products of the deboronation of BPh_4^- in different configurations (Fig. 6.6). Single molecules are imaged with a bright protrusion, corresponding to recombination process. The different behavior of the ionic salt on Cu(111) in comparison to Au(111), can be explained on the basis of commensurability and/or a stronger interaction of the Cu substrate and present Cu adatoms with molecular complex. Another important parameter, namely the electronic configuration of the system, should be considered. The interaction between the copper adatom and the OEt functional groups should be different in the case of Cu(111) compared to Au(111). In this case the charge state of a metal adatom can be no more favorable for the creating a stable pattern. Therefore it seems that a success of the 2D-coordinated polymer formation depends not only on the resulting reaction product, substrate symmetry, their commensurability, but also on the specific adatom-substrate interaction. Notably, in XP spectra for Cu(111) samples B1s signature was not observed as well. And presented STM topograph Fig.6.6 shows all steps of the deboronation, which were

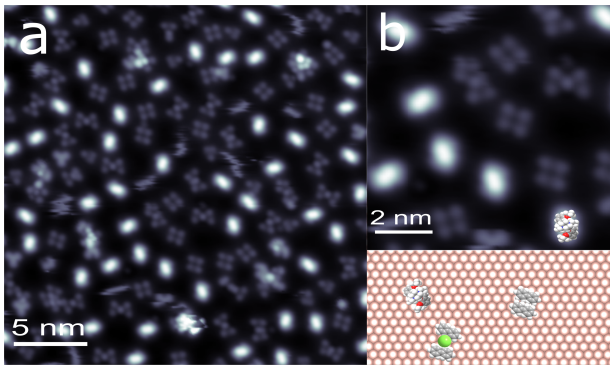

Figure 6.6: *Manganese ionic complex at the Cu(111) surface.* ***a*** *overview of the assembly,* ***b*** *closer overview and proposed model. STM details: 400 mV, 10 pA.*

proposed in Fig.6.4.

Mn(3-ON$_2$-sal)$_2$pip assembly on the Au(111) substrate

To investigate, if Kagome or closed pack lattice formation is driven by presence of biphenyl layer, was investigated similar but neutral Mn(3-ON$_2$-sal)$_2$pip triangular prismatic complex at the Au(111) surface by use of the STM Fig. 6.1, 6.7. Analysis of STM images Fig. 6.7 shows that neutral complex was assembled as sheets with a rectangular chiral shape and an extended lateral dimension. Chirality is a common phenomenon in nature and exists at nearly all scale ranges, from single organic molecules to living organisms and the universe. For example, almost all key molecules in life, including proteins and sugars, are chiral and appear in only one enantiomer. Moreover, adsorption and assembly of organic molecules on achiral solid surfaces should be an effective approach to construct chiral architectures and chiral surfaces. Mn(3-ON$_2$-sal)$_2$pip is functionalized by two NO$_2$ groups, which are widely known as strong electron withdrawing. As it was recently studies by Yang *et al.,* [183] according to the molecular packing model, a quarter of nitro groups in the monolayers are tilted from pyrazine ring plane with torsion angle of 154^{circ}. Under tip force, the most deformation of assemblies is taken up by rotation of the nitro groups, because the elastic deformation caused by van der Waals forces is very small compared with the twisted deformation of the tilted nitro groups. One would expect that in case of the NO$_2$ functional groups they should point up and to repel. This fact might be investigated by nc-AFM or XPS, to see the reaction.

Sodium tetraphenylborate at Au(111)

In order to test if, BPh$_4$ recombination is surface driven, was performed experiment with sodium tetraphenylborate - NaBPh$_4$. It is a salt, wherein the anion consists of four phenyl rings bonded to boron. This white crystalline solid is used to prepare other tetraphenylborate salts, which are often highly soluble in organic solvents. The compound is used in inorganic and organometallic chemistry as a precipitating agent for

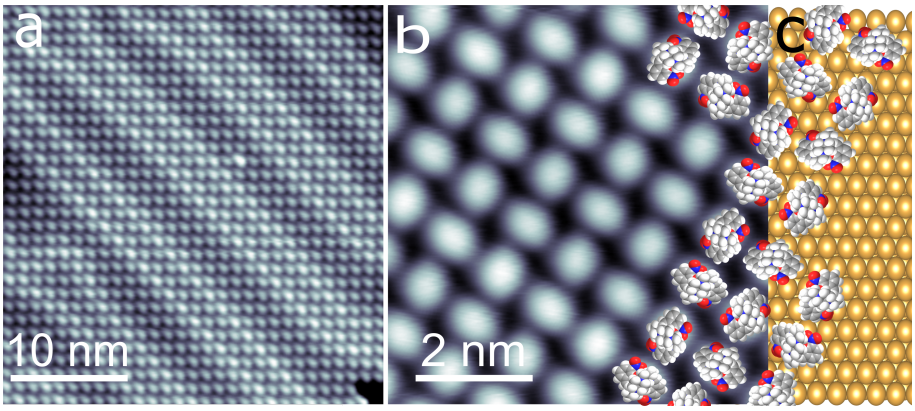

Figure 6.7: *STM topography of the neutral manganese complex at the Au(111) substrate.*

[top!]

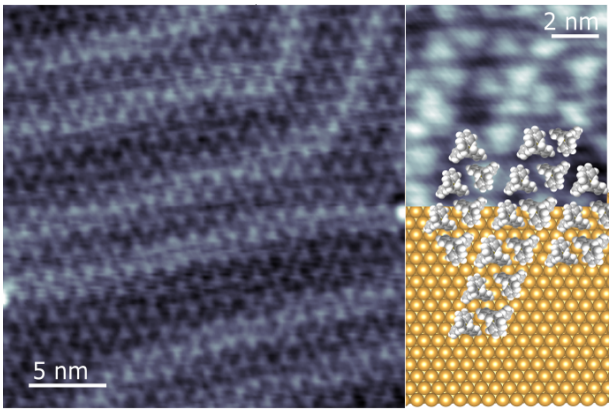

Figure 6.8: *STM topography of the $NaBPh_4$ at the Au(111) surface. STM details: 400 mV, 10 pA.*

potassium, ammonium, rubidium, and cesium ions, and some organic nitrogen compounds. Tetraphenylborates are often studied in organometallic chemistry because of their favorable solubility in nonpolar solvents and their crystallinity. Atomically clean Au(111) surface was prepared and investigated under ultrahigh vacuum (UHV) conditions with a base pressure of $\sim 10^{-10}$ mbar. The crystal substrates was cleaned by cycles of sputtering with Ar^+ ions and subsequent annealing to ~450°C. The molecules were deposited on the surface by means of thermal evaporation at ~50°C from a commercial evaporator (Kentax GmbH, Germany). The amount of the sublimed compound was controlled by a quartz crystal microbalance. Afterwards sample was stored at RT in UHV conditions over night. STM images were obtained at 5 K, in constant current mode – typical tunneling current 10-50 pA, and the sample bias was selected in the range of 5 mV to 1 V, such that the molecules appear in high contrast. Scanning probe tips were made from Pt/Ir wire (90% Pt, 10% Ir) and cleaned by sputtering with ions Ar^+.

Notably, due to the fact, that $NaBPh_4$ is a strong ionic salt it behaves completely different at the metal substrate. We assume, that molecule is anchored to the substrate

with Na atom, as from STM it is clear that prismatic shape of the compound is imaged as a triangle. Worth to notice, that scientific reports about ionic $NaBPh_4$ studied by STM or AFM are not available.

6.3 Conclusion

Unlike [Er(trensal)] tThe charge in the manganese complexes are charged molecules, each manganese complex is 1+, charge balanced in the crystal by a polyatomic counter-anion. This preliminary work demonstrates that sublimation of mono- and multilayers of positively charged trigonal prismatic Mn(III) metal-organic complexes on non-magnetic Au(111) substrate is possible. Combination of STM and XPS was used to investigate the self-assembly of magnetic triangular prismatic molecules on Au(111) and Cu(111) substrates at the submolecular level. In particular, newly proposed ionic salt undergoes two-step recombination process at the surface. The formation of regular Kagome lattices demonstrates that Au(111) can act as a wonderful template for fabrication of unique nanoarchitectures with remarkable properties. Varying the central metal ion of the prismatic molecules potentially can afford Kagome lattices with tunable molecular spins, providing ideal 2D model systems for studying frustration physics. This approach will provide valuable insight into how the interactions of magnetic molecules can be enhanced as it is useful towards both the fundamental understanding of the mechanism and potential device applications.

6.4 Details about experimental methods

All samples were prepared and investigated under ultrahigh vacuum (UHV) conditions with a base pressure of $\sim 10^{-10}$ mbar. The crystal substrates were cleaned by cycles of sputtering with Ar^+ ions and subsequent annealing to $\sim$450°C. The molecules were deposited on the surface by means of thermal evaporation at $\sim$150°C from a commercial evaporator (Kentax GmbH, Germany). The amount of the sublimed compound was controlled by a quartz crystal microbalance. Afterwards sample was stored at RT in UHV conditions over night. STM images were obtained at 5 K, in constant current mode – typical tunneling current 10-50 pA, and the sample bias was selected in the range of 5 mV to 1 V, such that the molecules appear in high contrast. Scanning probe tips were made from Pt/Ir wire (90% Pt, 10% Ir) and cleaned by sputtering with ions Ar^+.

Variable temperature magnetization measurements were performed on a polycrystalline sample between 10 K and 300 K. The χMT value of 3 cm^3 mol^{-1} K is in line with an S = 2 high-spin Mn^{2+} complex. The sharp decrease in the χMT value below $\sim$30 K is indicative of a non-negligible zero field splitting. To further investigate its presence, experiments were performed at low temperature from 0 T to 6.5 T.

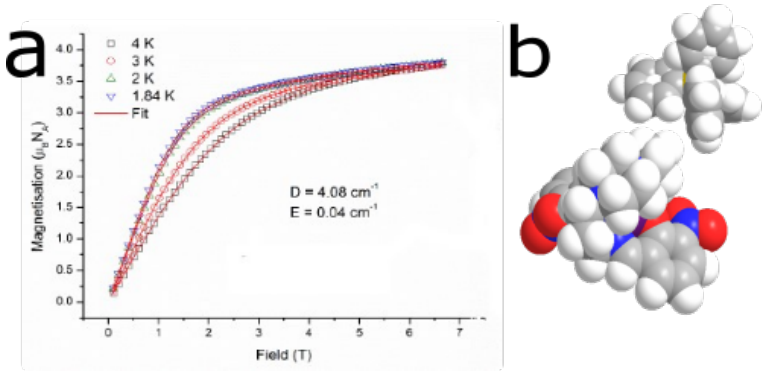

Figure 6.9: *Field dependence of the magnetization of complex. Red line represents fit to the data.*

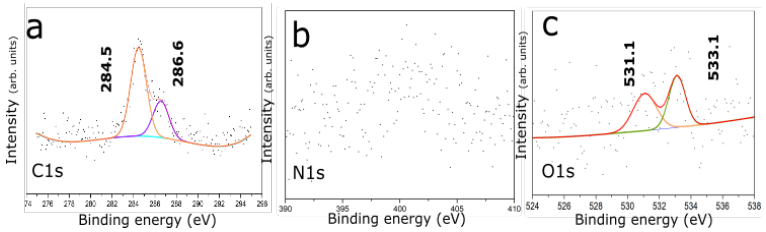

Figure 6.10: *XPS data for monolayer of manganese complex at the Cu(111) substrate. Corresponding spectra for C1s, N1s and O1s elements. B1s signature was not observed.*

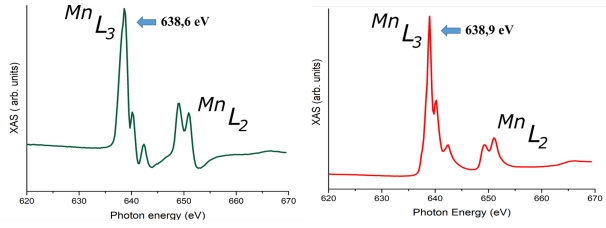

Figure 6.11: *Manganese ionic powder compounds investigated with XAS.* ***a*** *XAS of the proposed Mn^{3+} ionic complex,* ***b*** *XAS spectra of the Mn^{2+} complex. Initially both compounds corresponds to the Mn^{2+} oxidation state in the bulk.*

Conclusion

The complexity found in nature with its highly developed nanomachines demonstrates the possibilities and the prospects of molecular nanotechnology and molecular electronics. In contrast to nature, the metal-organic complexes are simple and well understood and the single-crystal surfaces are well defined. The electronic, mechanics and magnetic properties of low-dimensional on-surface architectures has been studied. By the combination of number of surface sensitive techniques, it was possible to investigate the relationship between the structural and electronic, mechanic and magnetic properties. For example, local access to electronic structure which provides STS in combination with ARPES averaging technique led to unique observation of the "nano pillow" effect in extended on-surface architectures. For presented quantum confinement arrays investigated in this thesis, the scalability of the determining physics has been evidenced by ARPES and XAS demonstrating the long range order, reproducibility of manufacturing and the possibility to determine macroscopic cooperative properties by the self-assembled nanoscale architectures. Moreover the effective mass of the partially confined electrons in the pores of a network was measured experimentally by ARPES and it was shown that in case of the Cu-coordinated 3deh-DPDI network on Cu(111) it is higher than the effective mass of electrons of the Shockley surface state. Simulations by the semi-empirical electron boundary element method in combination with the electron plane wave expansion has been used throughout this thesis. This has allowed us to model and understand the scattering potential landscape of the different configurations of the nanoporous network and simulate the LDOS and electronic band structures.

Previously described study revealed that upon deposition of Cu(111) surface at room temperature, CoOEP molecules form extended periodic nanoporous network due to the dipole-dipole interaction between Co ion and underlying substrate, and electrostatic potentials. The represented 2D porous metal-organic structure is one of the examples that can be used as host-guest systems. And in this case, the simplest way to test the suitability of the engineered 2D architecture for organization of functional materials and host-guest chemistry is to study their structural ability and steering effects in the co-adsorption of nanoscale objects. As a trial spices, one could choose C_{60} molecules,

which can be easily brought to the surface. Controlling C_{60} – quantum confinement interaction and positioning is both scientific and technological interest.

It is evident that the electronic environment (i.e. presence of the quantum confinement) act as an input to control the magnetic properties of single molecular adsorbates. We are aware of the fact that the electronic stimuli used as input in these studies are distinct from physical stimuli (e.g. light or electric fields) as commonly used in solid-state devices for information processing. But the above examples from nature show that complex logic operations can be based on inputs via chemical stimuli. The complexity of the obtained results asks for theoretical investigations which may capture the complex interaction of the molecular adsorbates with a present quantum confinement. This approach is able to provide benchmark results for first principle calculations to be assessed and improved towards the more accurate prediction of the properties of nanostructures.

It would be exciting to study the on-surface magnetochemistry of metal-organic complexes by a local probe like STM, in particular by spin-polarized or inelastic tunneling. The results shown in this thesis may pave a green light for the future development of organic spintronics, in particular at the organic – inorganic interface. Presented results also may find applications in magnetochemical sensors or as a means to control and fine tune the magnetic properties of complexes in spintronic molecular devices. We hope to contribute to the understanding of electronic and magnetic properties of metal-oganic complexes specifically magnetochemistry at the surface. The studies demonstrate the successful use merged surface sensitive techniques such as XAS, ARPES, XMCD as experimental methods to get a spectroscopic insight into the electronic and mechanic mechanisms of the present molecular adsorbates across the network and their impact on magnetic properties. Since the magnetochemical approach provides a straightforward way to control the magnetic quantum-state in a molecule, this may serve as an input for spintronic few-molecule data storage devices or even devices exploiting the quantum nature of spin and its entanglement. The complexity of the obtained results asks for theoretical investigations which may capture the complex interaction of the molecular adsorbates with a present quantum confinement. This approach is able to provide benchmark results for first principle calculations to be assessed and improved towards the more accurate prediction of the properties of nanostructures.

Bibliography

[1] Harrison, P. *Quantum Wells, Wires and Dots: Theoretical and Computational Physics of Semiconductor Nanostructures* (John Wiley & Sons, Ltd, Chichester, UK, 2005). URL http://doi.wiley.com/10.1002/0470010827.

[2] Forster, F., Bendounan, A., Ziroff, J. & Reinert, F. Systematic studies on surface modifications by ARUPS on Shockley-type surface states. *Surface Science* **600**, 3870–3874 (2006). URL http://www.sciencedirect.com/science/article/pii/S0039602806004158.

[3] Cottin, M. C. *et al.* Anisotropic scattering of surface state electrons at a point defect on Bi(111). *Applied Physics Letters* **98**, 022108 (2011). URL http://scitation.aip.org/content/aip/journal/apl/98/2/10.1063/1.3536528.

[4] Müller, K. *et al.* Multimorphism in molecular monolayers: Pentacene on Cu(110). *Physical Review B* **79** (2009). URL https://link.aps.org/doi/10.1103/PhysRevB.79.245421.

[5] Kepčija, N., Huang, T.-J., Klappenberger, F. & Barth, J. V. Quantum confinement in self-assembled two-dimensional nanoporous honeycomb networks at close-packed metal surfaces. *The Journal of Chemical Physics* **142**, 101931 (2015). URL http://scitation.aip.org/content/aip/journal/jcp/142/10/10.1063/1.4913244.

[6] Baumberger, F., Greber, T., Delley, B. & Osterwalder, J. Tailoring Confining Barriers for Surface States by Step Decoration: CO $/$Vicinal Cu(111). *Phys. Rev. Lett.* **88**, 237601 (2002). URL http://link.aps.org/doi/10.1103/PhysRevLett.88.237601.

[7] Lobo, J. *et al.* Tuning the Surface State Dimensionality of Cu Nanostripes. *Physical Review Letters* **93** (2004). URL https://link.aps.org/doi/10.1103/PhysRevLett.93.137602.

[8] Oka, H. *et al.* Spin-polarized quantum confinement in nanostructures: Scanning tunneling microscopy. *Reviews of Modern Physics* **86**, 1127–1168 (2014). URL https://link.aps.org/doi/10.1103/RevModPhys.86.1127.

[9] Crommie, M. F., Lutz, C. P. & Eigler, D. M. Confinement of electrons to quantum corrals on a metal surface. *Science* **262**, 218–220 (1993).

[10] Li, J., Schneider, W.-D., Crampin, S. & Berndt, R. Tunnelling spectroscopy of surface state scattering and confinement. *Surface Science* **422**, 95–106 (1999). URL http://www.sciencedirect.com/science/article/pii/S0039602898008905.

[11] Rodary, G. *et al.* Quantization of the electron wave vector in nanostructures: Counting k -states. *Physical Review B* **75** (2007). URL https://link.aps.org/doi/10.1103/PhysRevB.75.233412.

[12] Mugarza, A. & Ortega, J. E. Electronic states at vicinal surfaces. *J. Phys.: Condens. Matter* **15**, S3281 (2003). URL http://iopscience.iop.org/0953-8984/15/47/006.

[13] Klappenberger, F. *et al.* Dichotomous Array of Chiral Quantum Corrals by a Self-Assembled Nanoporous Kagomé Network. *Nano Letters* **9**, 3509–3514 (2009). URL http://pubs.acs.org/doi/abs/10.1021/nl901700b.

[14] Lobo-Checa, J. *et al.* Band Formation from Coupled Quantum Dots Formed by a Nanoporous Network on a Copper Surface. *Science* **325**, 300–303 (2009). URL http://www.sciencemag.org/cgi/doi/10.1126/science.1175141.

[15] Heller, E. J. Bound-State Eigenfunctions of Classically Chaotic Hamiltonian Systems: Scars of Periodic Orbits. *Phys. Rev. Lett.* **53**, 1515–1518 (1984). URL http://link.aps.org/doi/10.1103/PhysRevLett.53.1515.

[16] Crommie, M. F., Lutz, C. P. & Eigler, D. M. Imaging standing waves in a two-dimensional electron gas. *Nature* **363**, 524–527 (1993). URL http://www.nature.com/nature/journal/v363/n6429/abs/363524a0.html.

[17] Negulyaev, N. N. *et al.* Direct Evidence for the Effect of Quantum Confinement of Surface-State Electrons on Atomic Diffusion. *Phys. Rev. Lett.* **101**, 226601 (2008). URL http://link.aps.org/doi/10.1103/PhysRevLett.101.226601.

[18] Avouris, P. Real space imaging of electron scattering phenomena at metal surfaces. *Journal of Vacuum Science & Technology B: Microelectronics and Nanometer Structures* **12**, 1447 (1994). URL http://scitation.aip.org/content/avs/journal/jvstb/12/3/10.1116/1.587314.

[19] Jensen, H., Kröger, J., Berndt, R. & Crampin, S. Electron dynamics in vacancy islands: Scanning tunneling spectroscopy on Ag(111). *Physical Review B* **71** (2005). URL https://link.aps.org/doi/10.1103/PhysRevB.71.155417.

[20] Gross, L. *et al.* Scattering of Surface State Electrons at Large Organic Molecules. *Physical Review Letters* **93** (2004). URL http://link.aps.org/doi/10.1103/PhysRevLett.93.056103.

[21] Pawin, G. A Homomolecular Porous Network at a Cu(111) Surface. *Science* **313**, 961–962 (2006). URL http://www.sciencemag.org/cgi/doi/10.1126/science.1129309.

[22] Klappenberger, F. Two-dimensional functional molecular nanoarchitectures – Complementary investigations with scanning tunneling microscopy and X-ray spectroscopy. *Progress in Surface Science* **89**, 1–55 (2014). URL http://www.sciencedirect.com/science/article/pii/S0079681613000373.

[23] Matena, M. *et al.* On-surface synthesis of a two-dimensional porous coordination network: Unraveling adsorbate interactions. *Phys. Rev. B* **90**, 125408 (2014). URL http://link.aps.org/doi/10.1103/PhysRevB.90.125408.

[24] Piquero-Zulaica, I. *et al.* Precise engineering of quantum dot array coupling through their barrier widths. *Nature Communications* **8** (2017). URL http://www.nature.com/articles/s41467-017-00872-2.

[25] Shchyrba, A. *et al.* Covalent assembly of a two-dimensional molecular "sponge" on a Cu(111) surface: confined electronic surface states in open and closed pores. *Chem. Commun.* **50**, 7628–7631 (2014). URL http://pubs.rsc.org/en/content/articlelanding/2014/cc/c4cc02463j.

[26] Shchyrba, A. *et al.* Controlling the Dimensionality of On-Surface Coordination Polymers via Endo- or Exoligation. *J. Am. Chem. Soc.* **136**, 9355–9363 (2014). URL http://dx.doi.org/10.1021/ja5020103.

[27] Dong, L., Gao, Z. & Lin, N. Self-assembly of metal–organic coordination structures on surfaces. *Progress in Surface Science* **91**, 101–135 (2016). URL http://linkinghub.elsevier.com/retrieve/pii/S007968161630017X.

[28] Klappenberger, F. *et al.* Tunable Quantum Dot Arrays Formed from Self-Assembled Metal-Organic Networks. *Phys. Rev. Lett.* **106**, 026802 (2011). URL http://link.aps.org/doi/10.1103/PhysRevLett.106.026802.

[29] Stepanyuk, V. S., Negulyaev, N. N., Niebergall, L., Longo, R. C. & Bruno, P. Adatom Self-Organization Induced by Quantum Confinement of Surface Electrons. *Phys. Rev. Lett.* **97**, 186403 (2006). URL http://link.aps.org/doi/10.1103/PhysRevLett.97.186403.

[30] Stepanow, S. *et al.* Surface-Assisted Assembly of 2d Metal–Organic Networks That Exhibit Unusual Threefold Coordination Symmetry. *Angewandte Chemie International Edition* **46**, 710–713 (2007). URL http://doi.wiley.com/10.1002/anie.200603644.

[31] Nowakowska, S. *et al.* Configuring Electronic States in an Atomically Precise Array of Quantum Boxes. *Small* **12**, 3757–3763 (2016). URL http://doi.wiley.com/10.1002/smll.201600915.

[32] Hoffmann, R. A chemical and theoretical way to look at bonding on surfaces. *Reviews of Modern Physics* **60**, 601–628 (1988). URL https://link.aps.org/doi/10.1103/RevModPhys.60.601.

[33] Nowakowska, S. *et al.* Interplay of weak interactions in the atom-by-atom condensation of xenon within quantum boxes. *Nat Commun* **6** (2015). URL http://www.nature.com/ncomms/2015/150121/ncomms7071/full/ncomms7071.html.

[34] Cheng, Z. *et al.* Power of Confinement: Adsorbate Dynamics on Nanometer-Scale Exposed Facets. *Nano Letters* **10**, 3700–3703 (2010). URL http://pubs.acs.org/doi/abs/10.1021/nl1022018.

[35] Cheng, Z. *et al.* Adsorbates in a Box: Titration of Substrate Electronic States. *Phys. Rev. Lett.* **105**, 066104 (2010). URL http://link.aps.org/doi/10.1103/PhysRevLett.105.066104.

[36] Pivetta, M., Pacchioni, G. E., Schlickum, U., Barth, J. V. & Brune, H. Formation of Fe Cluster Superlattice in a Metal-Organic Quantum-Box Network. *Phys. Rev. Lett.* **110**, 086102 (2013). URL http://link.aps.org/doi/10.1103/PhysRevLett.110.086102.

[37] Oura, K., Katayama, M., Lifshits, V. G., Saranin, A. A. & Zotov, A. V. *Surface Science An Introduction* (Springer Berlin Heidelberg, Berlin, Heidelberg, 2003).

[38] Binnig, G., Rohrer, H., Gerber, C. & Weibel, E. Surface studies by scanning tunneling microscopy. *Physical Review Letters* **49**, 57–61 (1982).

[39] Olesen, L. *et al.* Apparent Barrier Height in Scanning Tunneling Microscopy Revisited. *Phys. Rev. Lett.* **76**, 1485–1488 (1996). URL http://link.aps.org/doi/10.1103/PhysRevLett.76.1485.

[40] Merzbacher, E. *Quantum Mechanics* (Wiley, New York, 1970), 2 edition edn.

[41] Tersoff, J. & Hamann, D. R. Theory of the scanning tunneling microscope. *Physical Review B* **31**, 805–813 (1985). URL https://link.aps.org/doi/10.1103/PhysRevB.31.805.

[42] Bardeen, J. Tunnelling from a Many-Particle Point of View. *Physical Review Letters* **6**, 57–59 (1961). URL https://link.aps.org/doi/10.1103/PhysRevLett.6.57.

[43] Lang, N. D. Theory of Single-Atom Imaging in the Scanning Tunneling Microscope. *Phys. Rev. Lett.* **56**, 1164–1167 (1986). URL http://link.aps.org/doi/10.1103/PhysRevLett.56.1164.

[44] Morr, D. K. Theory of scanning tunneling spectroscopy: from Kondo impurities to heavy fermion materials. *Reports on Progress in Physics* **80**, 014502 (2017). URL http://stacks.iop.org/0034-4885/80/i=1/a=014502?key=crossref.23aae9723641852065dbf2b1f6939f9e.

[45] Rieder, K.-H. *et al.* The scanning tunnelling microscope as an operative tool: doing physics and chemistry with single atoms and molecules. *Phil. Trans. R. Soc. Lond. A* **362**, 1207–1216 (2004). URL http://rsta.royalsocietypublishing.org/content/362/1819/1207.

[46] Chen, C. J. *Introduction to Scanning Tunneling Microscopy* (Oxford University Press, New York, 1993).

[47] Morita, S., Gießibl, F. J., Meyer, E. & Wiesendanger, R. (eds.) *Noncontact atomic force microscopy. Volume 3: ...* NanoScience and technology (Springer, Cham, 2015). OCLC: 918469789.

[48] Hla, S.-W., Braun, K.-F., Iancu, V. & Deshpande, A. Single-Atom Extraction by Scanning Tunneling Microscope Tip Crash and Nanoscale Surface Engineering. *Nano Letters* **4**, 1997–2001 (2004). URL `http://pubs.acs.org/doi/abs/10.1021/nl0487065`.

[49] Gopakumar, T. G. *et al.* Broken Symmetry of an Adsorbed Molecular Switch Determined by Scanning Tunneling Spectroscopy. *Angewandte Chemie International Edition* **52**, 11007–11010 (2013). URL `http://doi.wiley.com/10.1002/anie.201305027`.

[50] Krenner, W., Kühne, D., Klappenberger, F. & Barth, J. V. Assessment of Scanning Tunneling Spectroscopy Modes Inspecting Electron Confinement in Surface-Confined Supramolecular Networks. *Sci. Rep.* **3** (2013). URL `http://www.nature.com/srep/2013/130315/srep01454/full/srep01454.html`.

[51] Vitali, L. *et al.* Portrait of the potential barrier at metal-organic nanocontacts. *Nat Mater* **9**, 320–323 (2010). URL `http://www.nature.com/nmat/journal/v9/n4/full/nmat2625.html`.

[52] Reinert, F. & Hüfner, S. Photoemission spectroscopy—from early days to recent applications. *New Journal of Physics* **7**, 97–97 (2005). URL `http://stacks.iop.org/1367-2630/7/i=1/a=097?key=crossref.628e43da34de03ceaf654ceb005bc987`.

[53] Braun, S., Salaneck, W. R. & Fahlman, M. Energy-Level Alignment at Organic/Metal and Organic/Organic Interfaces. *Advanced Materials* **21**, 1450–1472 (2009). URL `http://onlinelibrary.wiley.com/doi/10.1002/adma.200802893/abstract`.

[54] Ishii, H., Sugiyama, K., Ito, E. & Seki, K. Energy level alignment and interfacial electronic structures at organic/metal and organirganic interfaces. *Advanced materials* **11**, 605–625 (1999).

[55] Watts, J. F. & Wolstenholme, J. *An introduction to surface analysis by XPS and AES* (J. Wiley, Chichester, West Sussex, England ; New York, 2003).

[56] van der Heide, P. *X-Ray Photoelectron Spectroscopy: An Introduction to Principles and Practices* (John Wiley & Sons, Inc., Hoboken, NJ, USA, 2011). URL `http://doi.wiley.com/10.1002/9781118162897`.

[57] Schindler, K.-M. Energy scan photoelectron diffraction: An integrated method for adsorbate structure determinations. *Applied Physics A Materials Science and Processing* **63**, 605–611 (1996). URL http://link.springer.com/10.1007/BF01567216.

[58] Shalaeva, E. V. & Kuznetsov, M. V. X-Ray Photoelectron Diffraction. Possibilities of Surface Structural Analysis. *Journal of Structural Chemistry* **44**, 465–498 (2003). URL http://link.springer.com/10.1023/B:JORY.0000009675.42838.de.

[59] Fasel, R. *et al.* Orientation of Adsorbed C 60 Molecules Determined via X-Ray Photoelectron Diffraction. *Physical Review Letters* **76**, 4733–4736 (1996). URL https://link.aps.org/doi/10.1103/PhysRevLett.76.4733.

[60] Kuznetsov, M. V., Ogorodnikov, I. I. & Vorokh, A. S. X-Ray photoelectron diffraction and photoelectron holography as methods for investigating the local atomic structure of the surface of solids. *Russian Chemical Reviews* **83**, 13–37 (2014). URL http://stacks.iop.org/0036-021X/83/i=1/a=13?key=crossref.43ce150e884370cd4d075c949bdcfac3.

[61] Öhrwall, G. *et al.* Observation of elastic scattering effects on photoelectron angular distributions in free Xe clusters. *J. Phys. B: At. Mol. Opt. Phys.* **36**, 3937 (2003). URL http://iopscience.iop.org/0953-4075/36/19/005.

[62] Osterwalder, J. *et al.* Angle-scanned photoelectron diffraction. *Surface Science* **331-333**, 1002–1014 (1995). URL http://linkinghub.elsevier.com/retrieve/pii/0039602895000763.

[63] *Magnetism* (Springer Berlin Heidelberg, Berlin, Heidelberg, 2006). URL http://link.springer.com/10.1007/978-3-540-30283-4.

[64] Piamonteze, C., Miedema, P. & de Groot, F. M. F. Accuracy of the spin sum rule in XMCD for the transition-metal L edges from manganese to copper. *Physical Review B* **80** (2009). URL https://link.aps.org/doi/10.1103/PhysRevB.80.184410.

[65] Muntwiler, M. *et al.* Surface science at the PEARL beamline of the Swiss Light Source. *Journal of Synchrotron Radiation* **24**, 354–366 (2017). URL http://scripts.iucr.org/cgi-bin/paper?S1600577516018646.

[66] Abajo, F. J. G. d., Cordón, J., Corso, M., Schiller, F. & Ortega, J. E. Lateral engineering of surface states – towards surface-state nanoelectronics. *Nanoscale* **2**, 717–721 (2010). URL http://pubs.rsc.org/en/content/articlelanding/2010/nr/b9nr00386j.

[67] Della Pia, A. *et al.* Anomalous Coarsening Driven by Reversible Charge Transfer at Metal–Organic Interfaces. *ACS Nano* **8**, 12356–12364 (2014). URL http://dx.doi.org/10.1021/nn505063w.

[68] Gottfried, J. M. Surface chemistry with reactive aromatic molecules and metal complexes. *EPS-CMD26 Conference* (2016).

[69] Würtz, P., Langen, T., Gericke, T., Koglbauer, A. & Ott, H. Experimental Demonstration of Single-Site Addressability in a Two-Dimensional Optical Lattice. *Phys. Rev. Lett.* **103**, 080404 (2009). URL http://link.aps.org/doi/10.1103/PhysRevLett.103.080404.

[70] Chilukuri, B., Mazur, U. & Hipps, K. W. Effect of dispersion on surface interactions of cobalt(ii) octaethylporphyrin monolayer on Au(111) and HOPG(0001) substrates: a comparative first principles study. *Phys. Chem. Chem. Phys.* **16**, 14096–14107 (2014). URL http://xlink.rsc.org/?DOI=C4CP01762E.

[71] Koch, N. *et al.* Conjugated organic molecules on metal versus polymer electrodes: Demonstration of a key energy level alignment mechanism. *Applied Physics Letters* **82**, 70–72 (2003). URL http://aip.scitation.org/doi/10.1063/1.1532102.

[72] Yoshimoto, S., Higa, N. & Itaya, K. Two-Dimensional Supramolecular Organization of Copper Octaethylporphyrin and Cobalt Phthalocyanine on Au(111): Molecular Assembly Control at an Electrochemical Interface. *Journal of the American Chemical Society* **126**, 8540–8545 (2004). URL http://pubs.acs.org/doi/abs/10.1021/ja0485210.

[73] Bhattarai, A., Mazur, U. & Hipps, K. W. Desorption Kinetics and Activation Energy for Cobalt Octaethylporphyrin from Graphite at the Phenyloctane Solution–Graphite Interface: An STM Study. *The Journal of Physical Chemistry C* **119**, 9386–9394 (2015). URL http://pubs.acs.org/doi/10.1021/acs.jpcc.5b01444.

[74] Bai, Y. *et al.* Adsorption of cobalt (II) octaethylporphyrin and 2h-octaethylporphyrin on Ag(111): new insight into the surface coordinative bond. *New Journal of Physics* **11**, 125004 (2009). URL http://stacks.iop.org/1367-2630/11/i=12/a=125004?key=crossref.303ebff05678d2dbc9e8b1100f76fadc.

[75] Bai, Y. *et al.* Interfacial coordination interactions studied on cobalt octaethylporphyrin and cobalt tetraphenylporphyrin monolayers on Au(111). *Physical Chemistry Chemical Physics* **12**, 4336 (2010). URL http://xlink.rsc.org/?DOI=b924974p.

[76] Girovsky, J. *et al.* Long-range ferrimagnetic order in a two-dimensional supramolecular Kondo lattice. *in the second stage of review at Nat Commun* **8**, 15388 (2017). URL http://www.nature.com/doifinder/10.1038/ncomms15388.

[77] Scudiero, L., Hipps, K. W. & Barlow, D. E. A Self-Organized Two-Dimensional Bimolecular Structure. *J. Phys. Chem. B* **107**, 2903–2909 (2003). URL http://dx.doi.org/10.1021/jp026875c.

[78] Heinrich, B. W., Braun, L., Pascual, J. I. & Franke, K. J. Tuning the Magnetic Anisotropy of Single Molecules. *Nano Letters* **15**, 4024–4028 (2015). URL http://pubs.acs.org/doi/abs/10.1021/acs.nanolett.5b00987.

[79] Écija, D., Urgel, J. I., Seitsonen, A. P., Auwärter, W. & Barth, J. V. Lanthanide-Directed Assembly of Interfacial Coordination Architectures–From Complex Networks to Functional Nanosystems. *Accounts of Chemical Research* **51**, 365–375 (2018). URL http://pubs.acs.org/doi/10.1021/acs.accounts.7b00379.

[80] Kiebele, A. *et al.* Adsorption and Dynamics of Long-Range Interacting Fullerenes in a Flexible, Two-Dimensional, Nanoporous Porphyrin Network. *ChemPhysChem* **7**, 1462–1470 (2006). URL http://doi.wiley.com/10.1002/cphc.200600186.

[81] Schwarz, M. *et al.* Adsorption Conformation and Lateral Registry of Cobalt Porphine on Cu(111). *The Journal of Physical Chemistry C* **122**, 5452–5461 (2018). URL http://pubs.acs.org/doi/10.1021/acs.jpcc.7b11705.

[82] Leung, K. *et al.* Density Functional Theory and DFT+U Study of Transition Metal Porphines Adsorbed on Au(111) Surfaces and Effects of Applied Electric Fields. *Journal of the American Chemical Society* **128**, 3659–3668 (2006). URL http://pubs.acs.org/doi/abs/10.1021/ja056630o.

[83] Han, Y. *et al.* Observing the Electrochemical Oxidation of Co Metal at the Solid/Liquid Interface Using Ambient Pressure X-ray Photoelectron Spectroscopy. *The Journal of Physical Chemistry B* **122**, 666–671 (2018). URL http://pubs.acs.org/doi/10.1021/acs.jpcb.7b05982.

[84] Piquero-Zulaica, I. *et al.* Temperature dependence of the partially localized state in a 2d molecular nanoporous network. *Applied Surface Science* **391**, 39–43 (2017). URL http://linkinghub.elsevier.com/retrieve/pii/S0169433216304147.

[85] Bürgi, L., Knorr, N., Brune, H., Schneider, M. A. & Kern, K. Two-dimensional electron gas at noble-metal surfaces. *Appl Phys A* **75**, 141–145 (2002). URL http://link.springer.com/article/10.1007/s003390101062.

[86] Wäckerlin, C. *et al.* On-surface coordination chemistry of planar molecular spin systems: novel magnetochemical effects induced by axial ligands. *Chemical Science* **3**, 3154 (2012). URL http://pubs.rsc.org/en/Content/ArticleLanding/2012/SC/c2sc20828h?utm_source=toc-alert&utm_medium=email&utm_campaign=pub-sc-vol-3-issue-11.

[87] Wäckerlin, C. *et al.* Ammonia Coordination Introducing a Magnetic Moment in an On-Surface Low-Spin Porphyrin. *Angew. Chem. Int. Ed.* **52**, 4568–4571 (2013). URL http://onlinelibrary.wiley.com/doi/10.1002/anie.201208028/abstract.

[88] Lyo, I.-W., Kaxiras, E. & Avouris, P. Adsorption of boron on Si(111): Its effect on surface electronic states and reconstruction. *Phys. Rev. Lett.* **63**, 1261–1264 (1989). URL http://link.aps.org/doi/10.1103/PhysRevLett.63.1261.

[89] Tseng, T.-C. *et al.* Charge-transfer-induced structural rearrangements at both sides of organic/metal interfaces. *Nature Chemistry* **2**, 374–379 (2010). URL http://www.nature.com/nchem/journal/v2/n5/full/nchem.591.html.

[90] Deimel, P. S. *et al.* Direct quantitative identification of the "surface trans-effect". *Chemical Science* **7**, 5647–5656 (2016). URL http://xlink.rsc.org/?DOI=C6SC01677D.

[91] Fiete, G. A. & Heller, E. J. Colloquium: Theory of quantum corrals and quantum mirages. *Rev. Mod. Phys.* **75**, 933–948 (2003). URL http://link.aps.org/doi/10.1103/RevModPhys.75.933.

[92] Seufert, K. *et al.* Controlled Interaction of Surface Quantum-Well Electronic States. *Nano Lett.* **13**, 6130–6135 (2013). URL http://pubs.acs.org/doi/abs/10.1021/nl403459m.

[93] Wyrick, J. *et al.* Do Two-Dimensional "Noble Gas Atoms" Produce Molecular Honeycombs at a Metal Surface? *Nano Letters* **11**, 2944–2948 (2011). URL http://pubs.acs.org/doi/abs/10.1021/nl201441b.

[94] Stöhr, M. *et al.* Controlling Molecular Assembly in Two Dimensions: The Concentration Dependence of Thermally Induced 2d Aggregation of Molecules on a Metal Surface. *Angewandte Chemie International Edition* **44**, 7394–7398 (2005). URL http://doi.wiley.com/10.1002/anie.200502316.

[95] Echenique, P. M. & Pendry, J. B. The existence and detection of Rydberg states at surfaces. *Journal of Physics C: Solid State Physics* **11**, 2065–2075 (1978). URL http://stacks.iop.org/0022-3719/11/i=10/a=017?key=crossref.0b650e02b42372fdbd3e4512ba195a6c.

[96] Armbrust, N., Güdde, J., Höfer, U., Kossler, S. & Feulner, P. Spectroscopy and Dynamics of a Two-Dimensional Electron Gas on Ultrathin Helium Films on Cu(111). *Physical Review Letters* **116** (2016). URL http://link.aps.org/doi/10.1103/PhysRevLett.116.256801.

[97] Müller, K., Enache, M. & Stöhr, M. Confinement properties of 2d porous molecular networks on metal surfaces. *Journal of Physics: Condensed Matter* **28**, 153003 (2016). URL http://stacks.iop.org/0953-8984/28/i=15/a=153003?key=crossref.d9b7ba4be71d850733fb51f1898e9612.

[98] Hipps, K. W., Scudiero, L., Barlow, D. E. & Cooke, M. P. A Self-Organized 2-Dimensional Bifunctional Structure Formed by Supramolecular Design. *J. Am. Chem. Soc.* **124**, 2126–2127 (2002). URL http://dx.doi.org/10.1021/ja017561q.

[99] Barth, J. V. *et al.* Building Supramolecular Nanostructures at Surfaces by Hydrogen Bonding. *Angewandte Chemie International Edition* **39**, 1230–1234 (2000). URL http://onlinelibrary.wiley.com/doi/10.1002/(SICI)1521-3773(20000403)39:7<1230::AID-ANIE1230>3.0.CO;2-I/abstract.

[100] Auwärter, W., Écija, D., Klappenberger, F. & Barth, J. V. Porphyrins at interfaces. *Nat Chem* **7**, 105–120 (2015). URL http://www.nature.com/nchem/journal/v7/n2/full/nchem.2159.html.

[101] Nowakowska, S. *et al.* Quantum Boxes: Configuring Electronic States in an Atomically Precise Array of Quantum Boxes (Small 28/2016). *Small* **12**, 3741–3741 (2016). URL http://doi.wiley.com/10.1002/smll.201670135.

[102] Kawai, S. *et al.* Van der Waals interactions and the limits of isolated atom models at interfaces. *Nature Communications* **7**, 11559 (2016). URL http://www.nature.com/doifinder/10.1038/ncomms11559.

[103] Fölsch, S., Martínez-Blanco, J., Yang, J., Kanisawa, K. & Erwin, S. C. Quantum dots with single-atom precision. *Nat Nano* **9**, 505–508 (2014). URL http://www.nature.com/nnano/journal/v9/n7/full/nnano.2014.129.html.

[104] Seufert, K., Auwärter, W. & Barth, J. V. Discriminative Response of Surface-Confined Metalloporphyrin Molecules to Carbon and Nitrogen Monoxide. *Journal of the American Chemical Society* **132**, 18141–18146 (2010). URL http://pubs.acs.org/doi/abs/10.1021/ja1054884.

[105] Wintjes, N. *et al.* A Supramolecular Multiposition Rotary Device. *Angewandte Chemie International Edition* **46**, 4089–4092 (2007). URL http://doi.wiley.com/10.1002/anie.200700285.

[106] Vázquez, H., Flores, F. & Kahn, A. Induced Density of States model for weakly-interacting organic semiconductor interfaces. *Organic Electronics* **8**, 241–248 (2007). URL http://linkinghub.elsevier.com/retrieve/pii/S1566119906001078.

[107] Vázquez, H., Dappe, Y. J., Ortega, J. & Flores, F. Energy level alignment at metal/organic semiconductor interfaces: "Pillow" effect, induced density of interface states, and charge neutrality level. *The Journal of Chemical Physics* **126**, 144703 (2007). URL http://scitation.aip.org/content/aip/journal/jcp/126/14/10.1063/1.2717165.

[108] Flores, F., Ortega, J. & Vázquez, H. Modelling energy level alignment at organic interfaces and density functional theory. *Phys. Chem. Chem. Phys.* **11**, 8658–8675 (2009). URL http://pubs.rsc.org/en/content/articlelanding/2009/cp/b902492c.

[109] Pennec, Y. *et al.* Supramolecular gratings for tuneable confinement of electrons on metal surfaces. *Nat Nano* **2**, 99–103 (2007). URL http://www.nature.com/nnano/journal/v2/n2/abs/nnano.2006.212.html.

[110] Zhang, J. *et al.* Probing the spatial and momentum distribution of confined surface states in a metal coordination network. *Chem. Commun.* **50**, 12289–12292 (2014). URL http://pubs.rsc.org/en/content/articlelanding/2014/cc/c4cc03941f.

[111] Nowakowska, S. *et al.* Adsorbate-Induced Modification of the Confining Barriers in a Quantum Box Array. *ACS Nano* **12**, 768–778 (2018). URL http://pubs.acs.org/doi/10.1021/acsnano.7b07989.

[112] Piquero-Zulaica, I. *et al.* Effective determination of surface potential landscapes from metal-organic nanoporous network overlayers. *New Journal of Physics* (2019). URL http://iopscience.iop.org/article/10.1088/1367-2630/ab150e.

[113] Seufert, K. *et al.* Cis-dicarbonyl binding at cobalt and iron porphyrins with saddle-shape conformation. *Nature Chemistry* **3**, 114–119 (2011). URL http://www.nature.com/nchem/journal/v3/n2/full/nchem.956.html.

[114] Wahl, M., Stöhr, M., Spillmann, H., Jung, T. A. & Gade, L. H. Rotation-libration in a hierarchic supramolecular rotor-stator system: Arrhenius activation and retardation by local interaction. *Chemical Communications* 1349 (2007). URL http://xlink.rsc.org/?DOI=b700909g.

[115] Ji, H.-X., Hu, J.-S. & Wan, L.-J. ZnOEP based phototransistor: signal amplification and light-controlled switch. *Chemical Communications* 2653 (2008). URL http://xlink.rsc.org/?DOI=b805204b.

[116] Malterre, D. *et al.* ARPES and STS investigation of Shockley states in thin metallic films and periodic nanostructures. *New Journal of Physics* **9**, 391–391 (2007). URL http://stacks.iop.org/1367-2630/9/i=10/a=391?key=crossref.2d213a58cfba6be90b7dade14fe89597.

[117] Krenner, W. *et al.* Unraveling the Hierarchic Formation of Open-porous Bimolecular Networks. *J. Phys. Chem. C* **116**, 16421–16429 (2012). URL http://dx.doi.org/10.1021/jp301226p.

[118] Ortega, J. E. *et al.* Scattering of surface electrons by isolated steps versus periodic step arrays. *Phys. Rev. B* **87**, 115425 (2013). URL http://link.aps.org/doi/10.1103/PhysRevB.87.115425.

[119] Gambardella, P. Giant Magnetic Anisotropy of Single Cobalt Atoms and Nanoparticles. *Science* **300**, 1130–1133 (2003). URL http://www.sciencemag.org/cgi/doi/10.1126/science.1082857.

[120] Wäckerlin, C. *et al.* Controlling spins in adsorbed molecules by a chemical switch. *Nature Communications* **1**, 1–7 (2010). URL http://www.nature.com/doifinder/10.1038/ncomms1057.

[121] Ishihara, S. *et al.* Porphyrin-based sensor nanoarchitectonics in diverse physical detection modes. *Phys. Chem. Chem. Phys.* (2014). URL http://pubs.rsc.org/en/content/articlelanding/2014/cp/c3cp55431g.

[122] Bogani, L. & Wernsdorfer, W. Molecular spintronics using single-molecule magnets. *Nat Mater* **7**, 179–186 (2008). URL http://www.nature.com/nmat/journal/v7/n3/full/nmat2133.html.

[123] Park, J. *et al.* Coulomb blockade and the Kondo effect in single-atom transistors. *Nature* **417**, 722–725 (2002). URL http://www.nature.com/doifinder/10.1038/nature00791.

[124] Wäckerlin, C. *et al.* Giant Hysteresis of Single-Molecule Magnets Adsorbed on a Nonmagnetic Insulator. *Advanced Materials* **28**, 5195–5199 (2016). URL http://doi.wiley.com/10.1002/adma.201506305.

[125] Wäckerlin, C., Siewert, D., Jung, T. A. & Ballav, N. On-surface coordination chemistry: direct imaging of the conformational freedom of an axial ligand at room temperature. *Phys. Chem. Chem. Phys.* **15**, 16510–16514 (2013). URL http://pubs.rsc.org/en/content/articlelanding/2013/cp/c3cp50966d.

[126] Crispin, X. *et al.* Characterization of the Interface Dipole at Organic/ Metal Interfaces. *J. Am. Chem. Soc.* **124**, 8131–8141 (2002). URL http://dx.doi.org/10.1021/ja025673r.

[127] Tsukahara, N., Minamitani, E., Kim, Y., Kawai, M. & Takagi, N. Controlling orbital-selective Kondo effects in a single molecule through coordination chemistry. *The Journal of Chemical Physics* **141**, 054702 (2014). URL http://scitation.aip.org/content/aip/journal/jcp/141/5/10.1063/1.4890654.

[128] Zhao, A. *et al.* Controlling the Kondo Effect of an Adsorbed Magnetic Ion Through Its Chemical Bonding. *Science* **309**, 1542–1544 (2005). URL http://www.sciencemag.org/content/309/5740/1542.

[129] Umbach, T. R. *et al.* Ferromagnetic Coupling of Mononuclear Fe Centers in a Self-Assembled Metal-Organic Network on Au(111). *Physical Review Letters* **109** (2012). URL https://link.aps.org/doi/10.1103/PhysRevLett.109.267207.

[130] Tsukahara, N. *et al.* Evolution of Kondo Resonance from a Single Impurity Molecule to the Two-Dimensional Lattice. *Physical Review Letters* **106** (2011). URL http://link.aps.org/doi/10.1103/PhysRevLett.106.187201.

[131] Chen, X. & Alouani, M. Effect of metallic surfaces on the electronic structure, magnetism, and transport properties of Co-phthalocyanine molecules. *Physical Review B* **82** (2010). URL `https://link.aps.org/doi/10.1103/PhysRevB.82.094443`.

[132] Brune, H. & Gambardella, P. Magnetism of individual atoms adsorbed on surfaces. *Surface Science* **603**, 1812–1830 (2009). URL `http://linkinghub.elsevier.com/retrieve/pii/S003960280900034X`.

[133] Pang, R., Shi, X. & Van Hove, M. A. Manipulating Magnetism at Organic/-Ferromagnetic Interfaces by Molecule-Induced Surface Reconstruction. *Journal of the American Chemical Society* **138**, 4029–4035 (2016). URL `http://pubs.acs.org/doi/abs/10.1021/jacs.5b10967`.

[134] Donati, F. *et al.* Magnetism of Ho and Er Atoms on Close-Packed Metal Surfaces. *Physical Review Letters* **113** (2014). URL `http://link.aps.org/doi/10.1103/PhysRevLett.113.237201`.

[135] Chandra, R. *et al.* Metalloporphyrins—Applications and clinical significance. *Indian Journal of Clinical Biochemistry* **15**, 183–199 (2000). URL `http://link.springer.com/10.1007/BF02867558`.

[136] Aragonès, A. C. *et al.* Large Conductance Switching in a Single-Molecule Device through Room Temperature Spin-Dependent Transport. *Nano Letters* **16**, 218–226 (2016). URL `http://pubs.acs.org/doi/10.1021/acs.nanolett.5b03571`.

[137] Loth, S., Baumann, S., Lutz, C. P., Eigler, D. M. & Heinrich, A. J. Bistability in Atomic-Scale Antiferromagnets. *Science* **335**, 196–199 (2012). URL `http://www.sciencemag.org/content/335/6065/196`.

[138] Kittelmann, M. *et al.* Controlled Activation of Substrate Templating in Molecular Self-Assembly by Deprotonation. *J. Phys. Chem. C* **117**, 23868–23874 (2013). URL `http://pubs.acs.org/doi/abs/10.1021/jp408664n`.

[139] Heinrich, B. W. *et al.* Change of the Magnetic Coupling of a Metal–Organic Complex with the Substrate by a Stepwise Ligand Reaction. *Nano Lett.* **13**, 4840–4843 (2013). URL `http://dx.doi.org/10.1021/nl402575c`.

[140] Franke, K. J., Schulze, G. & Pascual, J. I. Competition of Superconducting Phenomena and Kondo Screening at the Nanoscale. *Science* **332**, 940–944 (2011). URL `http://www.sciencemag.org/content/332/6032/940`.

[141] Zhong, J.-Q. *et al.* Reversible Tuning of Interfacial and Intramolecular Charge Transfer in Individual MnPc Molecules. *Nano Letters* **15**, 8091–8098 (2015). URL `http://pubs.acs.org/doi/10.1021/acs.nanolett.5b03520`.

[142] Betti, M. G. *et al.* Formation of Hybrid Electronic States in FePc Chains Mediated by the Au(110) Surface. *J. Phys. Chem. C* **116**, 8657–8663 (2012). URL http://dx.doi.org/10.1021/jp300663t.

[143] Betti, M. G. *et al.* Localized and Dispersive Electronic States at Ordered FePc and CoPc Chains on Au(110). *The Journal of Physical Chemistry C* **114**, 21638–21644 (2010). URL http://pubs.acs.org/doi/abs/10.1021/jp108734u.

[144] Gargiani, P., Betti, M. G., Taleb Ibrahimi, A., Le Fèvre, P. & Modesti, S. Orbital Symmetry of the Kondo State in Adsorbed FePc Molecules on the Au(110) Metal Surface. *The Journal of Physical Chemistry C* **120**, 28527–28532 (2016). URL http://pubs.acs.org/doi/abs/10.1021/acs.jpcc.6b07805.

[145] Rochford, L. A., Ramadan, A. J., Woodruff, D. P., Heutz, S. & Jones, T. S. Ordered growth of vanadyl phthalocyanine (VOPc) on an iron phthalocyanine (FePc) monolayer. *Phys. Chem. Chem. Phys.* **17**, 29747–29752 (2015). URL http://xlink.rsc.org/?DOI=C5CP03724G.

[146] Cuadrado, R. *et al.* CoPc adsorption on Cu(111): Origin of the C4 to C2 symmetry reduction. *The Journal of Chemical Physics* **133**, 154701 (2010). URL http://aip.scitation.org/doi/10.1063/1.3502682.

[147] Schulz, F., Drost, R., Hämäläinen, S. K. & Liljeroth, P. Templated Self-Assembly and Local Doping of Molecules on Epitaxial Hexagonal Boron Nitride. *ACS Nano* (2013). URL http://pubs.acs.org/doi/abs/10.1021/nn404840h.

[148] Mugarza, A. *et al.* Electronic and magnetic properties of molecule-metal interfaces: Transition-metal phthalocyanines adsorbed on Ag(100). *Physical Review B* **85** (2012). URL http://link.aps.org/doi/10.1103/PhysRevB.85.155437.

[149] Scheybal, A. *et al.* Induced magnetic ordering in a molecular monolayer. *Chemical Physics Letters* **411**, 214–220 (2005). URL http://www.sciencedirect.com/science/article/pii/S0009261405008626.

[150] Peisert, H., Petershans, A. & Chassé, T. Charge Transfer and Polarization Screening at Organic/Metal Interfaces: Distinguishing between the First Layer and Thin Films. *The Journal of Physical Chemistry C* **112**, 5703–5706 (2008). URL http://pubs.acs.org/doi/abs/10.1021/jp800674z.

[151] Annese, E., Fujii, J., Vobornik, I. & Rossi, G. Structure and Electron States of Co-phthalocyanine Interacting With the Cu(111) Surface. *The Journal of Physical Chemistry C* **115**, 17409–17416 (2011). URL http://pubs.acs.org/doi/abs/10.1021/jp203200s.

[152] Fanetti, M. *et al.* Structure and Molecule–Substrate Interaction in a Co-octaethyl Porphyrin Monolayer on the Ag(110) Surface. *The Journal of Physical Chemistry C* **115**, 11560–11568 (2011). URL http://pubs.acs.org/doi/abs/10.1021/jp2011233.

[153] Lu, X., Hipps, K. W., Wang, X. D. & Mazur, U. Scanning Tunneling Microscopy of Metal Phthalocyanines: d ^{7} and d ^{9} Cases. *Journal of the American Chemical Society* **118**, 7197–7202 (1996). URL https://pubs.acs.org/doi/10.1021/ja960874e.

[154] Widmer, R., Passerone, D., Mattle, T., Sachdev, H. & Gröning, O. Probing the selectivity of a nanostructured surface by xenon adsorption. *Nanoscale* **2**, 502–508 (2010). URL http://pubs.rsc.org/en/content/articlelanding/2010/nr/b9nr00431a.

[155] Dil, H. *et al.* Surface Trapping of Atoms and Molecules with Dipole Rings. *Science* **319**, 1824–1826 (2008). URL http://www.sciencemag.org/cgi/doi/10.1126/science.1154179.

[156] Abdurakhmanova, N. *et al.* Superexchange-Mediated Ferromagnetic Coupling in Two-Dimensional Ni-TCNQ Networks on Metal Surfaces. *Physical Review Letters* **110** (2013). URL https://link.aps.org/doi/10.1103/PhysRevLett.110.027202.

[157] Donati, F. *et al.* Tailoring the Magnetism of Co Atoms on Graphene through Substrate Hybridization. *Physical Review Letters* **113** (2014). URL https://link.aps.org/doi/10.1103/PhysRevLett.113.177201.

[158] Corradini, V. *et al.* CoTPP molecules deposited on graphene/Ni (111): Quenching of the antiferromagnetic interaction induced by gold intercalation. *Journal of Applied Physics* **125**, 142904 (2019). URL http://aip.scitation.org/doi/10.1063/1.5063562.

[159] Girovsky, J. *et al.* Antiferromagnetic coupling of Cr-porphyrin to a bare Co substrate. *Physical Review B* **90** (2014). URL http://link.aps.org/doi/10.1103/PhysRevB.90.220404.

[160] Lodi Rizzini, A. *et al.* Coupling of single, double, and triple-decker metal-phthalocyanine complexes to ferromagnetic and antiferromagnetic substrates. *Surface Science* **630**, 361–374 (2014). URL http://linkinghub.elsevier.com/retrieve/pii/S0039602814002003.

[161] Wende, H. *et al.* Substrate-induced magnetic ordering and switching of iron porphyrin molecules. *Nature Materials* **6**, 516–520 (2007). URL http://www.nature.com/doifinder/10.1038/nmat1932.

[162] Hermanns, C. F. *et al.* Magnetic Coupling of Porphyrin Molecules Through Graphene. *Advanced Materials* **25**, 3473–3477 (2013). URL http://doi.wiley.com/10.1002/adma.201205275.

[163] Maki, G. Ligand Field Theory of Ni(II) Complexes. I. Electronic Energies and Singlet Ground-State Conditions of Ni(II) Complexes of Different Symmetries. *The Journal of Chemical Physics* **28**, 651–662 (1958). URL http://aip.scitation.org/doi/10.1063/1.1744207.

[164] Armaroli, N., Marconi, G., Echegoyen, L., Bourgeois, J.-P. & Diederich, F. Charge-Transfer Interactions in Face-to-Face Porphyrin-Fullerene Systems: Solvent-Dependent Luminescence in the Infrared Spectral Region. *Chemistry – A European Journal* **6**, 1629–1645 (2000). URL http://onlinelibrary.wiley.com/doi/10.1002/(SICI)1521-3765(20000502)6:9<1629::AID-CHEM1629>3.0.CO;2-Z/abstract.

[165] Wiesendanger, R. *Scanning Probe Microscopy and Spectroscopy: Methods and Applications* (Cambridge University Press, Cambridge, 1994). URL http://ebooks.cambridge.org/ref/id/CBO9780511524356.

[166] Wang, Y., Hamers, R. J. & Kaxiras, E. Atomic Structure and Bonding of Boron-Induced Reconstructions on Si(001). *Phys. Rev. Lett.* **74**, 403–406 (1995). URL http://link.aps.org/doi/10.1103/PhysRevLett.74.403.

[167] Wäckerlin, C. *et al.* Assembly of 2d ionic layers by reaction of alkali halides with the organic electrophile 7,7,8,8-tetracyano-p-quinodimethane (TCNQ). *Chemical Communications* **47**, 9146 (2011). URL http://xlink.rsc.org/?DOI=c1cc12519b.

[168] Dreiser, J. *et al.* Exchange Interaction of Strongly Anisotropic Tripodal Erbium Single-Ion Magnets with Metallic Surfaces. *ACS Nano* **8**, 4662–4671 (2014). URL http://pubs.acs.org/doi/abs/10.1021/nn500409u.

[169] Fitzpatrick, A. J. *et al.* Challenges in assignment of orbital populations in a high spin manganese(iii) complex. *Dalton Transactions* **45**, 6702–6708 (2016). URL http://xlink.rsc.org/?DOI=C5DT03914B.

[170] Realista, S. *et al.* A Mn(iii) single ion magnet with tridentate Schiff-base ligands. *Dalton Trans.* **45**, 12301–12307 (2016). URL http://xlink.rsc.org/?DOI=C6DT02538B.

[171] Morchutt, C., Björk, J., Krotzky, S., Gutzler, R. & Kern, K. Covalent coupling via dehalogenation on Ni(111) supported boron nitride and graphene. *Chem. Commun.* **51**, 2440–2443 (2015). URL http://pubs.rsc.org/en/content/articlelanding/2015/cc/c4cc07107g.

[172] Cai, L. *et al.* Direct Formation of C–C Double-Bonded Structural Motifs by On-Surface Dehalogenative Homocoupling of *gem* -Dibromomethyl Molecules. *ACS Nano* (2018). URL http://pubs.acs.org/doi/10.1021/acsnano.8b02459.

[173] Grill, L. *et al.* Nano-architectures by covalent assembly of molecular building blocks. *Nature Nanotechnology* **2**, 687–691 (2007). URL http://www.nature.com/doifinder/10.1038/nnano.2007.346.

[174] Li, Z. & Kosov, D. S. Nature of well-defined conductance of amine-anchored molecular junctions: Density functional calculations. *Physical Review B* **76** (2007). URL https://link.aps.org/doi/10.1103/PhysRevB.76.035415.

[175] Kanuru, V. K. *et al.* Sonogashira Coupling on an Extended Gold Surface in Vacuo: Reaction of Phenylacetylene with Iodobenzene on Au(111). *J. Am. Chem. Soc.* **132**, 8081–8086 (2010). URL http://dx.doi.org/10.1021/ja1011542.

[176] Wang, Y., Lingenfelder, M., Classen, T., Costantini, G. & Kern, K. Ordering of Dipeptide Chains on Cu Surfaces through 2d Cocrystallization. *J. Am. Chem. Soc.* **129**, 15742–15743 (2007). URL http://dx.doi.org/10.1021/ja075118v.

[177] Ditze, S. *et al.* Activation Energy for the Self-Metalation Reaction of 2h-Tetraphenylporphyrin on Cu(111). *Angewandte Chemie International Edition* **51**, 10898–10901 (2012). URL http://doi.wiley.com/10.1002/anie.201205464.

[178] Aresta, M., Dibenedetto, A. & Quaranta, E. Reaction of alkali-metal tetraphenylborates with amines in the presence of CO2: a new easy way to aliphatic and aromatic alkali-metal carbamates. *Journal of the Chemical Society, Dalton Transactions* 3359 (1995). URL http://xlink.rsc.org/?DOI=dt9950003359.

[179] Di Santo, G. *et al.* Conformational Adaptation and Electronic Structure of 2h-Tetraphenylporphyrin on Ag(111) during Fe Metalation. *The Journal of Physical Chemistry C* **115**, 4155–4162 (2011). URL http://pubs.acs.org/doi/abs/10.1021/jp111151n.

[180] Bazarnik, M., Brede, J., Decker, R. & Wiesendanger, R. Tailoring Molecular Self-Assembly of Magnetic Phthalocyanine Molecules on Fe- and Co-Intercalated Graphene. *ACS Nano* **7**, 11341–11349 (2013). URL http://pubs.acs.org/doi/abs/10.1021/nn405172q.

[181] Kühne, D. *et al.* Self-Assembly of Nanoporous Chiral Networks with Varying Symmetry from Sexiphenyl-dicarbonitrile on Ag(111). *J. Phys. Chem. C* **113**, 17851–17859 (2009). URL http://dx.doi.org/10.1021/jp9041217.

[182] Sun, H., Tan, S., Feng, M., Zhao, J. & Petek, H. Deconstruction of the Electronic Properties of a Topological Insulator with a Two-Dimensional Noble Metal–Organic Honeycomb–Kagome Band Structure. *The Journal of Physical Chemistry C* (2018). URL http://pubs.acs.org/doi/10.1021/acs.jpcc.8b03353.

[183] Yang, G. *et al.* Synthesis of one-molecule-thick single-crystalline nanosheets of energetic material for high-sensitive force sensor. *Scientific Reports* **2** (2012). URL http://www.nature.com/articles/srep00698.

List of Figures

List of Figures

List of Tables

Nomenclature

Symbols

Latin letters

a_1	lattice constant
a_2	lattice constant
E	energy
E_{Fermi}	Fermi energy
$E_{F,T}$	Fermi energy of the tip
$E_{F,S}$	Fermi energy of the sample
e	elementary charge
e^-	electron
f	frequency
$\overrightarrow{G}$	reciprocal lattice vector
d	thickness of the barrier
h	height
$\hbar$	Planck constant
I_t	tunneling current
k_b	boltzmann's constant
m_e	mass of the electron
$M_{T,S}$	tunneling matrix
p	dipole moment
R	radius of curvature of the tip
T	temperature
$T(d, E, eV)$	transmission coefficient
U	potential difference between tip and sample
V_{AC}	Alternative Current voltage
V_{bias}	bias voltage
V_{DC}	Direct Current voltage

x	coordinate of one horizontal axis in the sample surface plane
y	coordinate of one horizontal axis in the sample surface plane
z	coordinate of the vertical axis between tip and sample
z_{offset}	offset distance

Greek letters

Δf	frequency shift
$\Delta\phi$	work function difference
Δp	dipole moment density difference
$\delta+$	positive partial charge
$\delta-$	negative partial charge
κ	decay length of bounding interaction
ρ	angle along which the molecular rows are aligned with respect to the [010] direction
ρ_S	LDOS of the sample
ρ_T	LDOS of the tip
μ	total chemical potential of electrons
σ	equilibrium distance
ϕ	work function
Φ_T	work function of the tip
Φ_S	work function of the sample
$\psi_n(0)$	value of the 1D electron function
Ψ	electron wave function of the tip
ω	Angular frequency of the oscillation

Abbreviations

AC	Actual Current
ARPES	Angle-Resolved Photoelectron Spectroscopy
BE	Binding Energy
CB	Conduction Band
COF	Covalent Organic Framework
CoOEP	Cobalt (||) Octaethylporphyrin
DC	Dirrect Current
DOS	Density of States
DPDI	4,9-diaminoperylene quinone-3,10-diimine
EBEM	Electron Boundary Element Method
EPWE	Electron Plane Wave Expansion
ESCA	Electron Spectroscopy for Chemical Analysis
HOMO	Highest occupied molecular orbital
H_2OEP	free based Octaethylporphyrin
LEED	Low-Energy Electron Diffraction
LDOS	Local Density of States
LUMO	Lovest Unoccupied Molecular Orbital
LT	Low Temperature
LD	Linear Dichroism
ML	Monolayer
MOF	Metal-Organic Framework
NiOEP	Nickel (||) Octaethylporphyrin
OEP	Octaethylporphyrin
PES	Photoelectron Spectroscopy
PhD	Photoelectron Diffraction
PLS	Partially Localized State
QD	Quantum Dot
QWs	Quantum Well state
QCMB	Quartz Micro Balance
RT	Room Temperature
SPM	Scanning Probe Microscopy/Microscope
SS	Surface State
STM	Scanning Tunneling Microscopy/Microscope
STS	Scanning Tunneling Spectroscopy
TEY	Total Emission Yield
TM	Transition Metal
UHV	Ultra-high Vacuum
UV	ultraviolet
UPS	Ultraviolet Photoelectron Spectroscopy
VB	Valence Band
WF	Work Function
XAS	X-Ray Absorption Spectroscopy
XMCD	X-Ray Magnetic Circular Dichroism
XPD	X-Ray Photoelectron Diffraction

XPS	X-ray Photoelectron Spectroscopy
ZnOEP	Zinc Octaethylporphyrin
1D	One-dimensional
2D	Two-dimensional
2PLS	Second Partially Localized State
2DEG	Two-dimensional Electron Gas
3D	Three-dimensional

Acknowledgements

Here I would like to express my gratefulness to all people, who have helped and supported me during my doctoral study. However, I am extremely happy that I had a chance to be on this journey, which would be impossible without help and support of many people. I am sincerely thankful to everyone for their priceless contribution to it. During this journey, learned a lot not only professionally about physics, but also about people, relations, the way we think and perceive things around us, about life. It is never an easy task to write this part on the paper, I tried to come back to it thousands times, but it was never easy to continue...

Here I would like to acknowledge my PhD supervisor Prof. Dr. Thomas A. Jung for allowing me to be myself, take control over my own research, and make it my own with the occasional direction prod in the right way. I always felt independent, which I am very grateful for.

Also I would like to say thank you to Prof. Dr. Ernst Meyer, for joining my examination comity, external help and creating great group, with whom I spent almost all my years of PhD inside and outside of the university. And for organizing amazing ski events - I literally felt as a part of Nanolino group.

Separate acknowledge goes to Prof. Richard Warburton, who was very kind to be a chairman at my defense, and for his motivating private talks before and after my exam.

I sincerely grateful to my non-official supervisor Dr. Jorge Lobo-Checa, who is the greatest scientist, I have ever met. With his patience and great sense of humor, being present, or via long skype discussions was always ready to share his deep knowledge and experience, to support at least half of my crazy ideas and to guide me in the right direction by end of this thesis. Thank you so much for showing me that it is not that scary to jump in at the deep end and learn by a hands-on approach during my numerous experiments. I gained a vast amount of my experience and knowledge thanks to your guidance and help.

Secondly, I would like to express my gratefulness to the former Nanolab and PSI groups members : Milos Baljozovic, Aneliia Waeckerlin, Sylwia Nowakowska, Christian Waeckerlin, Jan Nowakowski, Harald Rossmann, Jan Girovsky, and Dorota Stewert, who took me as a "new fresh meat", and with a lot of enthusiasm introduced me to the beautiful "night life" of the synchrotron experiments. In particular, I would like to acknowledge Milos here, who basically became my PhD buddy, for staying all those countless long night-shifts at SLS and measuring innumerable spectras, coffee breaks at 4 am at the Phoenix hatch and pizza for breakfast before the shift:D I should say, that we had a lot of disagreements, but I realized real value of your help only during last beamtimes and while writing this thesis, and see ya soon :D At the same time, I would like to thank all beamline and SLS staff that was helping during experiments: Jan Dreiser, Cinthia Piamonteze and Stephan Zeugin from XTREME, Armin Kleibert from SIM, Matthias Muntwiler and Dariia Sostina from PEARL. Thank you for your support not only during beamtimes, but also while data analysis and interpreting.

Separate acknowledgment goes to Marco Martina, who was always a "Chuck Norris of UHV" at Nanolab, was always kind to help to fix whatever happened. Marco, I hope, our root jokes from the office and lab times would not disappear:D , and I hope you still have your ventilator! Another acknowledgment goes to Matthes Senn, who replaced Marco on some point. I am really grateful to you for spending 3 days while Christmas holidays with me in the lab, when I crushed manipulator. Twice. Also, I can not mention here Rolf Schelldorfer – our technician from Nanojunction lab, who was always ready to make a joke and to help to fix a problem. And finally only by the end of my PhD Ive been awarded by Rolf, mayor of the city of Shilda, as a new member:D On this point i should also mention Electronic and Mechanics workshop from Basel - Sascha Martin, Stefan Gentsch, Patrick Stoecklin and Dominik Sifrig - for all your help amd being always positive, Michael Steinacher and Sascha Linder - for help, whenever it was needed.

I sincerely thank all my collaborations Prof. Lutz H. Gade (Heidelberg, Germany), who was official DPDI supplier for Nanolab, Dr. Grace Morgan and Vibe Jackobsen (Dublin, Ireland) - for molecular magnets supply, Ignacio Piquero (yes, Inaki, it is snowing in Basel right now when I am writing it, and it is beginning of May:D) and Zakaria Abd El-Fattah for performing EPWE calculations in very short time, Dr. Jorge Iribas Cerda for DFT calculations (Jorge, I am literally amazed how great you are! hope we will continue collaboration in future), Prof. Cornelia G. Palivan and Stefano Di Leone (Chemistry Department, UniBasel), for fruitful discussions with an aim to fill gaps in my chemistry knowledge, Dr. Jonas Bjoerk - my crazy conference buddy:) you are great:)

Also, I would like to acknowledge bachelor and master students which I was lucky to supervise over my PhD journey. There were at least 15, but in particular, I would like to acknowledge Laurent Clarissou – my summer student – who was one of the most clever kids I ever supervised. It was a lot of fun to spend time in the lab with you. Well, as Milos once told about our performance during the experiments - "you created a monster", but in my humble opinion it was one of the most productive matches so far:)

The group, who fully adopted me over my PhD years, deserves separate "thank You, guys!" – among them in particular: self-proclaimed office "project Manhattan" Marcin Kisiel, Remy Pawlak and Lucas Moser, who not only spent a lot of time with me in the lab environment, but also helped me to understand my own value. Tobias, Sara, Marwa, Laurent, Roland, Philipp, Res, Shigeki San, Thilo, Antoine, Gui, Alexis, Urs, Mauro, Gustavo, Roman, Asalan, Sebastian, Carl, Marco, Alexina it has been great time. I will miss you all. One additional time I would like to acknowledge Remy and Marcin for deep scientific discussions and proofreading parts of this thesis. Separate thank you goes to Remy, who destroyed every single slide of my presentation a week before the defense, HOWEVER, I really appreciate your criticism and input.

I am also very thankful to people I met here in Basel – Anna, Emma, Mira and Sime – you, guys, were always there to give me valuable advise and support me in the moments I was ready to give up. Here I would like to acknowledge Anna - I was brave enough to make friends with new neighbors, who has ukrainian surname:) and didn't regret any single moment especially our famous balcony wine sessions. And as we realized later on - we are also neighbors in Kyiv - the world is very small, and I believe that every person we meet during our lifetime is always for some reason or lesson. Anna, I could not even imagine better support, than you are.

Separate Thank you goes to my University friends Julia Reichert, who was not scared of my sense of humor and was always there for a cup of coffee and discussion. Sara Freund - my favorite french twin:D without you I would not be able to get over my darkest moments. I am happy that we became friends:D Sara, what was that phrase in french? :D Simon Philipp - next office buddy, for all your support, long life related chatting and redbull by request:D Alexina Ollier, who just recently joined the group, but decided to hang out with "old freaks" core team, you are sweet, and you will rock it!

I would also like to acknowledge my friends from university times who by visiting me here in Basel, reunions somewhere around the world (particular "cultural and not cultural program"(c)), or warm greetings back home made me feel like I have never left Kyiv or Radiophysics Faculty:) you all are great. I am really happy that distance and years didn't washed out our friendship, still years and years to go:) Also I am grateful to all of you, for keeping to call me with my unique nickname!

Finally, I would like to thank my family. My parents and sister who never stopped believing in me, and were always supportive in their own way.

List of publications & communications

Peer-reviewed journal publications

1. O. Popova, M. Baljozovic, D. Sostina, M. Muntwiller, M. Stöhr, C. Wäckerlin, J. Dreiser, J.I. Cerda, L.H. Gade, T.A. Jung, J. Lobo-Checa **Magnetic imprint from the periodically distributed molecular adsorbates with selected metal centers**, *in preparation*, (2019)

2. O. Popova, I. Piquero-Zulaica, Z. M. Abd El-Fattah, M. Baljozovic, M. Stöhr, L.H. Gade, T.A. Jung, J. Lobo-Checa **Guest-induced pillow effect upon the partially localized state of a quantum box array**, *in preparation*, (2019)

3. O. Popova, M. Baljozovic, D. Sostina, M. Muntwiller, L. H. Gade, J.I. Cerda, T.A. Jung, J. Lobo-Checa **A two-dimensional porphyrin based porous network assembled due to the electrostatic strain**, *in preparation*, (2019)

4. O. Popova, M. Baljozovic, V. Jacobsen, J. Nowakowski, J. Dreiser, C. Wäckerlin, G. Morgan and T. A. Jung, **XMCD Investigation of Highly anisotropic trigonal prismatic metal complexes**, *in preparation* (2019)

5. M. Baljozovic, O.Popova, J. Girovsky, J. Nowakowski, A. Hunter, C. Wäckerlin, F. Mousavi, M. Moradi, D. Siewert, F. Ravani, T. Nijs, E. Gradauskaite, M. Iwasaki, M. O'Doherty, H. Rossmann, I. Pasti, N. V. Skorodumova, S.-X. Liu, S. Decurtins, J. Dreiser, N. Ballav, T. A. Jung **Self-Assembly and Magnetic Order of 2D Spin Lattices on Surfaces** *manuscript in preparation* (2019)

6. M. Baljozovic, O.Popova, J. Nowakowski, M. Iwasaki, M. O'Doherty, H. Rossmann, T. Nijs. F. Mousavi, M. Moradi, A. Hunter, E. Gradauskaite, I.A Pasti, N.V Skorodumova, J. Dreiser, S.-X. Liu, S. Decurtins, J. Dreiser, N. Ballav, T. A. Jung **Spin Manipulations of Metal-Containing Phthalocyanine Molecules by H2/H* Ligation** *manuscript in preparation* (2019)

7. M. Baljozovic, O.Popova, J. Nowakowski, H. Rossmann, T. Nijs, A. Hunter, E. Gradauskaite, V. Müller, A. D. Schlüter, S.-X. Liu, S. Decurtins, J. Dreiser, A. Kleibert, N. Ballav, T.A. Jung **Magnetic Properties of Homo- and Hetero-Metallic Triply-Fused Porphyrins**, *manuscript in preparation* (2019)

8. M. Baljozovic, O.Popova, J. Nowakowski, Ali Md. E., A. Hunter, E. Gradauskaite, F. Mousavi, S.-X. Liu. J. Dreiser, S. Decurtins, P. M. Oppeneer, N. Ballav, T.A. Jung **Assembly and magnetic properties of chromium (II) phthalocyanine molecules on Au (111)** *manuscript in preparation* (2019)

9. P. Kröger, J. Nowakowski, M. Baljozovic, C. Wäckerlin, O.Popova, J. Dreiser, A. Wäckerlin, J. Girovsky, H. Rossmann, T. Nijs, F. Mousavi, F. Ravani, Jung T. A., Vollmers N. J., Schmidt W. G., Gerstmann U., Pfnür H. **Extreme magnetic anisotropy of Cr atoms embedded into ultrathin Bi(111) films** *manuscript in preparation* (2019)

10. F. Mousavi, A. Ahsan, T Nijs, B. Günther, M. Baljozovic, A. Wäckerlin, O. Popova, S. Nowakowska, M. Stöhr, C. Wäckerlin, J. Björk, T.A. Jung and L. H. Gade **Frustrated H-bonding of planar molecules on a weakly interacting semi-metallic Bi surface** *Chem Comm* (2019)

11. A. Ahsan, F. Mousavi, T. Nijs, S.Nowakowska, O. Popova, J. Björ, L.H. Gade and T.A. Jung **Watching nanostructure growth: Kinetically controlled diffusion and condensation of Xe in a surface metal-organic network** *Nanoscale* (2019)

12. I. Piquero-Zulaica, Z.M. Abd El-Fattah, O. Popova, S. Kawai, S. Nowakowska, M. Matena, M. Enache, M. Stöhr, A. Tejeda, A. Taleb-Ibrahimini, E. Meyer, J.E. Ortega, L.H. Gade, T.A. Jung and J. Lobo-Checa, **Effective Determination of Surface Potential Landscapes from Metal-Organic Nanoporous Overlayers** *New Journal of Physics* (2019)

13. M. Moradi, N. Opara, L. Tulli, C. Wäckerlin, S. Dalgarno, S. Teat, M. Baljozovic, O. Popova, E. van Genderen, A. Kleibert, H. Stahlberg, J. Pieter Abrahams, C. Padeste, P.F.-X. Corvini, T.A. Jung, P. Shahgaldian, **Supramolecular architectures of molecularly thin yet robust free-standing layers** *Science Advanced* (2018)

14. A. Ahsan, F. Mousavi, T. Nijs, S. Nowakowska, O. Popova, A. Wäckerlin, J. Björ, L.H. Gade, T.A. Jung, **"Phase transition" in quantum confinements: inducing mobility of Xe atoms in the pores of an on-surface networks** *Small, vol.* (2018)

15. S. Nowakowska, F. Mazzola, M. Alberti, F. Song, T. Voigt, J. Nowakowski, A. Wäckerlin, C. Wäckerlin, J. Wiss, W.B. Schweizer, M. Broszio, C. Polley, M. Leandersson, S. Fatayer, T. Ivas, F. Mousavi, A. Ahsan, T. Nijs, O. Popova, J. Zhang, M. Muntwiller, C. Thilgen, M. Stöhr, F. Diedrich, J. Wells, T.A. Jung,

Adsorbate induced modification of the confining barriers in quantum box array *ASC, Nano* **12(1)**, (2018)

16. A. Wäckerlin, S. Fatayer, T. Nijs, S. Nowakowska, F. Mousavi, O. Popova, A. Ahsan, T.A. Jung, C. Wäckerlin, **Molecular chessboard assemblies sorted by site-specific interactions of out-of-plane d-orbitals with a semimetal template** *Nano Letters* **17(3)** , (2017)

17. S. Nowakowska, A. Wäckerlin, I. Piquero-Zulaica, J. Nowakowski, S. Kawai, C. Wäckerlin, M. Matena, T. Nijs, S. Fatayer, O. Popova, A. Ahsan, F. Mousavi, T. Ivas, E. Meyer, M. Stöhr, J.E. Ortega, J. Björk, L.H. Gade, J. Lobo-Checa, T.A. Jung. **Configuring Electronic States in an Atomically Precise Breadboard of Quantum Boxes** *Small* **12**, 28, pp. 3759-3763 (2016)

18. O. Popova, R. Sydorov, A. Goriachko, I. Koval, P.V. Melnyk, M.G. Nakhodkin, **Creating of original nanopositioning system for scanning probe microscopy** *Ukrainian journal of young scientist's "Physics, Electronics, Electrical Engineering: 2014"*, (2014)

19. O. Popova, R. Sydorov, A. Goriachko, I. Koval, P.V. Melnyk, M.G. Nakhodkin, **Novel nanopositioning system for scanning probe microscopy** *Journal of Kyiv National Taras Shevchenko University, Series "Physics and Mathematics"* No21 (2014)

20. A. Goriachko, O. Popova, R. Sydorov, P.V. Melnik, M.G. Nakhodkin, **Scanning Probe Microscopy Investigation of Bi Film Surfaces on Ge (111) Substrate** *Ukrainian Journal of young scientists and graduate students "IEF'2013"*, (2013)

21. A.Goriachko, O. Popova, R. Sydorov, P.V. Melnik, M.G. Nakhodkin, **Bi/Ge(111) system: Investigation of adsorbtion and delta-doping by means of Scanning Tunneling Microscopy** *Ukrainian Journal of young scientists*, (2012)

Presentations

1. O. Popova **Electronic and magnetic properties of 2D on-surface architectures**, ESRF, Grenoble, France (December 2019)

2. O. Popova **Electronic and magnetic properties of 2D on-surface architectures**, Oak Ridge National Lab, Tennessee, USA (November 2019)

3. O. Popova, I. Piquero-Zulaica, Z. M. Abd El-Fattah, M. Baljozovic, M. Stöhr, L.H. Gade, J. Lobo-Checa and T.A. Jung, **"Pillow effect" induced by presence of adsorbates in the quantum box array**, *ECOSS 34*, Aarhus, Denmark (August 2018)

4. O. Popova, A. Wäckerlin, S. Fatayer, T. Nijs, S. Nowakowska, F. Mousavi, A. Ahsan, T.A. Jung, Ch. Wäckerlin, **Molecular chessboard assemblies sorted by site-specific interactions of out-of-plane d-orbitals with a semimetal template** *ECOSS 33*, Szeged, Hungary (September 2017)

5. O. Popova, I. Piquero-Zulaica, S. Nowakowska, J.E. Ortega, M. Matena, M. Stöhr, L.H. Gade, J. Lobo-Checa and T.A. Jung, **Temperature dependence of the partially localized state in molecular network**, *39th Internatioanl Conference on Vacuum Ultraviolet and X-Ray Physics*, Zürich, Switzerland (July 2016)

6. O. Popova, A. Wäckerlin, S. Nowakowska, J. Girovsky, A. Kleibert, N. Ballaw, S. Kawai, T. Ivas, J. Nowakowski, S. Fatayer, C. Wäckerlin, T. Nijs, E. Meyer, J. Björk, M. Stöhr, L.H. Gade and T.A. Jung, **Dimesionality control via metal-specific on-surface chemistry**, *International workshop: On-Surface Synthesis*, San Sebastian, Spain (June 2016)

7. O. Popova, A. Wäckerlin, S. Nowakowska, J. Girovsky, A. Kleibert, N. Ballaw, S. Kawai, T. Ivas, J. Nowakowski, S. Fatayer, C. Wäckerlin, T. Nijs, E. Meyer, J. Björk, M. Stöhr, L.H. Gade and T.A. Jung, **Programming the dimesionality of on-surface polymers by endo- and exo- ligation**, *ECOSS 31*, Barcelona, Spain (September 2015)

8. O. Popova, S. Nowakowska, A. Wäckerlin, S. Kawai, T. Ivas, J. Nowakowski, S. Fatayer, C. Wäckerlin, T. Nijs, J. Girovsky, S. Martens, A. Kleibert, N. Ballaw, E. Meyer, J. Björk, M. Stöhr, L.H. Gade and T.A. Jung, **Tunning on-surface coordination polymers to form form chains and networks forming quantum boxes to investigate Xenon condensation in an atom-by atom manner**, *DPG Spring meeting*, Berlin, Germany (March 2015)

9. O. Popova, R. Sydorov, A. Goriachko, I. Koval, P.V. Melnyk, M.G. Nakhodkin, **Creating of original nanopositioning system for scanning probe microscopy** *Young scientist competition in the direction " INSTRUMENT"*, Sumy, Ukraine (March 2014)

10. A. Goriachko, O. Popova, R. Sydorov, P.V. Melnik, M.G. Nakhodkin, **Bi/Ge(111) system: Investigation of adsorbtion and delta-doping by means of Scanning Tunneling microscopy** *Proceedings of the III-th International science conference "Nanostructure materials -2012: Russia-Ukraine-Belarus"*, Uzhgorod, Ukraine (May 2013)

Posters

1. O. Popova, I. Piquero-Zulaica, Z. M. Abd El-Fattah, M. Baljozovic, M. Stöhr, L.H. Gade, J. Lobo-Checa and T.A. Jung Title: **"Pillow effect" induced by presence of adsorbates in the quatum box array"** *International workshop: On-Surface Synthesis*, Sant Feliu de Guixols, Spain (September 2018)

2. O. Popova, S. Nowakowska, F. Mazzola, M. Alberti, J. Nowakowski, A. Wäckerlin, F. Song, T. Voigt, C. Wäckerlin, J. Wiss, W.B. Schweizer, M. Broszio, C. Polley, M. Leandersson, S. Fatayer, T. Ivas, F. Mousavi, A. Ahsan, T. Nijs, J. Zhang, M. Muntwiller, C, Thilgen, M. Stoehr, F. Diedrich, J. Wells, T. A. Jung, Title: **"Adsorbate induced modification of the confining barriers in quantum box array"** *QMol*, Ascona, Switzerland (October 2017)

3. O. Popova, M. Martina, U. Maier, T.A. Jung, Title: **"Portable Scanning Probe microscope in UHV suitcase"** *CTI micro-nano event*, Neuchatel, Switzerland (May 2015)

4. O. Popova, A. Wäckerlin, M. Nguyen, C. Wäckerlin, S. Martens, S. Nowakowska, T. Ivas, J. Roose, S. Boz, M. Schaer, C. Pignedoli, C.Thilgen, F. Diedrich, D. Passerone, T.A. Jung, Title: **"Chiral 1D and 2D metal-organic architectures"** *SpinMol*, Ascona, Switzerland (October 2014)

Curriculum Vitae

Olha Popova

Personal data: | Place, Date of Birth: Chernihiv, Ukraine, 14.12.1991 | Phone: +41788401405 | email: ollia.popova@gmail.com |

Education

2015- 2019 | **PhD student in Experimental Physics**, University of Basel, Switzerland

Title:"Electronic and magnetic properties of low dimensional on-surface organic systems"

Research area: on-surface magnetic and electronic properties of thin organic structures as well as individual transition metal atoms in ultra-high vacuum (UHV).

Leadership of seven projects involving collaboration with 10 international groups consisting of synthetic chemists, theoretical physicists, surface science physicists and synchrotron beamline scientists

PhD experience

Main proposer of 7 and co-proposer of 11 accepted beamtime proposals at the Swiss Light Source synchrotron; participation in more than 25 beamtimes

The investigations were performed via broad tool-kit of the Laboratory- and Synchrotron-based experimental techniques at University of Basel, Laboratory for Micro- and Nanotechnology at Paul Scherrer Institut and at the Swiss Light Source.

Presented posters and talks at 12 international conferences

Co-author of 21 scientific papers (4 manuscripts with first author are in preparation)

2014-2015 | **M. Sc. project in Technical Physics with major in Nanotechnology and Functional Materials** University of Basel and Paul Scherrer Institute, Villigen, Switzerland.
measurements for Master Thesis and participation in research projects concerning magnetic properties of organometallic molecules on a ferromagnetic surface in ultra-high vacuum (UHV).

2014 | **Internship** at Nanosurf Lab, Academy of Science of Czech Republic, Prague, Czech Republic.
Learning SPM technique on the base of q-Plus sensors and participation in research projects concerning on-surface assemblies and reactions of organic compounds.

2013-2015 | **M.Sc. in Applied Physics and Electronics** at the Department of Nanophysics and Nanoelectronics, Faculty of Radiohysics, Electronics and Computer systems, Taras Shevchenko National University of Kyiv, Ukraine.
(Individual course of studies with a broadened curriculum in nanoscience and ultra-high vacuum (UHV) technology).
Title:"Condensation of adsorbates in porous organic nanostructures investigated by STM/STS and XPS"
Obtained: Master Diploma with excellence in the field of study Radiophysics and Electronics.
Qualification of Master of radiophysics and applied physics, engineer radiophysicist, research fellow, research engineer.

2009-2013 | **B. Sc. in in Applied Physics and Electronics**, Radiophysics Department, Taras Shevchenko National University of Kyiv, Ukraine.
*Title:"Investigation of the thin Bi film growth on the Ge(111)c(2*8) surface"*

Awards

2015 Rector's award in distinguishing engagement in the work of student's society of Taras Shevchenko National University of Kyiv

2015 Best master Thesis Rector's award, Taras Shevchenko Natioanl Univesrity of Kyiv

2014 First place at all Ukraine competition among young scientist in the section "Instrument development"

Work Experiences

2014-2019	**Research Assistant at University of Basel and Paul Scherrer Institute**, Basel and Villigen, Switzerland. Teaching assistant in subjects: Surface science, Nanostructures: processing and Characterization techniques, supervision during 6 Nanowissenschaften Blockkurse, 4 Summer students and 3 Visiting scientists.
2013-2014	**Research Assistant** at Radiophysics Department, Taras Shevchenko National University of Kyiv.
2011-2014	**Graphic designer**, IT startup, Kyiv, Ukraine.
2011-2012	**Volunteer** at children health center, Crimea, Ukraine.
2009-2014	**Volunteer** at an orphanage, Kyiv, Chernihiv, Ukraine.

Languages

English: business fluent | **German:** intermidiate | **Ukrainian:** mother tongue | **Czech:** coversational | **Russian:** mother tongue.

IT Skills

Proficiency in: Latex, Origin, Pascal, Python, Microsoft Office, Power Point, Matlab, Unifit, Shell, SpecsLab, Graphics software;
Proficiency in: programs for control of XPS/local probe (SPM) experiments and data analysis, i.e. SpecsLab, IGOR and WSxM.
Experience of: C++, C♯, Labview.

Interests and Activities

Cooking, Handcrafting, Photography, Reading psychology literature and classical novels, Individual sports (Yoga, Snowboarding, jogging), Team sports (Tennis, Hiking, Football).